CUSTOMIZATION OF ANEURYSM SCAFFOLD GEOMETRIES FOR IN VITRO TISSUE-ENGINEERED BLOOD VESSEL MIMICS TO USE AS MODELS FOR NEUROVASCULAR DEVICE TESTING

A Thesis Presented to the Faculty of

California Polytechnic State University, San Luis Obispo

In Partial Fulfillment of the Requirements for the Degree

Master of Science in Biomedical Engineering

By

Camille D. Villadolid

August 2019

Committee Membership

Title: Customization of Aneurysm Scaffold Geometries for In Vitro Tissue-Engineered Blood Vessel Mimics to Use as Models for Neurovascular Device Testing

Author: Camille D. Villadolid

Date Submitted: August 2019

Committee Chair: Kristen O'Halloran Cardinal, Ph.D.
Professor of Biomedical Engineering

Committee Member: Lily Hsu Laiho, Ph.D.
Professor of Biomedical Engineering

Committee Member: Trevor Ryan Cardinal, Ph.D.
Professor of Biomedical Engineering

Abstract

Customization of Aneurysm Scaffold Geometries for In Vitro Tissue-Engineered Blood Vessel Mimics to Use as Models for Neurovascular Device Testing

Camille D. Villadolid

Cerebral aneurysms occur due to the ballooning of blood vessels in the brain. Rupture of aneurysms can cause a subarachnoid hemorrhage, which, if not fatal, can cause permanent neurologic deficits. Minimally invasive neurovascular devices, such as embolization coils and flow diverters, are methods of treatment utilized to prevent aneurysm rupture. The rapidly growing market for neurovascular devices necessitates the development of accurate aneurysm models for preclinical testing. In vivo models, such as the rabbit elastase model, are commonly chosen for preclinical device testing; however, these studies are expensive, and aneurysm geometries are difficult to control and often do not replicate the variety of geometries found in clinical cases. A promising alternative for preclinical testing of neurovascular devices is an aneurysm blood vessel mimic (aBVM), which is an in vitro tissue-engineered model of a human blood vessel composed of an electrospun scaffold with an aneurysm geometry and human vascular cells. Previous work in the Cal Poly Tissue Engineering Lab has established a process for creating different aneurysm scaffolds based on the shape of different geometries, and this work aimed to further advance these aneurysm geometries in order to enhance the versatility of the in vitro model.

The overall goal of this thesis was to customize the aBVM model through variations of different dimensions and to validate the scaffold variations for neurovascular device testing. First, a literature review was performed to identify critical ranges of aneurysm neck diameters and heights that are commonly seen in rabbit elastase models and in human clinical settings in order to set a foundation for creating new geometries. Based on the results, aneurysm geometries with varying neck sizes and heights were modeled and molded, and scaffolds were fabricated through electrospinning. Methods were developed to characterize scaffolds with internal measurements through imaging techniques using a scanning electron microscope. To validate these scaffolds for use as aBVMs for neurovascular device testing, constructs were created by

dual-sodding human endothelial cells and smooth muscle cells into scaffolds with varying neck sizes. Finally, flow diverters were deployed in constructs with varying neck sizes in order to evaluate feasibility and initial healing. Customized aneurysm scaffolds can eventually be used with a variety of device studies for screening of neurovascular devices or as a predecessor for in vivo preclinical testing.

Acknowledgements

Thank you to my friends and family back home who have supported me during my time here at Cal Poly and have always encouraged me to persevere no matter what. You've all raised me to be the person that I am today.

Thank you to all of my friends that I have made throughout my college years, and my fellow biomedical engineering classmates turned best friends. Thank you for sticking with me throughout all of these years, for providing me with support during the good times and bad, and for making memories with me of them both. These are friendships I will cherish forever.

Thank you to my friends from the Cal Poly Tissue Engineering lab for welcoming me with open arms when I joined just a year ago. Brandon and Ryan, thank you so much for teaching me everything that I know, for always being there during every crisis, and for your company as fellow electrospinners. Ben, Tessa, and Conor thank you for all the hours you spent helping me put the pieces of my thesis together and make an impact in the field. Gabby, Lily, Clare, and Ali, thank you for your support as I learned my way around the lab. Abby, Evan, Jason, Ben, Cami, Nicole, Henry, Ashley, and Alyssa, I am grateful that I got to learn with you, and I cannot wait to hear about the amazing things that you end up accomplishing in the future.

Thank you very much to my committee members Drs. Lily Laiho and Trevor Cardinal for your support. I've appreciated all the time that you've spent on my work, and providing me with insight that I'll carry on with me as an engineer.

Lastly, thank you Kristen, for absolutely everything that you've done for me, for all of the endless opportunities that you've given me from the MEDITEC projects to being in your research lab with you as my advisor. Thank you for taking a chance on me and for allowing me to discover my passions in research and in everything I love about being an engineer and a leader. You are a real inspiration, and I hope that we will work together again someday. Thank you.

Table of Contents

List of Tables

List of Figures

1 Introduction

1.1 Overview

Cerebral aneurysms occur when blood shear stresses cause a weakened spot in the wall of an artery in the brain to balloon, causing a change in blood flow velocity and endothelial cell dysfunction [1]. Without treatment, aneurysms can enlarge over time due to the changes in the complexity of proteins that comprise the extracellular matrix. Bulging is due to the diminishing tunica media and loss of collagen, which provides tensile strength and support. Aneurysm growth is due to the loss of fibronectin, which helps repair damaged vessels [2]. Upon rupture, brain aneurysms can cause a subarachnoid hemorrhage, or bleeding in the subarachnoid space in the brain, which can be a fatal event. 12% of hemorrhaging patients will die immediately after the event, while 40% of patients will die within one month [3]. Among the patients that survive a subarachnoid hemorrhage, almost a quarter of them will still have major neurologic deficits after four years [4].

Aneurysms occur in 1-5% of the population, and 10-30% of those patients have more than one aneurysm [5]. Most aneurysms occur in the Circle of Willis, which is a blood vessel complex in the brain that allows for redundancy in blood flow. The Circle of Willis is an evolutionary protective mechanism that allows for brain tissue to receive sufficient blood flow in case of an arterial blockage. Because of this, many different vascular variations have been observed in humans [6]. The complexity of the structure of the Circle of Willis and its surrounding vasculature, with its twists and variety of branching points, provide the ideal conditions for aneurysm formation (Figure 1).

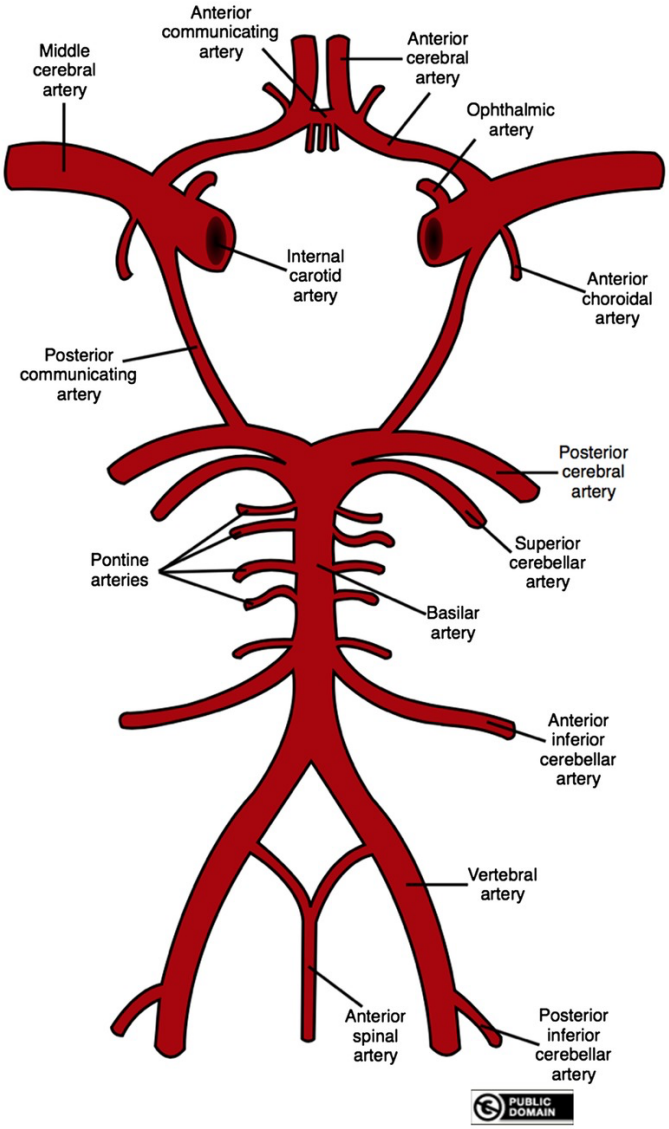

Figure 1: Circle of Willis and surrounding vascular anatomy [7]. Most cerebral aneurysms develop within the Circle of Willis because of the potential for weakened points in any part of the complicated vasculature. The inherent biological variability among each individual's Circle of Willis can also contribute to aneurysm formation. The most common artery where aneurysms occur is the anterior communicating artery.

Though aneurysms can develop in any weakened spot in the wall of an artery, the most common artery that an aneurysm can occur in is the anterior communicating artery, which is a small blood vessel that connects the left and right anterior cerebral artery. Aneurysms that occur in the anterior communicating artery account for nearly 25% of all aneurysms found in multiple large major studies [8]. Aneurysms are also commonly found in the internal carotid artery, the major artery that connects the aortic arch in the heart to the Circle of Willis, at points where it branches off into the posterior communicating artery and the ophthalmic artery. In many other cases, aneurysms occur in the middle cerebral artery, or in posterior circulation sites such as the tip of the basilar artery.

Cerebral aneurysms can be categorized into five main types based on their causes and relative geometries: saccular, blister, fusiform, dissecting, and mycotic. Saccular, or "berry" aneurysms account for 90% of all aneurysms found clinically, and are most commonly found in the crotch of major bifurcations within the Circle of Willis [9]. They are characterized by a large dome and a narrow neck at the junction of the parent artery. As the aneurysm grows, it develops a thick atherosclerotic-like fibromuscular-elastic layer throughout the dome [9]. Saccular aneurysms are at the largest risk of hemorrhage if a smaller aneurysm develops along the walls of the main aneurysm dome.

Blister aneurysms are most commonly found in the curvature of the ICA before feeding into the Circle of Willis, and are characterized by their hemispheric bulge, wide neck, and extremely fragile arterial wall composed of thin fibrotic tissue [10]. Fusiform aneurysms are a rare sub-type of intracranial aneurysm, accounting for less than 1% of clinical cases. They form when the circumference of the entire parent vessel dilates. Blood velocity streamlines of fusiform aneurysms demonstrate vortex-like profiles throughout the aneurysm before circling back

towards the parent artery [11]. Dissecting aneurysms occur when injury to the arterial wall causes a blood vessel tear through the endothelium, tunica media, and sometimes through the adventitia as well, creating a pocket within the arterial wall for blood to abnormally circulate [12]. Mycotic aneurysms are another rare type of aneurysms that are similar to saccular aneurysms geometrically; however, they are much more fragile and usually caused by an infection originating from either the adventitia layer or from septic emboli that sticks to the endothelium and spreads throughout the entire vessel wall [13]. With the exception of the mycotic subtype, aneurysms can grow from abnormal vessel wall weakness and constant shear stress due to dynamic blood flow.

1.2 Aneurysm Pathology

Initiation of aneurysm formation is mainly due to the weakness of a blood vessel wall, while growth occurs because of the constant hemodynamic shear stresses that affect the cell morphology. The risk for developing an aneurysm is increased due to genetic factors that affect the geometry of the blood vessels in the brain. Aneurysms are more likely develop at points of bifurcations or in areas of curvature where laminar blood flow is severely disrupted, causing uneven distribution of shear forces. Blood vessel lumens that were previously stenotic, such as in individuals who smoke tobacco, are also likely to develop aneurysms [14].

In weakened artery walls, high turbulent flow and abnormal vessel wall shear stress can lead to endothelial cell dysfunction. Endothelial cells are a specific type of simple squamous epithelial cells that line the lumen of blood vessels, and are sensitive to blood flow changes. Sudden or continual changes in wall shear stress cause them to change phenotype, disallowing them to perform their function.

Initial damage from increased shear stress to the vascular endothelium triggers an inflammation cascade [15]. The chemical signals are usually due to increased oxidative stress from the constant generation and destruction of free radicals, which are highly reactive molecules. Pro-inflammatory cells and molecules such as leukocytes, platelets, cytokines, adhesion molecules, immunoglobulins, and complement proteins are attracted to the site of the weakened point of the vessel and accumulate, sending more signals to keep the inflammation recurring [15]. Endothelial cells change shape and elongate, and the tunica intima layer swells, leading to the eventual loss of the tunica media, or smooth muscle, layer. During vascular injury, arterial smooth muscle cells undergo phenotypic modulation, causing them to switch to a pro-inflammatory state from their primary function of contracting and dilating the vessel [16]. The proliferation, migration and eventual loss of smooth muscle cells and phenotypic changes of the endothelial cells also lead to a decreased synthesis of collagen and laminin, important proteins that provide structural support to the artery wall. Once initiated, this cascade enters a positive feedback loop cycle, as the effect of blood shear stress grows larger proportionally to the growth of the aneurysm itself.

Unless the aneurysm grows so large that it presses against a nerve and causes notable damage to the sensory or motor control system, aneurysms can keep growing unnoticed. Many patients appear asymptomatic, and most aneurysms are discovered by chance [17]. Though larger aneurysms are at a greater risk for rupture, they can theoretically leak at any point during their growth. Most patients that have aneurysms discovered by chance will choose to treat it regardless of their symptoms in order to prevent rupture, unless other present physical conditions make the intervention risky [18]. Treatments range from drugs to treat the symptoms to surgical

intervention to remove the aneurysm, and many companies have developed different minimally invasive devices that can treat cerebral aneurysms, which will be discussed in the next section.

1.3 Aneurysm Treatments

1.3.1 Surgical Method

Surgical intervention is considered to be the only "cure" to completely remove an aneurysm, and it is the gold standard because it is the most tested and durable method of aneurysm treatments [19]. There are different methods of surgical approaches to treat aneurysms; the most common method is simple clipping.

Simple clipping is performed first with a craniotomy to expose the aneurysm neck. Once the location of the aneurysm is determined, the skull is opened at a specific part, and surgical flaps of skin and protective layers of the skull are created. Then, surgeons will dissect into the brain and retract excess tissue to isolate the aneurysm. This is done under controlled hypotension to prevent aneurysm rupture [20]. Surrounding arteries are temporarily occluded to prevent rupture. The aneurysm is then clipped using one or multiple clips at the neck region closest to the parent artery in order to prevent any more blood flow to the abnormal, weakened vascular wall (Figure 2).

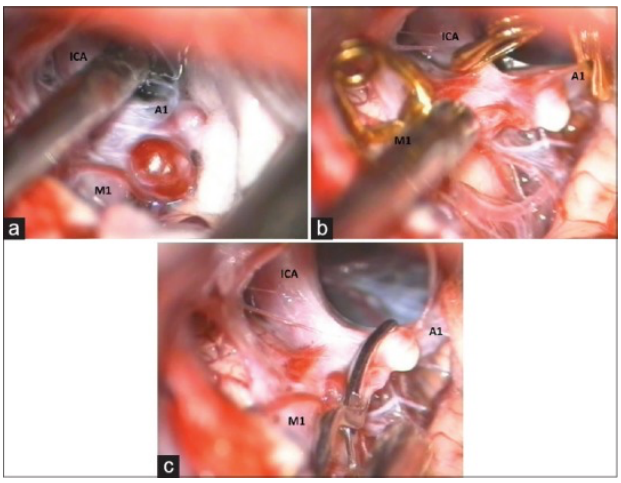

Figure 2: Aneurysm clipping surgical procedure [21]. A) Small aneurysm at a bifurcation. B) Surrounding vasculature is clipped at multiple areas using the gold clips. C) Aneurysm neck clipped using a silver clip. The gold clips are removed to relieve the surrounding vasculature.

Success of clipping relies on the surgeon's ability to obtain and maintain good neck exposure throughout the procedure [22]. Clipping has been a standard since it was introduced by American neurosurgeon, Walter Dandy M.D. in 1937 when he used a silver clip to obstruct blood flow from entering the neck of an internal carotid artery aneurysm [23]. From then until the modern day, this method has become more sophisticated over time as a larger variety of clips became available and operating room microscopes allowed for better visualization.

Another surgical technique to treat aneurysms that is less common includes wrapping, which is usually performed after an aneurysm has already ruptured [24]. The leakage is isolated and the tear is wrapped with tissue or an absorbable material such as cotton fiber in order to help reconstruct the parent artery. This surgical technique can ultimately be used in conjunction with simple clipping.

While surgery is considered the only procedure that will prevent recurrence of the same aneurysm, many patients do not have it as an option. Clipping involves open brain surgery, which is risky itself, specifically for older adults and others who suffer from other health conditions. Because of this, many companies have developed devices that minimally invasively treat cerebral aneurysms before their rupture.

1.3.2 Devices

There are three main categories of devices currently on the market used to treat cerebral aneurysms and prevent hemorrhagic stroke: embolization coils, stent devices, and flow diverters, which will be discussed more specifically in the next few sections. In all cases, these endovascular devices are delivered through a series of microcatheters from an access point in the femoral artery [25]. These catheters track the devices through the vasculature and up to the site of the aneurysm in the brain. All of these implants' goals are to clot off the sac or to completely direct blood flow away from the aneurysm to induce aneurysm shrinkage.

1.3.2.1 Embolization Coils

Embolization coils are used to pack aneurysm sacs with flexible metal to prevent blood from flowing into the dome. These coils are soft and flexible so that they can conform to various aneurysm shapes; however, they also have a minimum packing density and stiffness in order to resist shear stress due to constant blood flow. The Gugliemi detachable coil technique was one of the first established endovascular treatments [26]. During this procedure, microcatheters deliver detachable coils made up of stainless steel delivery wires with soft platinum soldered around it.

An applied current will detach the coils, leaving them inside the aneurysm sac (Figure 3). The current causes the coil to behave like a positively charged electrode in order to attract negatively charged blood particles to promote clot formation inside the aneurysm.

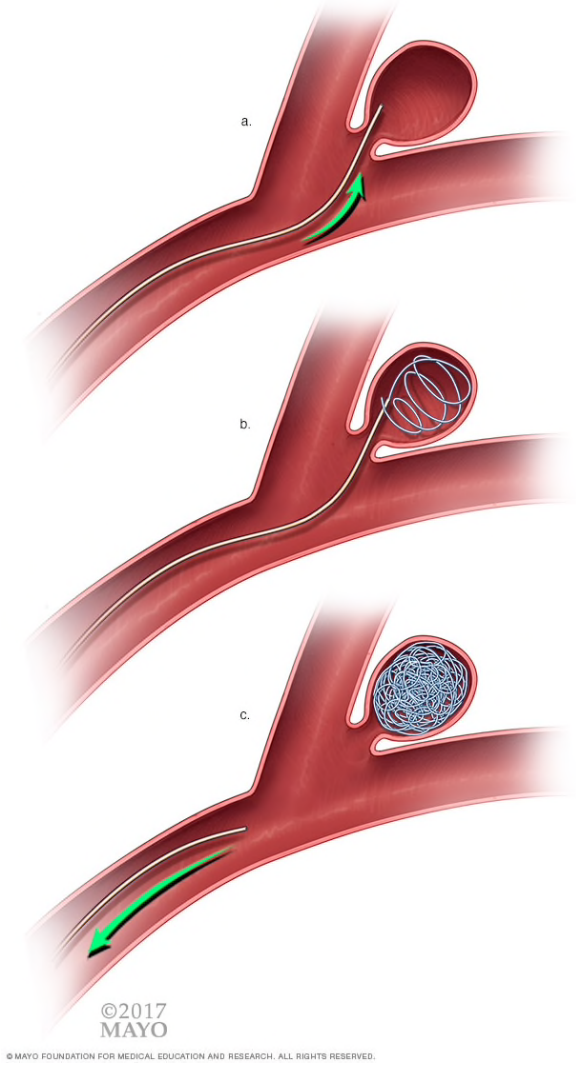

Figure 3: Endovascular Coil Devices [27]. A) Microcatheter is inserted minimally invasively into the dome of the aneurysm. B) Microcatheter delivers several coils to pack the aneurysm sac. C) Microcatheter is withdrawn.

Manufacturers will mass-produce coils of many lengths and diameters. Often, different types of coils are deployed into the dome of the aneurysm in one procedure in order to sufficiently fill all gaps. The stiffness of different coils is dependent on the shear modulus of the metal chosen as well as their primary, secondary, and tertiary structure, and this influences the packing density of the coil. The most commonly used metals to create coils are nitinol, platinum, nickel, iridium, and tungsten, with the most popular a platinum tungsten alloy that is inert, noncorrosive, non-immunogenic, and can be manufactured easily into wires with extremely small diameters [25, 28].

During a single treatment, coils of different material properties are often used. When deploying coils, framing coils, which are complex and spherical in shape, are first inserted to provide a specific architecture. Smaller, softer coils, or "finishing coils" will then be deployed in order to fill in the gaps left in the aneurysm dome to completely occlude blood flow. Though these coils are unable to maintain their shape, they are preferred during the final stages of embolization because their flexibility can achieve maximum packing density [29]. Softer coils can be more fined tuned in their flexibility to treat irregularly shaped aneurysms.

Coils have been increasingly modified to allow for increased packing efficiency to treat aneurysms, and also to improve usability. In addition to electrolytic detachment, mechanical mechanisms have been safely demonstrated [30, 31]. In addition, modifications such as PGA and PGLA bioactive coatings and expandable hydrogels have been developed in order to increase the packing density to promote clotting and to speed up neointimal proliferation [32].

Though coils have been widely used to treat a large variety of aneurysms, certain geometries may not be suitable for optimal treatment with them. In a published literature review comparing embolization coil treatment with surgical clipping of intracranial aneurysms, many

instances of incomplete occlusion after the first coiling treatment were on aneurysms with a wide neck greater than 4 mm [33]. In addition, poor outcomes of embolization coil treatment were associated with dome sizes greater than 10 mm [33]. Because of this, other devices have been developed to use in conjunction with coiling in order to increase the efficacy of blood flow occlusion in the neck and dome of the aneurysm.

1.3.2.2 Stents

Stents are a second type of medical device used to prevent blood from flowing into an aneurysm by using a technique called stent assisted coiling. Stents are most commonly used to treat atherosclerotic stenosis both with and without aneurysm formation [34]; however, they have been employed in conjunction with coil devices in order to stabilize the coils inside the sac of an aneurysm [25, 35]. Two major stent assisted coiling techniques are used by physicians: jailed and trans-cell coiling (Figure 4).

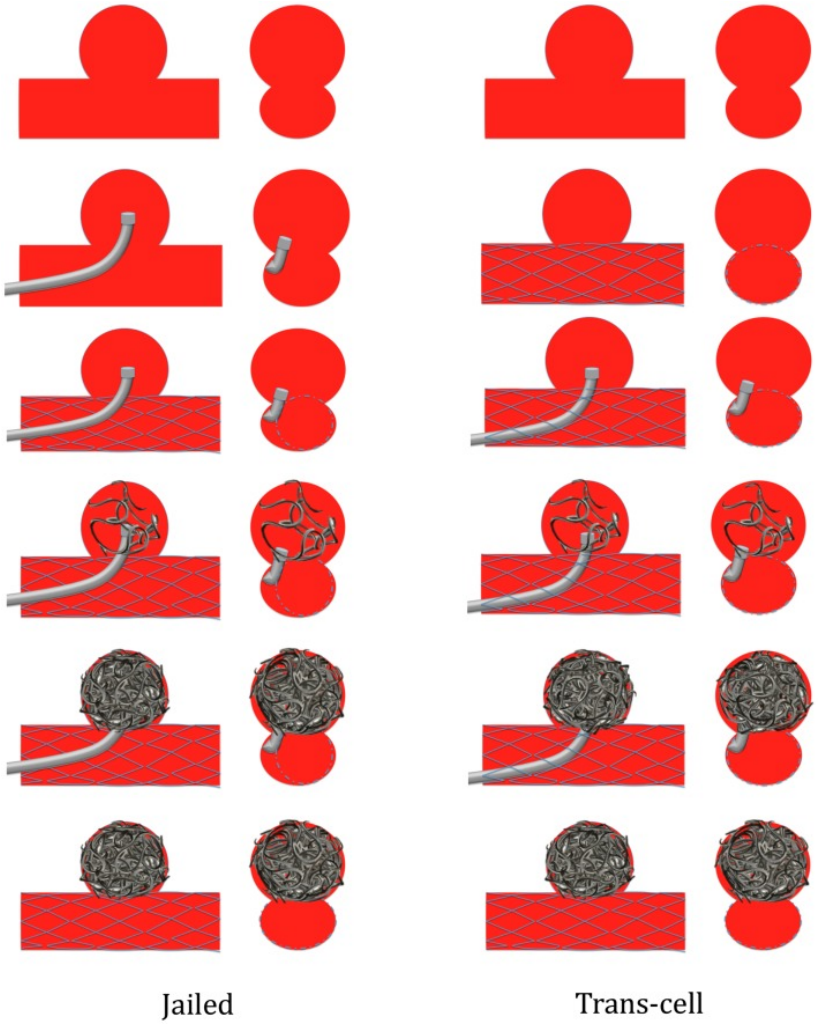

Figure 4: Jailed coiling versus trans-cell coiling [25, 36]. Jailed coiling occurs when a physician inserts the microcatheter delivering the coils first before deploying a stent to keep the microcatheter in place during device delivery [37]. Trans-cell coiling occurs when a stent is already deployed, and the microcatheter is advanced through the cells of the stent to deliver the coils [38].

Jailed coiling entails inserting the microcatheter of the embolization device first into the aneurysm sac, and then partially or fully deploying the stent on top of the catheter. This "jails" the microcatheter before coil deployment and the stent struts form against the parent artery walls

to seal the neck of the aneurysm [37]. On the other hand, trans-cell coiling consists of fully deploying the stent first, and then advancing the microcatheter through the stent lumen and within the struts of the stent to perform coiling [38]. In general, an advantage of using stent-assisted coiling is that higher metal coverage of stents can help provide structure and, subsequently, promote healing to diseased parent arteries in a combined aneurysm and arterial occlusion diagnosis.

A major design consideration for stents is the need for a high radial force throughout the length of the device once deployed in order to keep the blood vessel open; however, stents must also be flexible enough because of the inherent torturous anatomy of cranial blood vessels [39]. There are three types of stent designs based on the characteristics of the strut [25]: open celled, closed celled, and half-open celled. Open celled stent designs are defined by repeating structural elements, or cells, that are not bridged at the inflection points between each cell, while closed celled designs have cells that are connected at the inflection points [40]. Half-open celled stents have a combination of these patterns. Braided stents are most often closed celled stents, and they are advantageous because they inherently have a high compressive force that translates into a high radial force and uniform blood vessel dilation throughout [25]. Laser-cut stents are usually open celled or half open celled stents, which can conform to tortuous anatomy.

Material properties of the stent can also affect the radial force and flexibility. Most stents are bare metal made of nitinol, cobalt-based alloys or stainless steel alloys. Nitinol stents can expand to a heat treated shape once exposed to body temperature, but cobalt and stainless steel stents both need a balloon to expand the stent during deployment. Nitinol self-expanding stents are preferred for the delicate anatomy of blood vessels in the brain [25, 41].

In addition to coils and stents, the third type of device for aneurysm treatment is called a flow diverter. Flow diverters were developed from the idea of simplifying stent assisted coiling and to combat some of the problems that coiling delivery caused in irregular shaped aneurysms. Emerging technology of developing flow diverters shifted the focus of the neurovascular device industry to reconstruction of the parent artery underneath the aneurysm rather than clotting off the aneurysm itself, which was the purpose of coiling. The mechanism for flow diversion is described more below, in the following section.

1.3.2.3 Flow Diverters

The concept of flow diversion stemmed from neurovascular physicians that used stent-assisted coiling and started with an idea of overlapping multiple stents underneath an aneurysm to bridge the neck [42]. The resulting overlap formed by the stent struts decreased the total cell size of the stent. Though these cell sizes were inconsistent, blood flow was sufficiently redirected away from the aneurysm sac and there was no need for embolization coils to clot them off.

In other words, flow diverters were designed with a different purpose from intracranial stents. By halting the pulsatile flow into the aneurysm sac through reshaping the parent artery, flow diverters can completely shrink the aneurysm without the necessity of clotting off the sac itself (Figure 5).

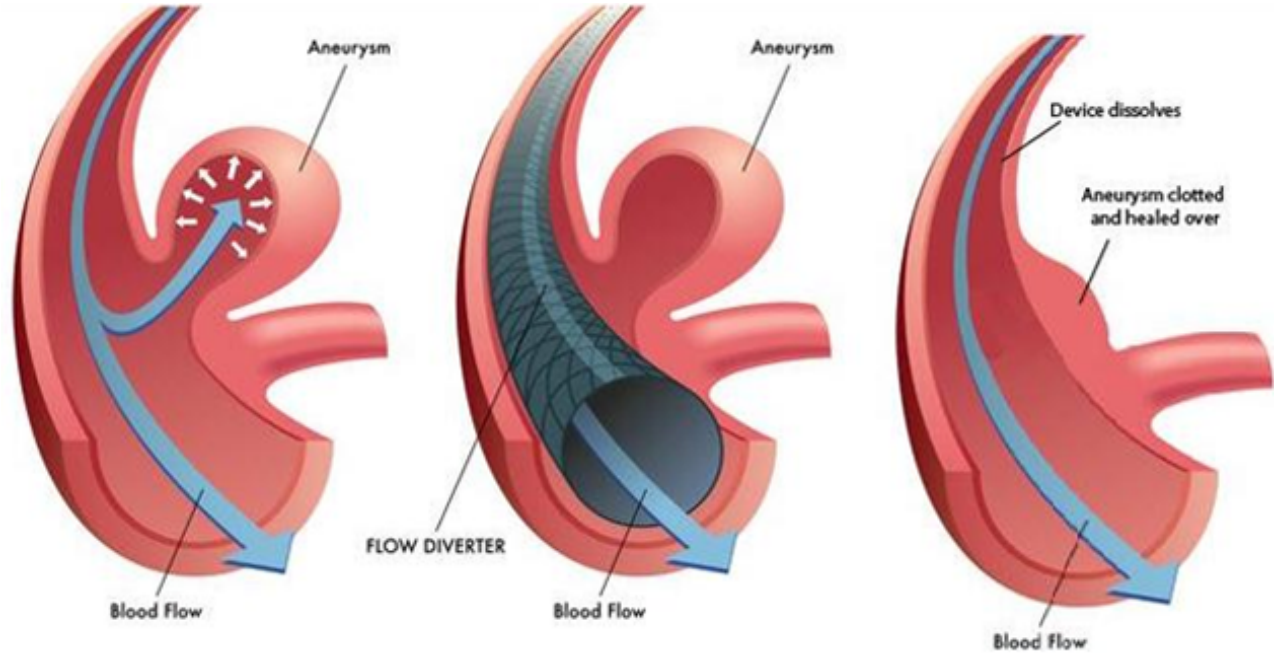

Figure 5: Flow diverter device mechanism [43]. Before treatment, blood flows into the aneurysm, which intensifies the inflammatory response at the weakened artery wall and causes it to grow. Deployment of the flow diverter stops blood from flowing into the aneurysm and only allows circulation through the parent artery. This allows the parent vessel endothelium to reconstruct over the neck, which clots and shrinks the aneurysm, leading to healing.

The development of flow diverters has focused on a main goal of completely healing and reconstructing the parent vessel through promoting endothelialization across the aneurysm neck [44]. The mechanism to allow for flow diversion heavily relies on reducing total flow velocity and leveling the peak kinetic blood energy entering the aneurysm to normal blood flow. In aneurysms, flow is slower and circular, which differs from the more linear flow profile of a healthy vessel. Flow diversion reduces this difference in hydrodynamic circulation by lessening the kinetic energy entering the aneurysm at each pulse. Without constant blood shear stress in its walls, thrombosis of the aneurysm will occur and it will reduce to a scar [45].

Two major design considerations are important for the hydrodynamic activity of flow diverters: porosity, which is represented by the areas uncovered from the stenting, and mesh density, which is the number of pores per surface area. An optimal diamond shape of the flow diverter strut has been shown to interact with blood flow shear stress to ensure that no exchange of flow between the aneurysm and parent vessel exists, and many manufacturers will often change the number of wires of the stent in order to keep this consistent [46]. Furthermore, the angles created from the intertwined wires must also stay the same despite changes in morphology over the neck of the aneurysm [47]. Though this can be achieved through a more traditional tubular stent, many companies have also designed intrasaccular flow diverters to fit inside of the sac [25, 48–51] (Figure 6). While this is effective, flow diverters of this type are used most with certain geometries, such as wide-neck aneurysms or aneurysms at bifurcations.

Figure 6: The Woven EndoBridge (WEB) Aneurysm Embolization System are examples of intrasaccular flow diverters [52]. Like classic flow diverters, these devices also reduce blood flow into the aneurysm dome; however, they are most effective in wide-neck or bifurcation aneurysms.

Though the concept of flow diverters grew from stent devices, they are increasingly growing in popularity to treat cerebral aneurysms [53]. Flow diversion technology has allowed physicians to only use one device, as opposed to multiple with endovascular coiling. In addition, they have been shown to completely occlude more than three quarters of aneurysms immediately after treatment, with the number only increasing after several follow-ups [51]. Though flow diverters were originally intended for treating wide-neck aneurysms, they are becoming more commonly used in challenging cases, such as those with aneurysms in difficult to access areas in the posterior circulation and in high-risk patients with ruptured aneurysms [54, 55].

1.4 Aneurysm Models for Device and Surgical Testing

The rapid growth of the neurovascular medical device industry specifically to treat hemorrhagic stroke due to aneurysm development has caused an increase in demand for different aneurysm models to properly test these devices. Device testing is performed in different stages in order to demonstrate safety of a device. This process usually begins with a series of bench and in vitro testing before progressing into more traditional in vivo models. In all cases, creating physiologically relevant models with the correct cell types, blood flow parameters, and ability to be mass-produced in order to provide statistically significant results prove to be extremely difficult. In the following sections, an overview of the most common in vivo models will be described, as well as more specifically, the rabbit elastase model, which is widely used for neurovascular device testing. Then, in vitro aneurysm models will be discussed as seen in literature, followed by the work done in Cal Poly's Tissue Engineering Lab.

1.4.1 In Vivo Models

The development and refinement of endovascular devices traditionally rely on animal models such as rabbits, swine, and canines; however, the most common in vivo models of aneurysms are canines and rabbits that incorporate effective and reproducible surgical reconstruction.

Anatomy and past-history as disease models of different animals have often determined the role of each species as a model for neurovascular device testing. Swine, for example, are well-established in the cardiovascular space because of their suitability for assessing the risk of in-stent stenosis [56], which is relevant in certain cases of testing neurovascular devices. The most common aneurysm model, however, is the canine bifurcation model [57]. Canines are most frequently used because they have a large geometry that is similar to humans [58]. Canines are also a practical choice for researchers because they react relatively well to anesthesia, and they can survive long term, allowing for extended studies with longer time points [57]. The second most common aneurysm model is created in rabbits using an enzyme called elastase [57]. Because of its low cost and convenience in handling [59], the New Zealand white rabbit species is a popular choice to test many types of medical devices, including those in the neurovascular space.

The rabbit elastase model is a widely used, well established disease model for understanding the pathophysiology of aneurysm development and for companies to test endovascular devices [60]. This model will be the main focus of this work, and will be outlined in more detail in the following section.

1.4.2 Rabbit Elastase Model

Surgically modified New Zealand white rabbits are commonly used as disease models in early stages of preclinical in vivo testing. They are categorized as a small animal in most local animal ethical committees and are used before testing medical devices in larger in vivo systems [59]. Compared to other strains, New Zealand white rabbits are easy to handle, often do not develop many health problems, and are bred quickly [61] because they reach skeletal maturity faster than many animals [62]. The practical advantages of using rabbit models make them a popular choice for testing high volumes of devices.

In the neurovascular device industry, the rabbit elastase model is a surgically constructed aneurysm model that is standard for testing devices [60]. First, an arteriotomy is performed to create an opening for a sheath introducer to be advanced into the common carotid artery. A balloon catheter is then navigated through the sheath introducer and to the subclavian artery and common carotid artery junction and is inflated. Porcine elastase is then pushed into the common carotid artery and left to incubate [63]. Elastase is a protease enzyme that can digest specific transmembrane peptides by cleaving the peptide bonds of the carboxyl-terminal of a variety of small amino acids [64]. The reasoning behind this method is that enzymes such as elastase have been hypothesized to contribute biochemically to the formation of aneurysms by causing the breakdown of the structure of the blood vessel.

After twenty minutes of elastase incubation, the balloon is deflated and the catheter is removed. The vessel is ligated at the mid portion above the incubated elastase, creating a stump-like structure. This segment of the artery dilates with time and forms the dome of the aneurysm (Figure 7).

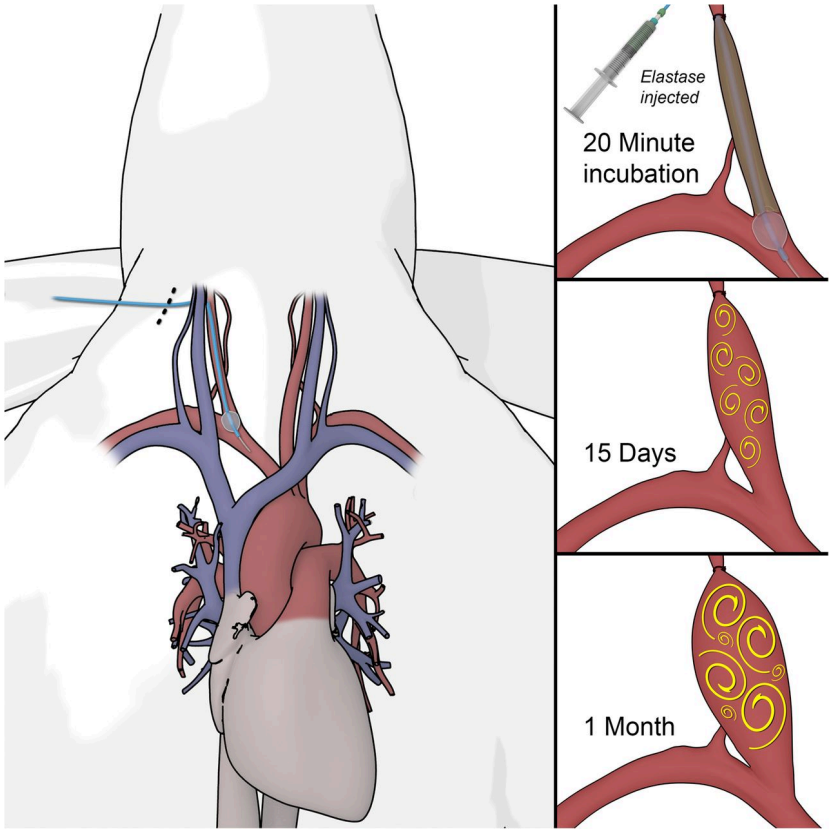

Figure 7: Rabbit elastase aneurysm model creation [60]. A balloon catheter is advanced into the rabbit common carotid artery and inflated near the junction of the subclavian artery. Elastase is then injected and incubated proximally to the balloon catheter. After twenty minutes, the balloon is deflated and removed, and the vessel is ligated proximally to the elastase incubation to prevent blood flow. In time, the continual weakening of the arterial wall at the areas exposed to elastase will cause the artery to balloon, creating the aneurysm.

The relevance of the rabbit elastase model to human clinical cases has been evaluated in many ways, and they have been found to be fairly similar in most cases. One study evaluated hemodynamic flow at different anatomical geometries and compared it to published clinical data [65]. Results illustrated similarities between flow types due to surrounding vascular effects and

arterial curvature as well as between fluid pressure changes within the dome of the aneurysm and at the parent artery. Another study looked at histological effects of the disease, and in both humans and rabbit models, there was a complete loss of elastic lamina and a decreased endothelium, leading to degeneration of the vessel wall [66]. The stark similarity of the pathophysiology of aneurysm formation in both humans and in rabbits combined with the practical advantages of using small animals make this model the most ideal for large scale preclinical endovascular device testing.

Modifications of the standard elastase models also exist in order to more accurately replicate a larger variety of aneurysms seen clinically. Researchers have attempted to control aneurysm height [67] and neck size [68] and created double aneurysms [69] to increase the range of aneurysm sizes produced by this model. Specific details and examples of these sizes and variations will be described in depth in Chapter 2.

While the rabbit elastase model and other animal models are important for in vivo hemorrhagic stroke studies, devices must first go through a series of bench and in vitro testing. In vitro studies are important for showing initial feasibility and biocompatibility. They provide essential data that can screen out device designs, and many companies will opt to perform more proof-of-concept studies at this step of the design process before proceeding to the more expensive in vivo studies. It is essential, therefore, desirable for in vitro testing to accurately replicate disease states in order to gain valid results, and while much work has been done modeling blood vessels, few studies have created a geometrically accurate and biologic aneurysm model. Examples of work done in this area of bench and in vitro models are described next in Section 1.4.3.

1.4.3 Bench and In Vitro Models

Before preclinical testing can progress into traditional in vivo models as described above, devices must first go through a series of biocompatibility and feasibility testing. The necessity of ample bench and in vitro models has grown because of the increased development of different kinds of devices and more scrutinized evaluation processes required for getting approval for animal testing. In addition, efficient bench and in vitro models can also greatly reduce the amount of animals used in in vivo studies. Bench models that study hemodynamic flow and device interactions will first be outlined, followed by in vitro blood vessel studies incorporating aneurysm geometries and disease states. Then, the work done in the Cal Poly Tissue Engineering lab, which is the foundation of this thesis work, will be reviewed.

1.4.3.1 Bench Models

For neurovascular devices used to treat hemorrhagic stroke, few bench and in vitro models exist that closely resemble the disease state of the tissue and hemodynamics of the blood flow; however, many bench models have been developed to study hemodynamic flow and have incorporated device testing. While these current models may not have biologically represented aneurysm disease states, they have allowed for evaluation of an important parameter and have clearly demonstrated the effect of pulsatile flow on neurovascular device deployment using computational fluid dynamics.

One example of a hemodynamic bench model was created and utilized by Chivukula et al. [70]. This group reconstructed silicone physical models of clinical aneurysms in order to image and recreate phantom flow to “treat” with virtual endovascular devices. Gester et al. [71], Boyle et al. [72], and Dhlolakia et al. [73] all used computational fluid dynamics to study device

interactions with dynamic flow, while also creating a physical model employing pulsatile flow to deploy actual devices. Gester et al. measured flow behavior using particle imaging velocity with and without different flow diverter iterations of varied material wires, braid angles, sizes, flexibilities, and deployment techniques. Boyle et al. molded negative impression aneurysm geometries to test a shape memory polymer foam-over-wire implant device. Dhlolakia et al. deployed five different devices into both sidewall and bifurcation silicone models and assessed the change in contrast due to hemodynamic flow changes within the treated aneurysm, as illustrated in Figure 8 below. In all of these cases, benchtop models with silicone aneurysms were used to understand and evaluate the impact of hemodynamics on neurovascular devices.

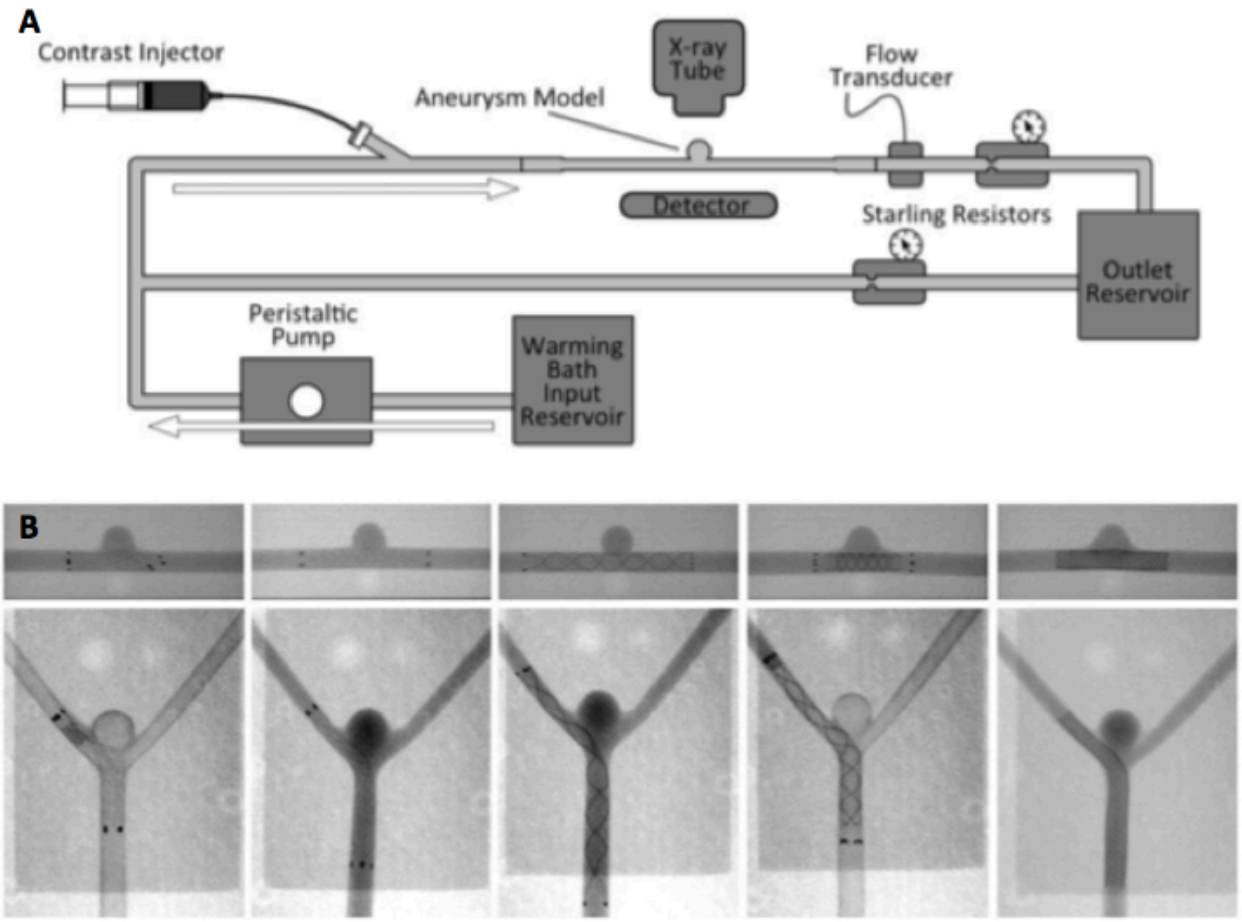

Figure 8: Benchtop silicone aneurysm model from Dhlolakia et al. [73]. A) Diagram of the hemodynamic flow-loop system. B) Hemodynamic device evaluations using the sidewall aneurysm geometry (top row) and bifurcation aneurysm geometry (bottom row). Devices evaluated were, from left to right: Neuroform, Enterprise, Low-Profile Visualized Intraluminal Support (LVIS), Flow-Redirection Endoluminal Device (FRED), Pipeline.

In addition to hemodynamic device testing, benchtop silicone aneurysm models have been useful for training physicians on neurovascular device deployment. Sugiu et al. [74] developed transparent silicone models that delivered pulsatile flow using an electrical pump

system. This model allowed physicians to practice access techniques through the femoral artery as well as vascular mapping during device delivery.

While hemodynamic bench models have all contributed to a greater understanding of aneurysms and neurovascular devices, these models and studies typically do not incorporate the aneurysm disease state of the tissue, or any vascular tissue components. Flow models allowed for the effects of hemodynamics to be studied in relation to device testing and aneurysm geometry; however, these models are not accurate enough for long term studies because of the lack of tissue degeneration and healing after treatment. Few studies have successfully incorporated cells into clinically accurate aneurysm model geometries; however, the work and studies that have been done in this area are outlined below.

1.4.3.2 In Vitro Models

Novel in vitro models have used different approaches to combine pulsatile flow effects with cell layers in aneurysm geometries to more accurately represent disease states. Kaneko et al. [75] and Levitt et al. [76] both created PDMS models seeded with cells to study the effect of dynamic flow on cell phenotype. In contrast, Touroo et al. [77] used tissue engineering to create an aneurysm model specifically suitable for neurovascular device testing, rather than only for studying blood flow hemodynamics. This work is summarized in more detail below.

Kaneko et al. [75] cultivated an endothelium in a PDMS model of a basilar tip aneurysm to study the effect of shear stress on cell behavior. To enhance cell adhesion, the scaffold was coated with fibronectin. The vascular models were transferred into a tube with bovine carotid artery endothelial cell suspension solution and rotated in order to allow the cells to adhere to the scaffold. The construct was then transferred into a perfusion bioreactor with constant laminar

flow and temperature. This model was created to study endothelial cell morphology impacted by pulsatile flow in the parent artery and in the aneurysm bifurcation geometry. Kaneko et al. saw a large drop in shear stress from linear flow in the parent artery to circulating flow inside the aneurysm dome, and, after being subjected to perfusion, endothelial cells were spindle-shaped, elongated, and aligned with the flow direction in the parent artery. In the aneurysm, cells were irregularly shaped and unaligned. Their results imply that the irregular flow profile in an aneurysm changes the spread of endothelial cells on the blood vessel luminal surface, which may contribute to the weakening of the arterial wall. Though this model did not take into account mechanical properties of the blood vessel itself, they were able to create complex geometries and depict endothelial cell morphology both in the aneurysm and parent artery. More notably, Kaneko et al. established a relationship between fluid dynamics and endothelial cell behavior in an aneurysm geometry.

Similar to Kaneko et al., Levitt et al. [76] created a PDMS model to study hemodynamic flow in an aneurysm using computational fluid dynamics and gene expression in endothelial cells using PCR. Before seeding cells onto their model, Levitt et al. plasma treated the inner surface to create a hydrophilic lumen. The plasma treatment consisted of 0.2% gelatin incubation at body temperature. Then, human carotid artery endothelial cells or human umbilical vein endothelial cells were seeded in the lumen. Like Kaneko et al.'s study, constructs were connected to a perfusion bioreactor to undergo pulsatile flow, and similar results were retrieved. In the parent artery, flow was directional. Velocity streamlines, wall shear stress and shear stress gradients were much lower in the disorganized flow profiles inside the aneurysm. Differences were also observed in mRNA levels of key vascular factors between the aneurysm dome and the parent artery, indicating that biochemical cell behavior is influenced by dynamic flow in the aneurysm

geometries. Like Kaneko et al., Levitt et al.'s study also demonstrated feasibility of replicating a clinical aneurysm scan and successfully seeding cells onto the model construct. In addition, they established connections between endothelial cell gene expression and fluid dynamics.

Kaneko et al. and Levitt et al. successfully studied vascular cell behavior due to hemodynamic flow changes in an aneurysm model; however, they did not demonstrate the potential of the model to study endovascular devices. Touroo et al. [77], whose study is described below, also did not deploy devices into their model; however, they created a completely different type of construct that was sized and potentially more appropriate for the purpose of evaluating endovascular devices.

Touroo et al. [77] used a different approach of creating a hemorrhagic stroke model using tissue engineering methodologies. The premise of their method consisted of creating a tubular scaffold with aneurysm geometries that have similar mechanical properties to a native artery and growing a confluent layer of cells in its lumen. An ePTFE vascular graft that was dilated using a balloon catheter to create a fusiform-like aneurysm served as a scaffold, as seen in Figure 9 below.

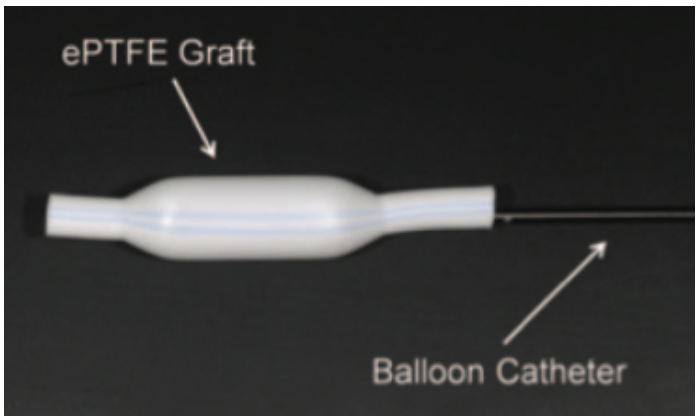

Figure 9: Aneurysm scaffold created by Touroo et al. [77]. An ePTFE vascular graft was expanded using a balloon catheter to create a geometry that resembled a fusiform aneurysm around 3 cm in length.

Isolated stromal vascular fraction cells derived from human adipose tissue were deposited intraluminally using a pressure sodding technique, and the construct was cultivated in a perfusion bioreactor chamber. Cultivation was done to grow a thick cell lining, which has potential to allow for healing to be tracked after device deployment. Through hematoxylin and eosin staining, Touroo et al. confirmed a confluent lining of human tissue in all regions of the scaffold; however, the thickness of the cell layers was inconsistent in the aneurysm and in the parent artery. Immunohistochemical analysis determined that the cells were of mesenchymal origin, and the fluid contacting layer had differentiated into vascular smooth muscle cells. SEM imaging also demonstrated alignment of these cells due to dynamic flow.

The biggest limitation of Touroo et al.'s model was the lack of endothelial cells, which reconstructs the parent artery, and dynamic shear stresses do not necessarily induce differentiation into this cell type. In addition, the mechanical properties of ePTFE were not consistent with those of blood vessels, most notably because of its limited compliance, even

though this material was more similar compared to the silicone in other models. Because ePTFE was already manufactured in tubes, it was difficult to customize aneurysm geometries. Despite these limitations, Touroo et al. successfully tissue-engineered an aneurysm model with a confluent cell lining and expected morphology that could potentially be used to track healing when evaluating the performance of endovascular devices.

As demonstrated by Touroo et al.'s work, tissue engineering has proven to be a promising approach to creating physiologically relevant models that can potentially help evaulate the effectiveness of endovascular device treatment. Unlike Touroo et al.'s work, however, it would be beneficial to be able to customize scaffold and aneurysm geometries and to use materials that have more similar properties to blood vessels. One promising way of creating scaffolds uses a method called electrospinning, which can make almost any shape of scaffold from polymer fibers. This method is currently being employed in the Cal Poly Tissue Engineering research lab to allow for increased customization of polymer blood vessel scaffolds. The work done in this lab will be outlined in more detail in the next section.

1.4.4 Cal Poly Tissue Engineering Research Lab

The work done in the Cal Poly Tissue Engineering research lab uses tissue engineering to create blood vessel models. These "blood vessel mimics" (BVMs) [77–81], which laid the foundation for Touroo et al.'s work, are vascular constructs composed of polymer scaffolds and human vascular cells. The purpose of these BVMs is to provide a preclinical model for medical device testing.

The foundation of a tissue-engineered construct consists of a scaffold and cells that are combined and cultivated in dynamic conditions in a bioreactor, resulting in an artificial tissue or

organ resembling native tissue. To make a tissue-engineered blood vessel, scaffolds are tubular in shape, and vascular cells are grown separately and seeded into the lumen to mimic the inner cell lining. In the Cal Poly lab, tubular scaffolds are created using a process called electrospinning, which can generate any scaffold shape out of fibers from a dissolved polymer solution. The basis of this thesis relies on the electrospinning process, which will be described in more detail later in this section. Cultured cells are human umbilical artery smooth muscle cells (HUASMCs) and human umbilical vein endothelial cells (HUVECs), which allow for growth of a sufficient vascular cell lining [81].

After cell culture and scaffold creation, the construct is cultivated in a perfusion bioreactor system that simulates flow using a peristaltic pump. The perfusion bioreactor is composed of a chamber to hold the construct, media reservoirs, tubing, and the pump. Once the scaffolds are electrospun, they are mounted onto fittings, sterilized, and placed inside the bioreactor chamber. Scaffolds are then conditioned in the bioreactor with protein-rich media to allow for enhanced cell adhesion. After conditioning, both endothelial cells and smooth muscle cells are pressure sodded using a dual sodding technique into the lumen of the tubular scaffolds [81]. These constructs are then cultivated in dynamic flow conditions. Once the constructs contain a sufficient cell lining, they can be used as a tissue-engineered blood vessel model for testing medical devices.

The BVMs created in the Cal Poly Tissue Engineering research lab have been successful in both scaffold creation and bioreactor cultivation. Electrospinning scaffolds has allowed for microfiber generation, which supports cell adhesion into the scaffold lumen. In addition, the dual-sodding technique of both smooth muscle cells and endothelial cells has created a sufficient layer of cells onto the scaffold lumen.

As previously stated, for neurovascular devices used to treat hemorrhagic stroke, it is important that better aneurysm models be developed, especially for early stage assessments. One way the BVM model can be improved for neurovascular device testing is the incorporation of different aneurysm geometries as part of the electrospinning process in scaffold generation. This process will be the focus of this thesis. The next few sections will outline scaffold creation using electrospinning in more detail, followed by the work of Shen et al. [82], a previous Cal Poly Master's student who tested neurovascular devices in BVMs and developed the first aneurysm BVM model in the Cal Poly Tissue Engineering research lab.

1.4.4.1 Electrospinning Polymer Scaffolds

Scaffold creation in the Cal Poly Tissue Engineering lab is executed using electrospinning, which is a technique that creates microfibers from polymers dissolved in a solvent. Components of an electrospinner include a syringe pump, voltage supply, and grounded collector, as seen in Figure 10 below. Dissolved polymer is loaded into a syringe and onto a syringe pump, which dispenses the polymer at a slow, constant flow rate while being charged with a high voltage. Once the voltage is high enough to break the surface tension of the solution, the polymer is then attracted to a grounded metal collector. As the collector draws polymer, the solvent evaporates and the polymer forms a stream of fibers that are several microns in diameter.

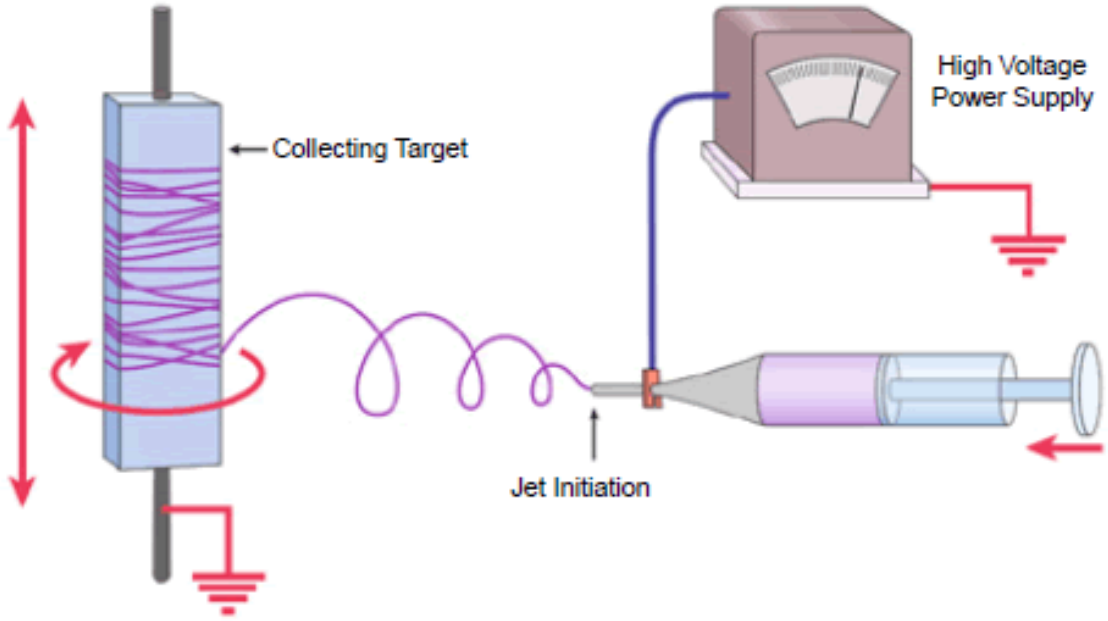

Figure 10: Electrospinning setup with a process flow from right to left [83, 84]. Polymer dissolved in a solvent is loaded onto a syringe and dispensed using a syringe pump at a low flow rates. The syringe needle is charged to a high voltage, and the circuit is grounded at the collector. When the polymer solution is dispensed out of the needle, the voltage breaks the surface tension, and the polymer is drawn out as continuous fibers towards the collector. To make a tubular scaffold, the collector is a metal mandrel, which rotates and translates to endure full coverage and random fiber orientation.

The electrospinning process allows for customizable scaffold creation depending on the shape and motion of the collector, which is the primary component that needs to be changed to be suitable for the application. To make a tubular scaffold, the collector must contain a grounded metal mandrel. To ensure random fiber orientation and full mandrel coverage, the collector must be motorized to allow for rotation and translation of the mandrel.

Electrospinning provides many advantages for scaffold creation. As mentioned previously, the freedom to change the collector allows for any scaffold shape to be electrospun. In addition, any polymer that can be dissolved in a solution can theoretically be spun using the process, which allows for increased tailoring of the mechanical properties of the scaffold material. The last advantage, specifically for tissue engineering blood vessels, is that the small, consistent, randomly oriented fibers generated from electrospinning create pores that result in high cell adhesion and, therefore, a thicker cell lining, which is essential for testing endovascular devices.

Shen et al. used the customizability of the electrospinning process to create a better aneurysm model for neurovascular device testing by creating tissue-engineered aneurysm BVMs. Through modification of the collector mandrel, she was able to fabricate different geometries that accurately represent the various types of aneurysms seen in clinical cases. Her work, which was documented in her Master's thesis as well as in a publication, is described in more detail in the next section.

1.4.4.2 Shen et al.

The Cal Poly Tissue Engineering research lab first used BVMs as a model for testing neurovascular devices in 2015 with Scott Herting and Kristen Temnyk as part of a contract for a major medical device company (unpublished), [81]. This initial work focused on the feasibility of evaluating neurovascular devices, specifically flow diverters, using BVMs by assessing cellular responses after reatment. Subsequently, Shen et al. [82] built upon this work and developed a method to create BVMs with clinically accurate aneurysm geometries (aBVMs).

The Shen et al. publication included feasibility of device studies using flow diverters, as performed by Herting and Temnyk. From this first study, they demonstrated simple, successful deployment techniques in straight BVMs and showed that the cell lining was robust enough to withstand the process. In addition, they found that cell growth occurred over the struts of the flow diverter during cultivation in the bioreactor after device deployment, signifying that healing can be evaluated by observing cell coverage. The amount of cell coverage over time is a measureable output that can evaluate these devices using the in vitro model. Shen et al. used these results as a foundation for the second aim, which was to develop the process for aBVM fabrication to establish a more accurate disease model.

Shen's expansion of the in vitro model to include the different aneurysm geometries on the electrospun scaffold was achieved by creating custom mandrels and developing scaffold post-processing steps. Saccular, fusiform, and blister geometries were first determined through literature on clinical and animal model cerebral aneurysms. Negative impressions of these geometries were then designed using Solidworks to make molds of the tubular scaffolds. Casts were created by inserting a smaller metal mandrel within the mold to allow for grounding to collect fibers and by injecting melted wax throughout the desired geometry. These mandrels were then wrapped with saran wrap and heat-shrunk before electrospinning to prevent wax residues from seeping into the fibrous pores of the scaffold. After electrospinning, the wax was melted and dissolved to remove the scaffold from the mandrel. These geometries were characterized and implemented in the perfusion bioreactor for cultivation studies [82]. Each geometry was tested for feasible use as an in vitro model using immortalized mouse fibroblasts (3T3s) for proof of concept.

The Cal Poly Tissue Engineering research lab, as documented through the Shen et al. paper, saw many successes through their feasibility testing and the development of their process. Not only were they able to demonstrate the ability to evaluate endovascular devices using the BVM model, but also, they were able to build upon it to create a more accurate representation of aneurysm clinical cases. In addition, the microstructure of the scaffold was consistent in morphology and in fiber diameter, aligning with results seen from the standard electrospinning process. The results from the aBVM feasibility studies using mouse fibroblasts were also promising, as were studies using smooth muscle cells (unpublished). Throughout the complex geometries of the aBVM scaffolds, cells deposited and grew consistently, demonstrating a thick cell lining even after only short time points. This suggested that the dual sodding method could potentially be employed in these complex geometries as well.

Though Shen et al. were able to develop a process to create distinct complex aneurysm geometries, further work was needed to refine the variations and characterize the outputs. Shen et al. used external dimensions of the scaffolds to define each of the geometries; however, internal dimensions are more accurate representations of clinical aneurysm scans, and many device studies are based off of internal measurements. In addition, expanding the capability of creating different geometries and being able to control different dimensions such as aneurysm neck and height, were determined to be beneficial to increase the model's compatibility with other neurovascular devices. The goal of this thesis was to use Shen et al.'s work as a foundation to further customize and characterize scaffold geometries for aBVM creation and to further develop the aBVM model.

1.5 Summary and Aims of the Thesis

Because of the rapidly growing industry of neurovascular devices to treat hemorrhagic stroke, the need for suitable aneurysm models is critical. The increasing demand for preclinical data from endovascular devices has driven researchers to develop in vitro aneurysm models in order to test earlier stage proof-of-concept designs and to reduce the amount of in vivo studies needed to test flow diverters and embolization coils, and demonstrate safety of their device. In order for in vitro models to properly evaluate these devices, many factors such as the aneurysm geometry must be replicated to adequately represent the disease state.

Aneurysm geometry is a crucial aspect of a successful preclinical in vitro model, as it may impact the effectiveness of the device treatment at both the tissue and cellular levels from delivery to long-term implantation. Surprisingly, some studies have suggested that increasing the size of aneurysms does not always directly increase the amount of time needed for healing to occur after treatment with a neurovascular device. Few studies have shown that in patients with smaller aneurysms, there is a higher risk for inadequate device delivery and lower long-term occlusion rates [85, 86]. Larger aneurysms are also difficult to treat because they may require more devices, and the risk for adverse thromboembolic events are much higher [86]. One study demonstrated that specific geometries of aneurysms with low aspect ratios, which equaled the dome height divided by the neck width, or low dome-to-neck ratios, which equaled the dome width divided by the neck width, are also difficult to treat minimally invasively, and often require adjunct techniques [87]. Results from in vivo studies have exhibited the importance of these geometries as well. Rabbit aneurysm models with varying neck widths and heights resulted in different hemodynamic changes, which affected the morphology of cells involved in healing. This compromised the time to complete aneurysm occlusion after treatment with endovascular

coiling [88]. It is important, therefore, for as many different types of geometries as possible to be incorporated into in vitro aneurysm models in order to better understand cellular responses and healing mechanisms so that better devices can be created.

A novel method for creating in vitro hemorrhagic stroke models that allows for control of the aneurysm geometry and also the assessment of the cellular response is tissue engineering. Tissue-engineered blood vessel mimics (BVMs) can be designed with similar vessel and aneurysm geometries and dimensions to clinical models, and the biological interaction between the model and an implanted device can be evaluated. Different aneurysm geometries in an aneurysm BVM (aBVM) scaffold have been developed and characterized using electrospinning methods, and more research would help build off this previous work to demonstrate specific or more desirable dimensions of the aneurysm dome. Therefore, the goal of this thesis was to create, characterize, and utilize variations of aneurysm geometries by electrospinning scaffolds with dimensions that encompass those seen clinically and in the rabbit elastase model. This goal was pursued through the completion of three specific aims:

1. Explore and identify different aneurysm geometries and dimensions found in rabbit models and human clinical settings.
2. Fabricate and characterize aneurysm geometry variations based on common rabbit and human anatomies.
3. Evaluate new aneurysm geometries for feasible use in blood vessel mimic models.

2 Identification and Review of Aneurysm Types in Human Clinical Settings and in Rabbit Models

2.1 Introduction

This chapter addresses the first specific aim of this thesis: explore and identify different aneurysm geometries found in rabbit models and human clinical settings. This goal will establish the foundation for the different aneurysm geometry variations that will be fabricated in the second aim of this thesis by providing a range of dimensions that are important to replicate in in vitro models.

The demand for accurate aneurysm models stems from the rapidly growing market of minimally invasive endovascular devices for prevention of hemorrhagic stroke [89]. In addition to studying aneurysm pathophysiology, these models are useful in a variety of ways in the development of neurovascular devices. In the United States, the FDA requires sufficient in vitro testing to demonstrate safety of a device before animal testing and approval for clinical trials [90, 91]. Appropriate anatomical models are important as well for mimicking surgical cases for doctors to practice device deployment [74, 92].

Geometric size, shape, position, blood vessel location, and type of the aneurysm are all important considerations that should be incorporated in in vitro and in vivo models to correctly simulate the disease state. Aneurysm size and geometry affects blood flow hemodynamics, which help determines the type and number of endovascular devices used to treat it [93]. Aneurysm position and cerebral blood vessel location also affect how the aneurysm is accessed during treatment. It is crucial to understand these factors before developing novel in vitro models.

The unique biological factors that contribute to aneurysm formation create an infinite clinical variability of shapes and sizes in the human population. Many studies have attempted to consolidate commonalities among different types of aneurysms from different locations in the cerebral vascular network [94–97]; however, it is nearly impossible to include examples from every unique clinical case that has been published. The rabbit elastase model, on the other hand, is well established in endovascular device preclinical testing to show safety and feasibility. This model has gained attention because of its simplicity and potential to control geometric properties of the aneurysm. Unlike many clinical cases, aneurysms produced from these methods are usually geometrically within the same ranges of height, dome diameter, and neck diameter [98, 99], which is useful for comparing different types of devices or testing specifications. Researchers have experimented with the rabbit elastase model in order to control some of the dimensions, such as the neck diameter [68] and height [67], so that the model can be more customizable depending on the desired study. Ultimately, however, the rabbit elastase model is the most useful if the range of geometries produced can match what is commonly seen in clinical settings.

The following sections describe a comprehensive literature review of aneurysm geometries found in both clinical and rabbit model studies. The purpose of this initial work was to gather dimensional data that have characterized the shape and geometry of clinical aneurysms and in vivo rabbit elastase aneurysms. Once analyzed, this information will then be used to establish a range of desired values of aneurysm dimensions that should be replicated and characterized in order to create appropriate in vitro versions of clinical cases and rabbit models.

2.2 Methods

A search strategy using PubMed was performed to find reports on cerebral aneurysm clinical case studies and in vivo experiments using rabbit elastase models. The key words included in the search were: cerebral aneurysm, cranial aneurysm, aneurysm geometry, rabbit cranial aneurysm model, and rabbit aneurysm geometry. A method of cross-reference checking was also performed, and older articles that were referenced in current studies were also included. Some clinical aneurysms or disease models reported were treated surgically, while others utilized endovascular devices, all of which were included in this review.

The most important data gathered from these studies encompassed a set of critical dimensions, and optional data included more obscure dimensions as well as other qualitative notes about the aneurysms. Studies were excluded from the results if there was no quantitative information given on the aneurysm itself. Critical dimensions of interest were the diameter of the neck and the height of the aneurysm. Optional data included lengths describing the width of aneurysm domes, parent artery diameters, and ratios comparing the aneurysm to the parent vessel. In addition to dimensions taken, the type and location of the aneurysm were also noted. Specific types of aneurysms with unique dimensions such as angles were also recorded.

Once the necessary and optional data was recorded from each article, aneurysms were diagrammed to highlight ranges and averages of key dimensions so that visual comparisons could be made among groups of aneurysms in each study. For more complicated human models specifically, aneurysms were also redrawn to visualize the shape and interaction with the surrounding vasculature. Artistic renditions of aneurysms were hand drawn for this thesis and scanned. Annotations and diagrams were created using Microsoft PowerPoint. In artistic

renditions, aneurysms were denoted with red dotted circles, and the parent artery was noted with PA.

Data on human aneurysms and rabbit model aneurysms were compiled into different tables with each entry separated by study. Each entry had a description of the different aneurysm groups in the review along with the corresponding dimensions and ratios that characterized the aneurysms. Common dimensions were noted, and values were compared between each study for both human and rabbit models. Then, dimensions from human and rabbit models were compared collectively with each other.

2.3 Results

The results of this review are divided into two sections: one comparing different human aneurysm clinical cases and the other comparing rabbit elastase model studies. For each section, a summary table will be provided, followed by diagrams or artistic renditions of notable studies from each part of the literature review. The following section, Section 2.3.1, presents the human aneurysm studies whereas the subsequent section, Section 2.3.2, presents aneurysms found in rabbit studies.

2.3.1 Human Aneurysms

Aneurysms from human models were gathered from clinical case articles and summarized in this literature review. Across the existing literature, there was not a uniform way of measuring the geometries of aneurysms. Some aneurysms were measured more comprehensively than others, and certain dimensions were described for specific types of

aneurysms that did not necessarily apply to all aneurysms. Because of the variety of aneurysms studied and the inconsistent measurements used, not one paper described all the dimensions of an aneurysm. A summary of the various dimensions used to characterize aneurysms in each study, along with the data that was provided, can be seen in Table 2.1. Aneurysms were depicted with diagrams and artistic renditions of clinical scans or computerized models and are provided in Appendix A.

Table 2.1: Summary of Human Aneurysm Dimensions

Author	Type	Neck Diam (mm)	Dome Diam #1 (mm)	Dome Diam #2 (mm)	Height (mm)	Parent Diam (mm)	Max Sac Size (mm)	Lateral Vessel Diam* (mm)	Angle* (^{o})	Size Ratio **
Wang et al. [94]	L/R MCA	1.35-6.16	1.86-12.3	1.53-9.65	1.27-9.28	-	-	-	-	-
	ACom	1.66-2.88	2.67-8.92	2.26-5.05	2.79-5.21	-	-	-	-	-
	L/R PCom	2.01-8.84	3.69-8.03	3.39-8.25	3.73-10.5	-	-	-	-	-
	L/R ICA	3.49-3.89	6.14-13.8	5.56-12.7	5.10-13.8	-	-	-	-	-
	L Vertebral	-	8.64	5.05	4.86	-	-	-	-	-
Seo et al. [95]	Fusiform / Branching	-	-	-	-	-	-	-	-	1.28
	Saccular / Sidewall	-	-	-	-	-	-	-	-	0.77-1.7
	Saccular / Bifurcation	-	-	-	-	-	-	-	-	1.33-1.87
Zhang et al. [96]	Basilar Bifurcation	-	-	-	-	2.1-8.3	-	0.7-6.8	118.1-173.3	-
Park et al. [100]	ICA / Ophthalmic Artery	9, 4.3	9.3	9.6	10.6	-	-	-	-	-
Shi et al. [101]	PCom, Type I	6.2 ± 3.5	-	-	-	-	-	-	-	-
	PCom, Type II	5.8 ± 2.5	-	-	-	-	-	-	-	-
	PCom, Type III	6.0 ± 2.4	-	-	-	-	-	-	-	-
Rajabzadeh-Oghaz et al. [97]	Blister ICA	2.31	-	-	-	-	2.5	-	-	-
	MCA	5.85	-	-	-	-	6.85	-	-	-
	Basilar	6.44	-	-	-	-	6.79	-	-	-
	ICA	4.47	-	-	-	-	10.35	-	-	-
	ACA	6.99	-	-	-	-	16.59	-	-	-
	Giant ICA	7.31	-	-	-	-	23.53	-	-	-
Oishi et al. [102]	ICA Segments C4, C3, C2	8.3 ± 4.4	-	-	-	-	16.9 ± 6.8***	-	-	-
Jiang et al. [103]	Thick wall MCA Bifurcation	6.1 ± 2.7	12.4 ± 4.2	13.2 ± 4.3	14.4 ± 5.1	2.2 ± 0.4	-	-	-	5.8 ± 2.3
	Thin wall MCA Bifurcation	4.8 ± 1.7	6.2 ± 2.9	5.3 ± 2.6	6.6 ± 2.5	2.6 ± 1.2	-	-	-	2.2 ± 1.0

* For Basilar Aneurysms Only, ** Aneurysm Size divided by Parent Vessel, *** Average Aneurysm Size

Among all aneurysms characterized, a wide range of dimensions was gathered from this literature review. Even though the same dimensions were often analyzed in different studies, ranges were extremely large and inconsistent such that it was difficult to determine specific ranges for each dimension. Comparing values among studies was also difficult because of the way the values were presented if more than one aneurysm was measured, which occurred in six out of the eight studies [94–96, 101–103]. Half of those studies [94–96] presented information in ranges, while the other half of those studies stated only the mean values [101–103].

Neck, dome, and height were the most common dimensions measured throughout all studies. The aneurysm neck diameter was the most common length reported. Six out of the eight studies [94, 97, 100–102] measured the diameter of the aneurysm neck. Wang et al. [94] reported the smallest value for neck diameter at 1.35 mm for an aneurysm in the middle cerebral artery. The largest values for neck diameter were 9 mm and 8.3 ± 4.4 mm from Park et al. [100] and Oishi et al. [102], respectively. Three of the six studies that measured the neck of the aneurysm [94, 100, 103] also incorporated two more dimensions that characterized the dome of the aneurysm, indicating that the aneurysm sacs were never completely circular, as well as a dimension for the aneurysm height. These three measurements were together the second most common dimension. Wang et al. [94] measured the smallest diameter for the aneurysm dome, which resulted in 1.53 mm. The largest diameter reported were from both Wang et al. as well and Jiang et al. [103], measuring 13.8 mm and 13.2 ± 4.3 mm and 13.8 mm. Like dome diameter, the range of heights throughout each study also followed a large variation pattern. Similarly, Wang et al. [94] measured the smallest aneurysm height at 1.27 mm, while Jiang et al. [103] found the largest height, which was at 14.4 ± 5.1 mm.

Though aneurysm neck diameter, height, and dome diameter were the most common dimensions given among the studies, a few other measurements were worth noting. Other dimensions recorded that were mentioned in two separate studies were the parent artery diameter [96, 103], maximum or average sac size [97, 102], and size ratio [95, 103]. The sac size referred to the largest dimensions characterizing the aneurysm dome, and could represent a height or dome diameter; however, in these studies, the exact directions were not specified. Size ratio referred to the largest aneurysm dome size divided by the diameter of the parent artery [104], indicating the growth of the aneurysm with respect to the vessel it originated from. Even though these dimensions were not given in most of the studies, the fact that they were recorded more than once shows that while they may not directly affect the aneurysm geometry, they are important for characterization.

Characterization methods of aneurysm geometries differed throughout all studies in this review; therefore, analysis of each dimension individually generated large ranges that were similar to each other and difficult to interpret. As exhibited by these large ranges of dimensions extracted from this review, there is no single perfect model that encompasses all potential human aneurysm geometries. This fact, however, does not diminish the importance of understanding the complexity of these different geometries in order to develop suitable treatments. A larger representation of these geometries must be incorporated into in vitro models for better development of neurovascular devices to demonstrate that these treatments can apply to a variety of already existing cases. **Specifically, these clinical studies make it clear that the neck diameter can range from 1.35 mm – 9 mm, with the range of 3 mm – 6 mm being the most common, and height can range from 1.27 mm – 14 mm, with the range of 3 mm – 10 mm being the most important to capture in preclinical models.**

Because of the large variation in aneurysm geometries described in humans, and even with the ranges of appropriate dimensions stated above, it is still difficult to develop models that encompass all clinical cases. It is easier to begin with established animal models, which mimic the dynamic environment of the disease state and have already been widely reproduced to test neurovascular devices. As mentioned in the previous sections, the rabbit elastase model has already been used for preclinical testing by many companies; hence, narrower, more established ranges of important dimensions could be extrapolated from this model. These ranges provide a simpler foundation for developing in vitro models, and can act as stepping stones towards making in vitro geometries that are more inclusive of unique clinical cases. In the following section, geometries and methods of characterizing aneurysms in both established and modified rabbit elastase models are outlined.

2.3.2 Rabbit Aneurysm Models

2.3.2.1 Overview

As mentioned in previous sections, the rabbit elastase model is a well-established aneurysm model used for studying aneurysm pathophysiology, or for testing hemorrhagic stroke devices and surgical treatments. While the rabbit elastase model serves many different purposes, most of the resulting characterization methods employed to describe baseline aneurysm dimensions were fairly similar throughout the literature summarized in this review. A summary of the dimensions of rabbit elastase aneurysm models can be seen in Table 2.2. Baseline characteristics of the rabbit elastase model will then be described in a preliminary overview,

followed by an analysis of certain notable studies [67–69] that have modified the rabbit elastase model in the next section.

Table 2.2: Summary of Rabbit Elastase-Induced Aneurysm Model Dimensions

Author	Treatment / Control	Neck Diam (mm)	Neck Cross-Section Area (mm^2)	Dome Diam (mm)	Dome: Neck Ratio	Height (mm)	Parent Diam (mm)	Volume (mm^3)	Max Sac Size (mm)
Kainth et al. [69]	Single	2.6-2.9	-	2.9-3.4	-	4.8-6.1	-	-	-
	Double	3.2-3.7	-	2.5-3.1	-	1.7-2.4	-	-	-
Brinjikji et al. [60]	-	-	-	4.5	-	7.5	4	-	-
Ding et al. [67]	Carotid-jugular AVF and Elastase	3.5-5.5	-	3.4-6.4	-	8.6-16.8	-	273 ± 172	-
	Control	2.5-4.3	-	2.9-4.3	-	6.4-9.5	-	77 ± 32	-
Altes et al. [63]	-	-	4.5x7.5	3-6.5	-	5-10	-	-	-
Li et al. [105]	-	2.81-5.48	-	2.81-6.73	-	2.67-9.23	2.09-3.05	-	-
Ding et al. [68]	Low Occlusion Balloon	3.4 ± 1.2	-	3.8 ± 1.0	1.2 ± 0.4	8.0 ± 1.7	-	-	-
	High Occlusion Balloon	2.3 ± 0.9	-	3.3 ± 0.9	1.7 ± 0.7	7.5 ± 2.2	-	-	-
Hoh et al. [106]	-	-	-	-	-	-	-	-	5.9 ± 1.9
King et al. [98]	PED with DAPT	3.8 ± 0.7	-	3.3 ± 0.8	-	6.3 ± 1.2	-	-	-
	PED without DAPT	4.1 ± 1.3	-	3.8 ± 0.9	-	7.7 ± 2.2	-	-	-
	sPED with DAPT	4.3 ± 1.8	-	3.4 ± 1.0	-	7.7 ± 2.3	-	-	-
	sPED without DAPT	3.9 ± 1.0	-	3.8 ± 0.9	-	7.6 ± 2.5	-	-	-
Marosfoi et al. [99]	48-wire Flow Diverter	5.3 ± 1.9	-	-	-	6.9 ± 1.7	4.2 ± 0.4 (prox.), 4.6 ± 1.0 (dist.)	-	-
	72-wire Flow Diverter	4.7 ± 1.3	-	-	-	7.1 ± 1.6	4.3 ± 0.5 (prox.), 4.4 ± 0.6 (dist.)	-	-
Li et al. [107]	30-day time point	4.57 ± 0.19	-	5.14 ± 0.24	-	7.21 ± 0.48	-	-	-

Results from the studies utilizing the rabbit elastase model proved to be much easier to interpret than those included in the review of human models. In general, much tighter ranges of dimensions were observed as well as smaller standard deviations, demonstrating a much smaller variation than in human models.

From this literature review, the rabbit elastase model has been used for many purposes. Some articles from this review used this model to study aneurysm pathology [106, 107], while most of them employed the model in conjunction to testing neurovascular devices [60, 63, 98, 99, 105]. Data from these studies describe the baseline measurements of the aneurysm before treatment or experimentation, so these results demonstrate the variation of the model only. Some articles were excluded from this preliminary overview because the goal of these studies was to modify the rabbit elastase model to purposefully change the geometry. In these studies, aneurysm neck [68] or height [67] were controlled, or double aneurysms were created [69]. These studies are described further in the next section.

Regarding specific dimensions, almost all studies characterized the aneurysms in the same way. Similar to the human models, the most common dimensions were aneurysm height, dome diameter, and neck diameter. Unlike clinical cases, though, the most emphasis was placed on the height of the aneurysm. Nine out of the ten studies reported height [60, 63, 67–69, 98, 99, 105, 107]. Data from the established elastase model demonstrated that the smallest height throughout all studies was 2.67 mm from Li et al. [105], and the largest was 10 mm from Altes et al. [63]; however, most of the average heights were reported around 5-8 mm tall.

Eight out of the ten studies [60, 63, 67–69, 98, 105, 107] reported the diameter of the aneurysm dome. In contrast with many of the human studies, which included two dome lengths

characterizing a cross-section of the aneurysm dome, there was only one recorded value for each of the rabbit studies. The smallest dome diameter across the literature was 2.81 mm from Li et al. [105], and the largest of the range was 5.14 ± 0.24 mm from Li et al. [107]. Many of the dome diameters, however, tended to be around 3-4 mm, which was a much smaller range compared to the height data, demonstrating that these aneurysms were cylindrical in shape because they were taller than they were wide.

The last common dimension was the aneurysm neck. 2.5 mm was the smallest measurement from the control group in Ding et al. [67]. The largest neck sizes were noted to be 5.48 mm and 5.3 ± 1.9 mm from Li et al. [105] and Marosfoi et al. [99], respectively. Altes et al. [63] particularly denoted a neck size differently from the other studies; rather than measuring a single diameter, they reported a cross-sectional area using both diameters: 4.5 mm x 7.5 mm, implying that the aneurysm necks were not perfectly circular in all cases. In addition, these dimensions demonstrate that the aneurysm necks were either wider or similar to the dome size, which is not indicative of the saccular shape commonly found in humans.

In addition to the aneurysm dome and neck characteristics, three out of the ten studies [60, 99, 105] also measured the diameter of the parent artery, indicating that though this measurement is not as commonly seen, it can still add value to the model depending on the study. Marosfoi et al. [99] in particular measured the parent artery both proximally and distally to the aneurysm. The smallest measurement of the parent vessel diameter was 2.09 mm and the largest measurement was 4.6 ± 1.0 mm from Li et al. [105] and Marosfoi et al. [99], respectively.

Though not found quite as often as in human clinical case articles, few other specific measurements were incorporated in some of the rabbit elastase models. For example, Hoh et al. [106] measured “aneurysm size,” which was assumed to be the maximum size of the aneurysm

sac. This measurement was similar to the maximum or average sac size mentioned in some of the clinical cases. Ding et al. [68] also measured the dome to neck ratio, which compared the body of the aneurysm to its neck since the study looked at controlling the neck. Like the "aneurysm size" from Hoh et al., this dimension was also similar to the size ratio in the human studies.

The rabbit elastase model is commonly utilized throughout scientific research and in industry for device evaluation because it has a fairly established range of values in terms of its geometry. For proper medical device assessment, however, one can argue that the limited ranges of its geometry are detrimental because it only validates the treatment for similar aneurysms. Certain studies have devised techniques to modify the rabbit elastase model in order to control some of these dimensions or geometries to enhance the versatility of this model [67, 68]. These more unique techniques and modifications will be addressed next.

2.3.2.2 Modifications to the Rabbit Elastase Model

As mentioned previously, certain studies from this literature review specifically experimented with modifications to create more versatile rabbit elastase models. The articles that controlled neck diameter and height will first be outlined. Then, a study that successfully created double aneurysms will be described.

Ding et al. [68] changed the surgical procedure in order to control the aneurysm neck size. This group had conducted previous research and gained results implying that the position of the occlusion balloon dictated the area of blood vessel that was exposed to elastase. By protecting certain areas from enzymatic injury, the vessel did not dilate as much at those portions, resulting in a small aneurysm neck in comparison to its dome. Diagrammed results from this study can be seen in Figure 11 below. As exhibited by the relatively small variations,

Ding et al. demonstrated the possibility of reproducing aneurysms of various consistent neck sizes.

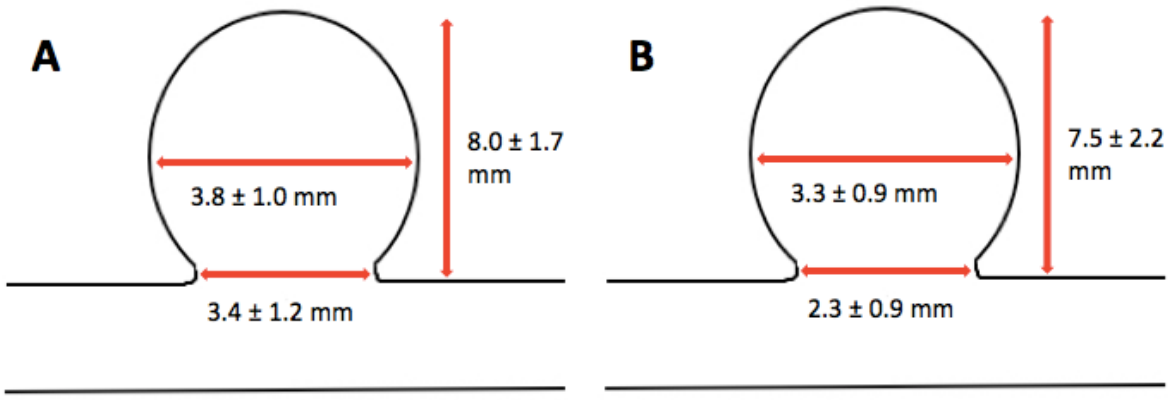

Figure 11: Right common carotid artery rabbit elastase-induced aneurysms with and without surgical modifications to control neck size from Ding et al. [68]. A) Average lengths characterizing resulting geometry from a low occlusion balloon. This procedure leads to a neck size that is similar to the aneurysm dome. B) Average lengths characterizing resulting geometry from a high occlusion balloon. This procedure leads to a neck size that is smaller than the aneurysm dome.

Another study from Ding et al. [67] used a different surgical modification to create extremely large aneurysms compared to those made using the standard procedure. By creating a carotid-jugular arteriovenous fistula, Ding et al. hoped to change the blood velocity profile of the common carotid artery to cause dilation and induce arterial remodeling [88, 108]. The resulting aneurysms were, in general, much larger, most particularly, in height. The tallest aneurysm was

more than twice as large as the tallest created without the arteriovenous fistula using the standard procedure (Figure 12).

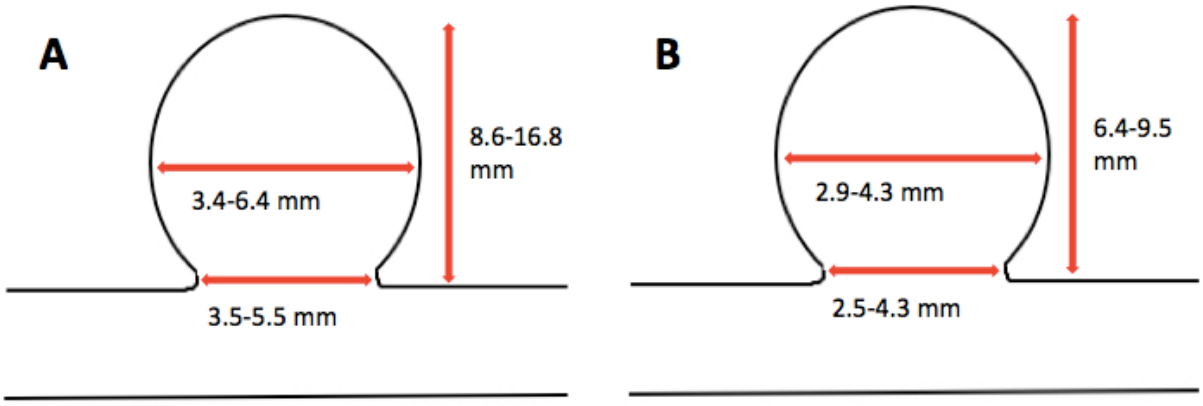

Figure 12: Elastase-induced rabbit common carotid artery aneurysms with and without the creation of an arteriovenous fistula from Ding et al. [67]. A) Ranges of measurements characterizing geometry for aneurysms after creation of the arteriovenous fistula. These aneurysms were larger than the standard model, especially in terms of height. B) Ranges of measurements characterizing geometry for control group of aneurysms using the standard procedure. These aneurysms were smaller than those made after creation of an arteriovenous fistula.

Successful attempts to control different aspects of the aneurysm geometry in the rabbit elastase model are small steps forward in creating more customizable models for neurovascular device testing. One interesting study from Kainth et al. [69] uses another surgical modification to address another drawback of in vivo testing. Their goal was to establish a double aneurysm model in both right and left common carotid arteries of a single rabbit, reducing the cost of running a study by decreasing the number of animals. The following figure depicts an artistic

rendition of a right and left common carotid artery ligation that resulted in double aneurysm geometries as well as a diagram of some of the ranges of the measurements that were taken to characterize the aneurysm.

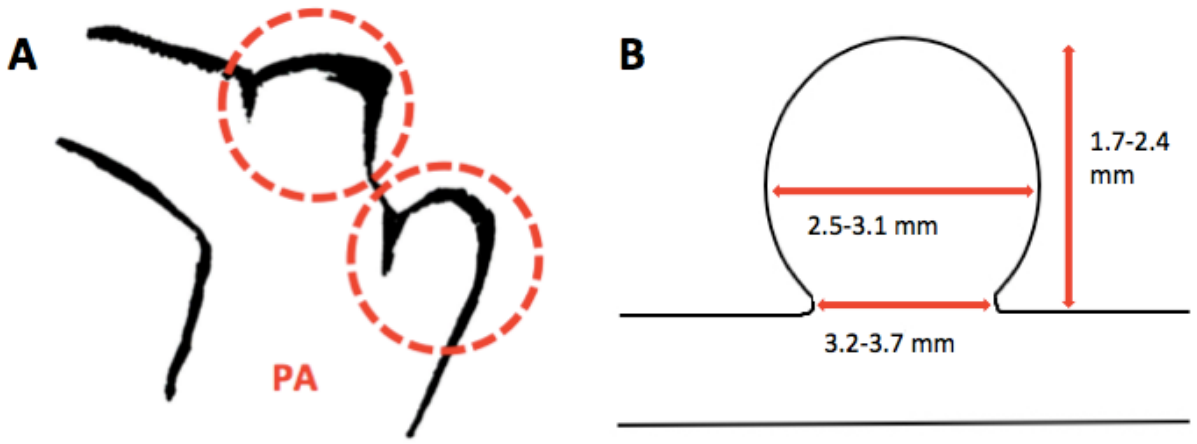

Figure 13: Rabbit elastase double aneurysms from the right and left common carotid artery established from Kainth et al. [69]. A) Artistic rendition of the double aneurysms. B) Ranges of measurements characterizing double rabbit common carotid artery aneurysms. Though the dome and neck diameters were somewhat consistent with the standard method, the aneurysm height was severely decreased.

Kainth et al.'s method was robust in creating elastase-induced double aneurysms; however, the resulting geometries were much smaller compared to their single aneurysm control group, especially regarding the height. The median height was 1.9 mm, which may not be effective for testing certain devices, such as those that focus on clotting off the sac of the aneurysm. Despite these limitations, Kainth et al. demonstrated a practical and reproducible

modification to the rabbit elastase model, though more work needs to be done to match the original geometry.

Another interesting modification to the rabbit elastase model from Kainth et al. was their ability to influence the orientation of the aneurysm as it pertained to the parent artery. They accomplished this by "anchoring" some of the aneurysms to the surrounding tissue using non-absorbable sutures (Figure 14).

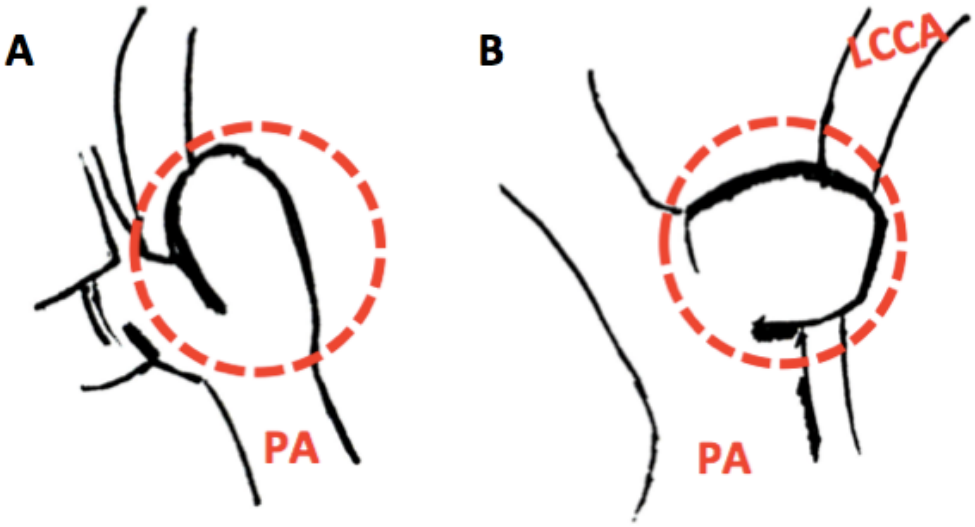

Figure 14: Artistic renditions of single rabbit elastase aneurysm models of different orientations pertaining to the parent artery from Kainth et al. [69]. A) Anchored orientation. B) Severed orientation.

Aneurysm orientation was a unique aspect of this study. While it is not a characteristic of the specific geometry, orientation can be a factor in determining the proper treatment of the aneurysm as well as a consideration when designing delivery systems. Though this thesis does

not specifically focus on incorporating this type of variation in aneurysm in vitro models, it is an important consideration that can be included in future studies.

Through consideration of baseline measurements and modifications to the rabbit elastase model, it can be seen that the neck diameter spans a narrow range of 2.3 mm – 5.5 mm. The height can range from 1.7 mm – 16.8 mm, with a more common range between 2 mm – 8 mm. The success of the established, reproducible rabbit elastase aneurysm model is apparent in the many articles that use it to study aneurysm pathophysiology and to test neurovascular devices. Emerging research demonstrates that many have attempted to modify this model in order to better control aspects of the geometry. Because the rabbit elastase model uses a dynamic, living environment with inherent biologic variation, it can be very difficult to establish modifications to the methods that also yield consistent results. In vitro models, in contrast, have a great potential to be customizable, though not much work has been done to create relevant aneurysm geometries. The rabbit elastase model can, therefore, serve as a good foundation for early stage research in developing these new in vitro models.

2.4 Discussions and Conclusion

From the literature review of human and rabbit elastase aneurysm models, few similarities were found among all studies, but overall trends and dimensions were determined. Through analyzing each model separately, it was determined that the standard rabbit elastase aneurysm model was fairly consistent in terms of methods and resulting geometries; however, the span of ranges only encompassed part of the variation found in human aneurysms in clinical settings. This result is expected because rabbit elastase aneurysms were created from an established method. Few deviations of the rabbit elastase method, which allow for geometries to

more accurately represent some of those found in humans, have been studied, although a few examples were noted.

A stark difference in characterization methods existed when comparing human and rabbit elastase aneurysm models. While it was fairly simple to analyze most of the rabbit aneurysm studies together, each human model was far too unique to be interpretable as a whole. Instead, conclusions were drawn about the importance of certain dimensions based on how commonly they were recorded throughout the studies. In human models, the neck diameter was the most common measurement taken, while in rabbit models, the most commonly noted measurement was the height of the aneurysm. The ranges of these specific dimensions were used to help determine the foundation of novel in vitro geometries, which is seen later in Chapters 3 and 4.

Many of the limitations of this literature review lie mostly with the inconsistencies of measurement throughout the human aneurysm studies. Human aneurysms were measured in such a variety of ways, whereas rabbit model aneurysms were measured very consistently. For most of the rabbit models, the height, neck diameter, and dome width were reported in addition to a few other unique measurements depending on the study. For clinical studies, only three articles completely characterized the aneurysms using all neck diameters, dome width measurements, and heights. Lastly, because of such a wide range of measurements found in the variety of aneurysms, it was difficult to compare the geometries because they could be further categorized differently into other subtypes. An improvement to this review would be to first categorize aneurysms based on their shape or location, and increase the sample size of aneurysms in each category. This could provide a more interpretable model within each category and would determine accurate ranges for different types of aneurysms.

The electrospinning work done in the Cal Poly Tissue Engineering research lab, as previously described, is an example of a method that can be manipulated to create customizable geometries of specified dimensions. The work done in this thesis uses such dimensions as design specifications to create different variations of aneurysm geometries. Before attempting to create scaffolds with newly specified dimensions, however, methods were developed in order to characterize aneurysm scaffolds consistently. In addition, these methods were then used to characterize current blister and saccular aneurysm models to provide insight into internal scaffold morphology in order to help determine the next steps of creating variable geometries. This method development and current model characterization are described further in the following chapter.

3 Method Development for Characterizing Aneurysm Geometries and Preliminary Characterization of Current Blister and Saccular Aneurysms

3.1 Introduction

In order to evaluate neurovascular devices, accurate preclinical geometric models are imperative; however, it is difficult to attempt to replicate the variety of aneurysms that are found in all clinical cases. As demonstrated in the previous chapter, no perfect human model exists that can replicate all aneurysm geometries. While the rabbit elastase aneurysm model is a more refined model, it still only encompasses a small range of dimensions that are present in humans. Only a few studies have attempted to modify the rabbit elastase model to expand the range of dimensions possible to replicate a greater number of clinical cases [67, 68]. This process of expanding the capabilities of the rabbit model, however, is slow because in vivo experimentation is expensive and outcomes are difficult to control. Preclinical in vitro models have a great potential to be customizable and scalable models to test neurovascular devices.

In order to make progress in eventually representing aneurysms found in humans, it is easier to start at a narrower range, such as the rabbit elastase model, and to determine and utilize consistent characterization methods. Although characterization of aneurysm size and geometry has been relatively well documented for in vivo models, especially for aneurysm neck and height, [60, 65, 66, 109], there has been little work exploring how to best characterize in vitro aneurysm models. The goal of this thesis was to establish a range of specific in vitro geometries, which requires accurate characterization methods. The purpose of this chapter was, therefore, to

establish the methods to characterize in vitro aneurysm geometries and to perform preliminary characterization of existing blister and saccular aneurysm geometries.

In Cal Poly's Tissue Engineering research lab, electrospun scaffolds have been characterized by their fiber morphology using SEM imaging. In addition to scaffold microstructure, previous work from Shen et al. established methods for documenting the external dimensions of various aneurysm geometries using calipers. Internal measurements of these geometries, however, remained unknown, despite their importance. This chapter will first, therefore, establish consistent characterization methods through measuring external diameters of the neck size and height, followed by the internal diameter of the aneurysm neck and the height. Additionally, methods will be presented to characterize current Solidworks models, which can be applied to the development of new geometries. Then, these methods will be used to determine dimensions of current blister and saccular aneurysms using the geometries and electrospinning protocol from Shen et al., which will also be helpful in establishing the new range of geometries for our in vitro models.

3.2 Methods

Sample preparation and calculations for determining external and internal measurements from aneurysm scaffolds as well as specifying dimensions from the Solidworks models are outlined in the following sections. First, sample preparation and aneurysm scaffold measurements will be described, beginning with external dimensions, and ending with scaffold cutting to acquire the internal dimensions to characterize the geometries. Then, the Solidworks calculations will be described in order to determine the actual dimensions of geometries from the CAD models.

3.2.1 Overview

Aneurysm scaffolds were characterized using both external and internal dimensions. After electrospinning, outer measurements of the aneurysm vessel were taken with calipers before samples of the scaffold were taken off of the mold or dissolved. Then, in order to take internal dimensions, the scaffold was cut in cross-sections depending on the type of measurement, and the inside of the aneurysm was imaged using a scanning electron microscope. The internal dimensions were measured in ImageJ, an image processing and analysis software.

3.2.2 External Measurements

First, external dimensions of the aneurysm were taken using calipers when the scaffold was still on the mandrel. Both neck diameters perpendicular and parallel to the parent artery were measured from the top of the scaffold. The height was measured with calipers from the side of the scaffold. All three measurements are diagrammed below in Figure 15.

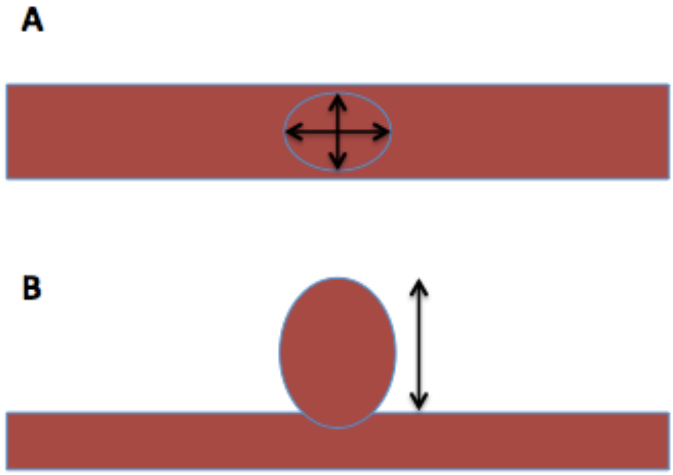

Figure 15: Diagram of external dimensions taken with calipers of the aneurysm neck and height. A) Aneurysm neck diameters (parallel and perpendicular to the parent artery) taken from the top view of the vessel. The horizontal dimension represents the neck diameter parallel to the parent vessel. The vertical dimension represents the neck diameter perpendicular to the parent vessel. B) Aneurysm height dimension.

3.2.3 Internal Measurements

In order to measure internal dimensions, scaffold samples were cut to expose the internal lumen based on whether its neck diameter or its height was measured. For the neck measurements, the bottom half of the parent vessel was cut off, and the rest of the scaffold lumen was opened up to reveal the bottom view of the inside of the aneurysm. The sample was then sputter coated on both sides for seventy seconds each in preparation for SEM imaging. After images were taken of the bottom of the aneurysm, neck diameters were measured at the axes parallel and perpendicular to the parent vessel using the "Straight Line" tool in ImageJ (Figure 16).

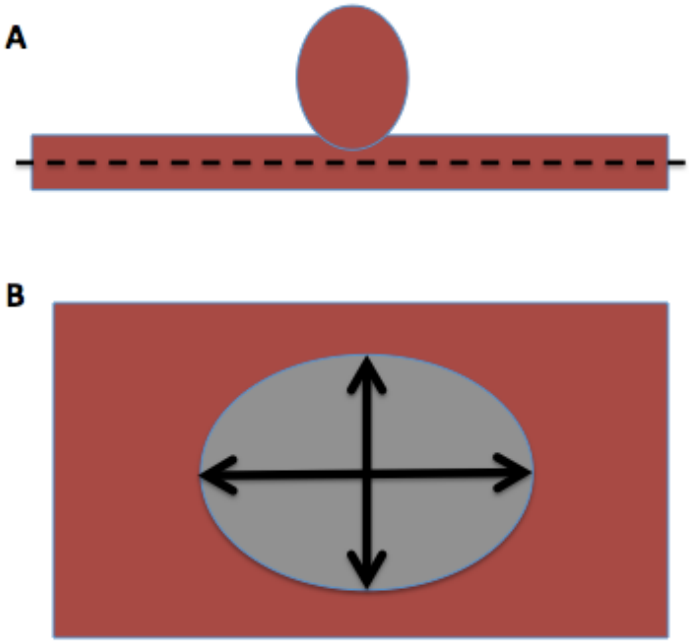

Figure 16: Diagram for sample preparation and internal aneurysm neck dimensions. Flow direction is horizontal for both diagrams in this case. A) To prepare the sample, the bottom half of the vessel is cut off and is folded out to expose the bottom view of the inside of the neck of the aneurysm. B) Aneurysm neck dimensions, with the gray area representing the bottom view of the aneurysm dome. The vertical dimension is the inner aneurysm neck diameter perpendicular to the parent artery and the horizontal dimension is the inner aneurysm neck diameter parallel to the parent artery.

For the aneurysm height measurements, separate scaffold samples were cut to expose symmetrical halves of the aneurysm connected to the parent vessel. Samples were prepared similarly to the samples designated for neck dimensions for SEM imaging. Once images were taken, heights were measured vertically from the very top of the dome of the aneurysm and lined

up horizontally with the inner lumen wall of the parent vessel (Figure 17). Similar to the neck measurements, the “Straight Line” tool in ImageJ was used to determine the height dimensions.

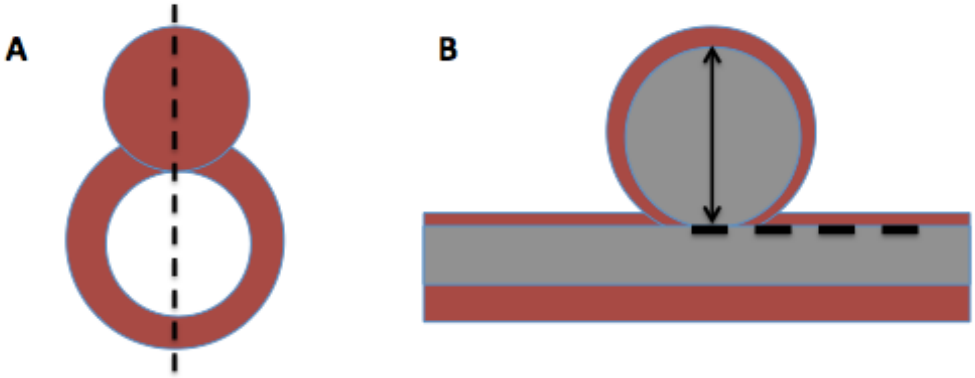

Figure 17: Diagram for sample preparation and internal aneurysm height dimensions. A) To prepare the sample, the vessel was cut into two symmetric halves both containing the aneurysm and the parent artery. B) Aneurysm neck dimensions, with the gray area representing lumen in the aneurysm and the parent vessel.

3.2.4 Solidworks Model Dimensions

In addition to scaffold characterization, neck diameters and heights of the aneurysm CAD models were calculated and applied to specify dimensions in Solidworks to allow for comparisons between the design and the output. The specified dimensions were calculated from the current geometries, and these methods could also be utilized to reverse-engineer new geometries. Because these dimensions were of the Solidworks molds, they were only representative of the inner dimensions of the aneurysm scaffold.

Height and parallel neck diameter were simple dimensions to specify. In order to specify the height, the vertical distance from the highest point of the aneurysm dome was measured to the top of the parent artery. The dimension of the neck at the parallel axis was found by specifying the width of the aneurysm collinear with the top of the parent artery. These dimensions did not require any extra calculations and could be specified on Solidworks when designing a different geometry.

The aneurysm neck dimension perpendicular to the parent vessel required more calculation steps. This length equaled the arc length created by the interface between the aneurysm and the parent artery, which is illustrated by the green curve in Figure 18 below.

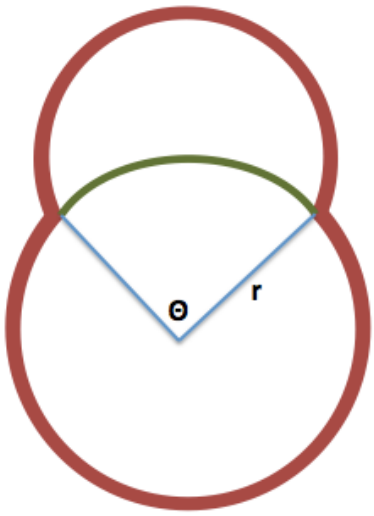

Figure 18: Diagram of the side view cross section of an aneurysm and parent vessel. The perpendicular neck diameter is indicated by the length of green curve, or the arc length of the section of the parent vessel. Other important dimensions needed to calculate this value are θ, or the angle the arc makes when measuring from the center of the parent vessel, and r, or the radius of the parent vessel.

In order to determine the length of the neck diameter, the arc length must be calculated. The equation equal to arc length is:

$$arc\ length = \frac{\theta}{360^o}\ x\ 2\pi r$$

where θ is equal to the angle of the arc in degrees with the vertex at the center of the parent vessel, and r is equal to the radius of the parent artery.

In Solidworks, the radius, r, was measured by first drawing a centerline through the parent artery. The outermost point of the aneurysm from the center of the parent artery was located, and the distance between that point and the centerline was measured to find the radius. This diagonal was split into corresponding x and y vector components by default, as depicted by the diagram below.

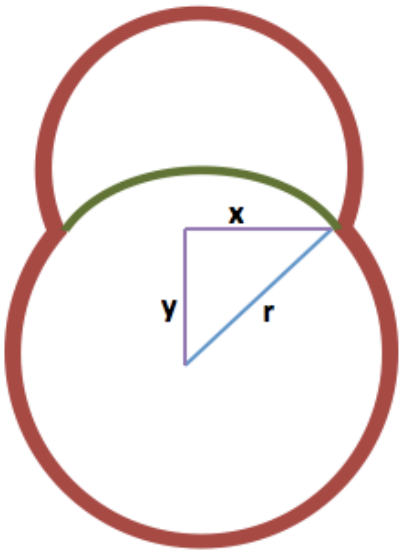

Figure 19: Diagram of side view cross section of an aneurysm and parent vessel depicting x and y vector components (in purple) of the radius (in blue). Using trigonometry, the x and y components can be used to find the angle equal to half of the arc length.

Using the rules of similar triangles, the angle equal to the arc length of half of the aneurysm neck can be found with the following equation that uses trigonometry:

$$\theta = tan^{-1}\left(\frac{opposite\ side\ length}{adjacent\ side\ length}\right)$$

θ can then be plugged back into the equation for arc length to find the arc length of half of the aneurysm since the angle only encompassed half of the mold. Multiplying the calculated arc length by two will determine the entire arc length bounded by the aneurysm and, therefore, the perpendicular neck diameter.

3.3 Results and Discussion

3.3.1 Overview

Characterization methods were employed for existing blister and saccular aneurysm geometries. First, external dimensions were taken. Then, the internal height measurements were made for both geometries from samples imaged with a scanning electron microscope. Measuring the internal height also allowed for visualization of the fiber morphology at the neck. These results are described in Sections 3.3.1 and 3.3.2.

The last two sections describe characterization of the scaffold aneurysm neck and Solidworks model for the blister aneurysm geometry only. As described later, it was determined through internal height measurements that the saccular aneurysm geometry was not robust because of inconsistent, aligned fiber morphology at the neck region, which did not result in the true mandrel geometry and made taking internal measurements difficult. From the success of SEM imaging of the blister aneurysm, it was concluded that new geometries should follow the same general shape. This work is depicted in more detail throughout the rest of the chapter.

3.3.2 External Dimensions for Blister and Saccular Aneurysms

Current blister and saccular aneurysm geometries were characterized externally with calipers measuring the neck diameters and the height. Two aneurysms were characterized from one scaffold and were categorized as "distal" or "proximal" depending on the relative position on the collector during electrospinning. The following table describes the measurements made of both neck diameters and the height for each aneurysm before it was cut off the mold. Values are presented as a mean ± standard deviation, and were measured on both the front and the back of each aneurysm in order to capture the variability due to the measurement system. Multiple measurements were taken from the same scaffold. The standard deviation represents the variation in these measurements from the same scaffold sample. Table 3.1 illustrates the external measurements of the current blister aneurysm.

Table 3.1: External Dimensions of Blister Aneurysm Scaffold

Aneurysm Position	Parallel Neck Diam. (mm)	Perpendicular Neck Diam. (mm)	Height
Distal	1.91 ± 0.042	3.05 ± 0.283	5.26 ± 0.113
Proximal	1.665 ± 0.134	2.965 ± 0.290	5.81 ± 0.042

Table 3.2 below contains the measurements of the current saccular aneurysm for two aneurysms on one scaffold.

Table 3.2: External Dimensions of Saccular Aneurysm Scaffold

Aneurysm Position	Parallel Neck Diam. (mm)	Perpendicular Neck Diam. (mm)	Height
Distal	6.84 ± 0.085	3.94 ± 0.057	3.065 ± 0.361
Proximal	5.825 ± 2.482	3.925 ± 0.205	3.43 ± 0.212

In general, the external dimensions of the saccular aneurysm were much more variable than the external dimensions of the blister aneurysm. The external dimensions of the saccular aneurysm were also unexpected because of the large difference between the parallel neck diameter and the perpendicular neck diameter.

For both blister and saccular scaffolds, measurements were variable between the distal and proximal aneurysms on each mandrel. It was difficult to tell whether the variability was due to the aneurysms themselves or due to the measurement tool. The biggest limitation of using the calipers to measure the external dimensions was that it relied on human judgment to position the caliper at the corresponding neck and height sizes. It was difficult to make accurate measurements without making a dent in the aneurysm because the scaffold is extremely small and delicate. In addition, securing the scaffold on a flat surface was not easy, and any resulting tilt could have skewed the measurements, especially when measuring aneurysm height. Improvements for external measurements could be made in the future by securing the scaffold using custom fixtures.

In summary, external dimensions can be used for preliminary characterization of the aneurysm geometries; however, they may not be the most accurate representation of whether the aneurysm actually conformed to the mandrel geometry. These external dimensions can be used

for determining changes in PLGA fiber coverage of aneurysms, but they are not an indication of the mandrel geometry. Internal dimensions taken from SEM images are more accurate in visualizing these geometries, and they perhaps provide a more consistent way to make measurements.

3.3.3 Internal Height Measurements for Blister and Saccular Aneurysm Geometries

After external measurements were taken, the same blister and saccular aneurysms from Section 3.3.1 were prepared accordingly to measure the internal height of the scaffold. First, the wax molds were melted and dissolved off the mandrel, and the saran wrap was removed. Once scaffolds were obtained, the aneurysm domes were cut symmetrically using small scissors so that the inside of the front or back of the aneurysm could be visualized. SEM images were taken of these samples, as seen in Figure 20 and Figure 21 for blister and saccular aneurysms, respectively. Because the saccular aneurysm was much larger than the blister aneurysm, multiple images were taken of the proximal aneurysm for better visualization.

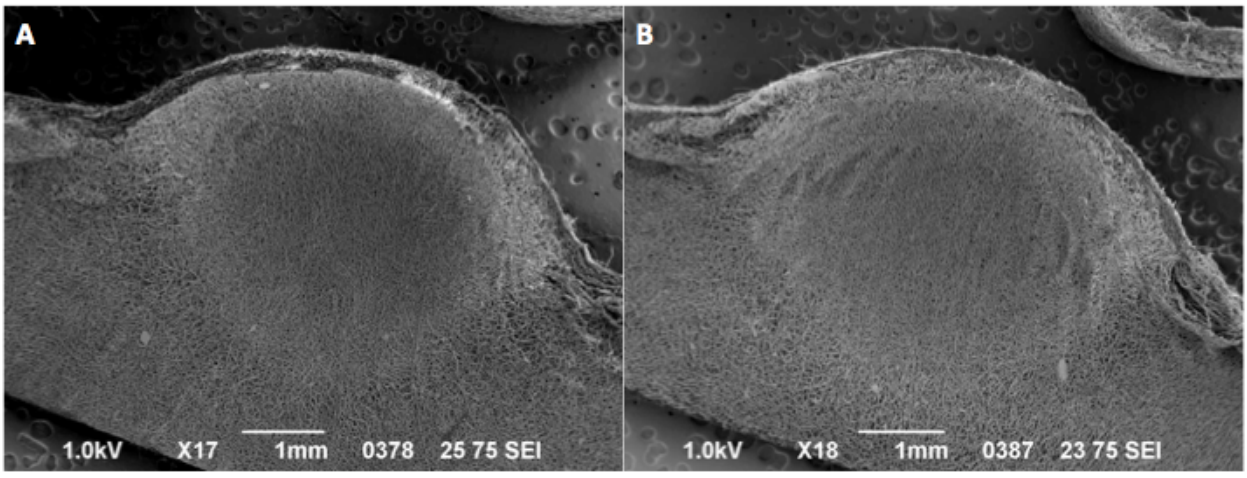

Figure 20: Blister aneurysm dome SEM images used to measure the internal height dimension. A) Distal blister aneurysm. B) Proximal blister aneurysm.

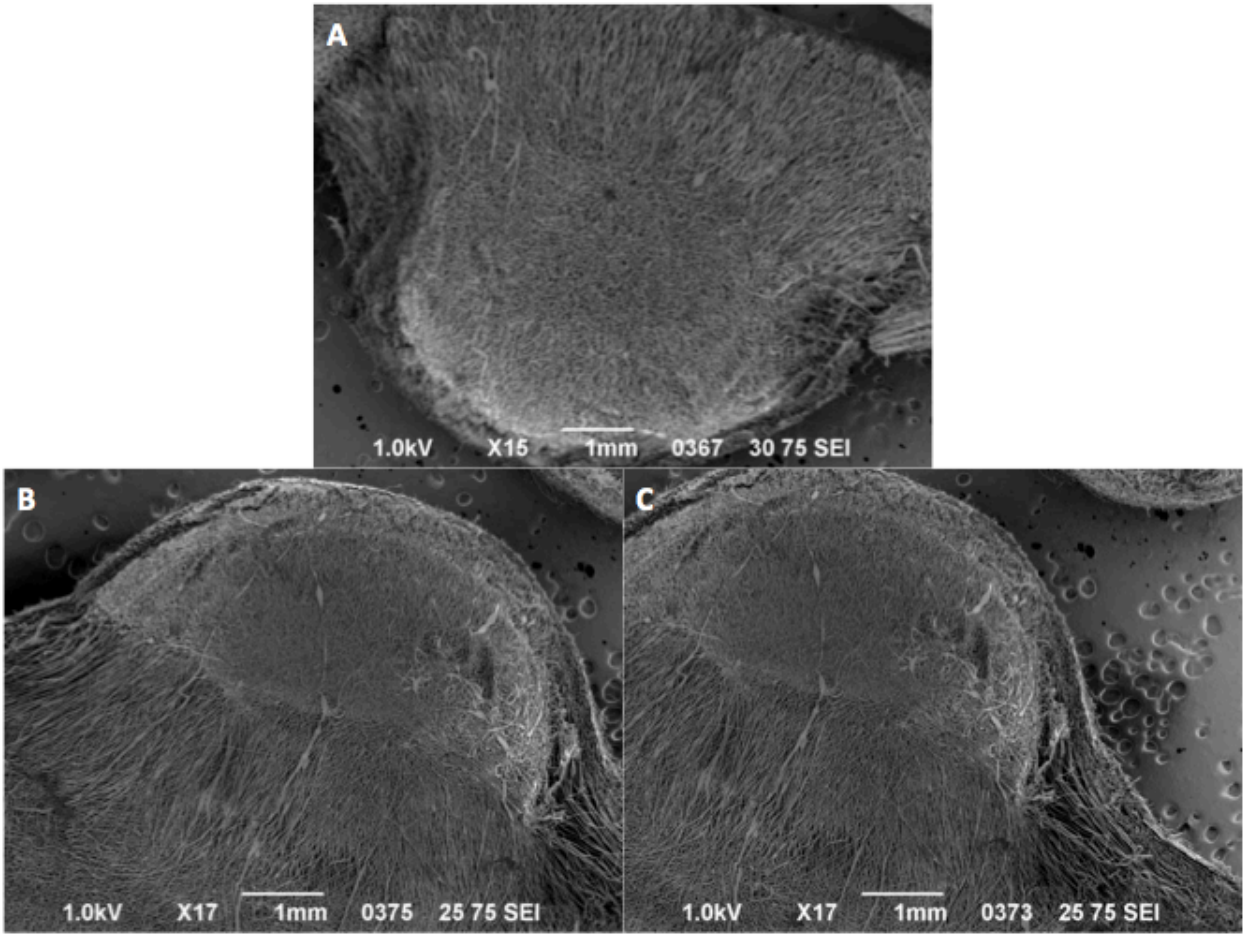

Figure 21: Saccular aneurysm dome SEM images used to measure internal height. A) Distal saccular aneurysm. B, C) Proximal saccular aneurysm.

The following table below contains the internal and corresponding external measurements for comparison of the blister and saccular aneurysm height. For external characterization, multiple measurements were taken from the same scaffold. Using these images, the parallel neck diameter was also measured. It was determined, however, that these measurements were not accurate due to sample preparation. Cutting the scaffolds longitudinally with scissors most likely elongated the neck, resulting in measurements that are larger than the specification. In addition, because of the stretched out fibers at the neck of the saccular

aneurysms specifically, it was more difficult to determine the edges of the neck. These neck diameters have been omitted from the table, but can be found in Table B.1, in Appendix B.

Table 3.3: Blister Aneurysm Dome Internal Height Measurements from SEM Images and External Heights from Caliper Measurements

Aneurysm Type	Aneurysm Position	Internal Height (mm)	External Height (mm)
Blister	Distal	1.71	5.26 ± 0.113
	Proximal	1.67	5.81 ± 0.042
Saccular	Distal	4.09	3.065 ± 0.361
	Proximal	3.09	3.43 ± 0.212

Similar to the external characterization of the aneurysm geometries, the internal height measurements were found to be consistent for both blister aneurysms, but not for the saccular aneurysms. The internal height of the distal and proximal saccular aneurysms differed by 1 mm. This variation was most likely due to the saran-wrapping step in the process because it was noted that the saccular geometry was not as robust in holding its shape when heat shrinking was applied. The heat most likely melted part of the proximal aneurysm dome, making it shorter than the distal aneurysm.

When comparing the external height measurements to the internal height measurements, the blister aneurysms were about 4 mm larger externally. The external saccular aneurysm heights, however, were around the same for the proximal aneurysm or slightly smaller for the distal aneurysm than the internal height measurements, demonstrating that external measurements may not be as accurate for all geometries. As mentioned previously, this also may

be an indication of a large measurement error due to variation in the measuring tool or due to human judgment.

In addition to measuring the aneurysm height, the general fiber morphology as the scaffold transitions from the parent artery to the aneurysm at the neck region was also observed between both saccular and blister geometries for this method of sample preparation. There was a notable difference observed at the neck portion of the aneurysm between the saccular and blister aneurysms, as illustrated in Figure 22 below. Specifically for the blister geometry, there was not much of a difference in fiber morphology among the neck, aneurysm, and parent artery; rather, the only way to distinguish these regions was to use the different planes of focus on the scanning electron microscope. In contrast, fibers were much more sparse in in the saccular geometry and oriented the same direction, which was unexpected.

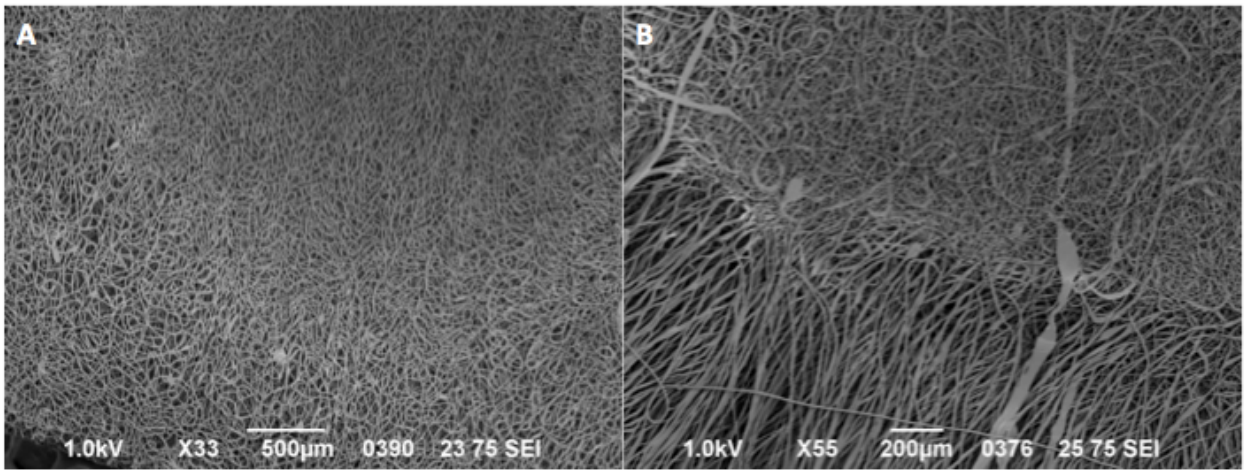

Figure 22: Neck region of blister and saccular aneurysm geometries at higher magnifications. A) Proximal blister aneurysm neck. The neck region was more subtle because fiber morphology was very similar that of the aneurysm dome and of the parent artery. B) Proximal saccular aneurysm neck. The neck region was very distinct because of the aligned and sparse fibers, indicating that the fibers did not conform to the geometry at the neck region.

One explanation of these results could be that there was a limitation of the electrospinning process itself in conjunction with this specific geometry. The largest difference between the saccular and blister geometry was the neck region; specifically, the saccular geometry had a much narrower neck compared to the width of the dome. Because the dome was circular, the narrow neck created a crevice between the aneurysm and the parent vessel in all directions, which may have been too deep and too narrow for the fibers to penetrate into. Without a mandrel to physically stick onto, the fibers stretch from the dome to the parent vessel, resulting in a unidirectional fibrous sheet without structure. Using this assumption, it was concluded that future aneurysms would need to be designed with an exposed neck for the fibers to catch onto in order for accurate replication of the mold geometries if the lab were to keep

electrospinning saccular scaffolds. This would be accomplished by exposing the neck region between the dome and the parent artery in all directions by changing the dome shape to be less spherical.

Another logistical limitation to this process of taking internal measurements itself was the amount of time that it took to obtain one image and gain one dimension. This required mixing solutions, electrospinning, and mandrel removal. Since sample preparation is different for each measurement, multiple scaffolds were created and, ultimately, the lengthy process was repeated in order to obtain each necessary dimension for full geometric characterization. One solution to cut the time that it would take to make these characterization measurements would be to cut the aneurysm scaffold directly off of the mold using a razor blade, eliminating the melting and dissolving steps of the process to remove the scaffold off the mandrel. These steps currently exist to allow for mandrel removal while keeping the scaffold intact for aBVM use; however, this may not necessary for geometric characterization. Before eliminating these steps; however, it needed to be demonstrated that the saran wrapping, melting, and dissolving process do not significantly change the aneurysm geometry so that characterization outputs directly reflect the scaffolds that are being used in the in vitro aBVM setups. Hence, characterization of the blister aneurysm neck with a scaffold that was saran wrapped and dissolved and with a bare scaffold that was cut off the mandrel was performed, and results were documented in the next section.

In summary, internal aneurysm heights were successfully measured and visualized using SEM imaging despite the lengthiness of the saran wrapping and scaffold removal process. Additionally, it was determined that saccular aneurysms did not have distinguishable neck regions because they were composed of aligned, sparse fibers. Therefore, these aneurysms were difficult to characterize, and future geometries should mimic the shape of the blister geometry

rather than the saccular geometry. As mentioned previously, one limitation to this characterization process was the lengthiness of the saran wrapping and the dissolving steps. In order to eliminate specific steps during characterization to save time, it was important to determine whether saran wrapping the mandrel, and melting and dissolving the mandrel off the scaffold would affect the overall geometry.

After characterizing internal aneurysm heights, the next step was measuring the internal neck dimensions. This process will be described in further detail in the next section. Since future geometries should mimic the shape of the blister rather than the saccular aneurysm, internal neck measurements were only made for the blister geometry. Additionally, in order to address the potential elimination of saran wrapping and dissolving, this neck characterization was done on two scenarios: a scaffold that was not saran-wrapped and cut straight off the aneurysm mold after electrospinning and a scaffold that was saran-wrapped, electrospun, and went through the entire mandrel removal process of melting and dissolving the wax.

3.3.4 Internal Neck Measurements for Blister Aneurysm Geometries

Based on the results of the height measurements for both blister and saccular aneurysms, it was clear that new geometries should be based off of the current blister geometry because the saccular geometry could not be accurately electrospun and resulted in a neck that was not well defined. Saccular aneurysm geometries, therefore, were omitted from the following characterization study.

In addition, neck characterization was done using two aneurysms from the same mandrel with one aneurysm saran wrapped and the wax melted and dissolved for scaffold removal, and with the other aneurysm cut straight off the mandrel. This was done to determine the impact of

the saran wrapping and mandrel removal steps of the process, which are both essential if the scaffolds are used in a bioreactor setup, but add potentially unnecessary time and complexity to the characterization steps. The "non-dissolved" scaffold was cut off the mandrel using a razor blade after it was electrospun and desiccated, and scissors were used to trim the bottom of the scaffold to get a good view of the internal aneurysm neck. The "dissolved" scaffold was saran-wrapped and went through the melting and dissolving process to remove the wax and plastic wrap. Then, the bottom half of the scaffold was trimmed off with scissors. Both scaffolds were opened and flattened as much as possible without destroying the integrity of the geometry in order to reveal the internal neck region. Figure 23 below shows the SEM images taken of the bottom view of the aneurysm neck for both dissolved and non-dissolved scaffolds.

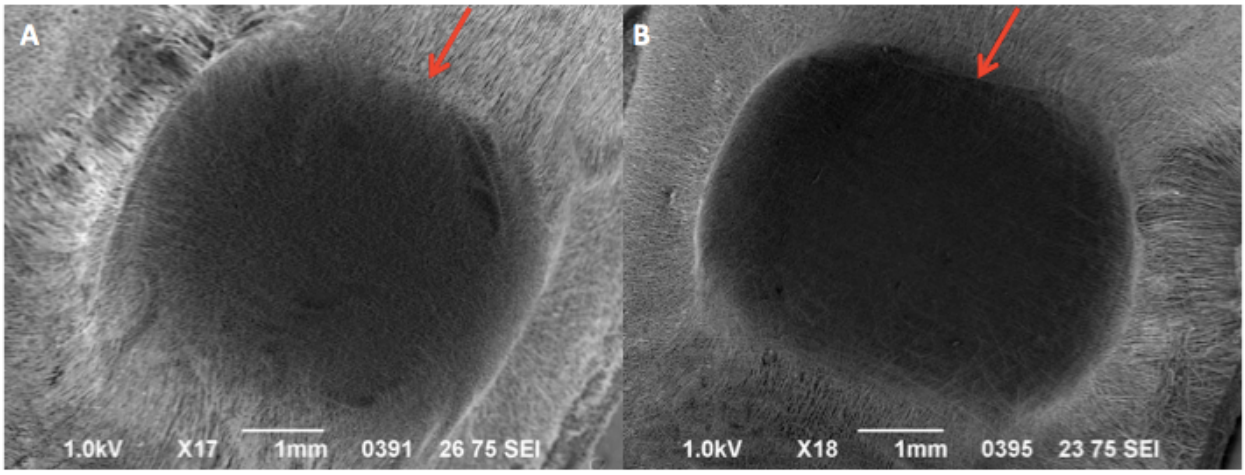

Figure 23: Blister aneurysm internal neck SEM images used to measure the diameter of the neck parallel and perpendicular to the parent vessel. Flow direction is indicated with red arrows. A) Dissolved blister aneurysm. B) Non-dissolved blister aneurysm.

SEM images of the bottom view of the neck were used to measure the perpendicular and parallel neck diameters, which are outlined in the following table. Measurements were taken with ImageJ, similar to the internal heights.

Table 3.4: Blister Aneurysm Internal Neck Diameters from SEM Images

Aneurysm Condition	Parallel Neck Diam. (mm)	Perpendicular Neck Diam. (mm)
Dissolved	4.14	5.19
Non-Dissolved	4.04	5.20

When comparing both neck diameters, it was seen that the perpendicular neck diameter was actually larger than that of the parallel neck diameter with a difference of 1 mm, contradicting the external measurements of the blister aneurysm scaffold. This outcome illustrated the importance of measuring the internal dimensions because external dimensions did not account for the curved surface of the parent artery and, therefore, curved perpendicular neck diameter. Physically flattening the curved surface of the neck region when preparing the sample for imaging is also essential for generating an accurate length measurement from the SEM image.

Variation in neck size measurements could result from difficulties in identifying the edges of the aneurysm neck. The measurements are not automated, so determining the edges of the aneurysm neck is purely based on human judgment. Since SEM images are displayed in a gray-scale, it can be difficult to determine a clear-cut edge. Measurements can vary depending on who is taking the measurement and where the edges are specified. Future work could be done in order to determine how much the measurements vary throughout different geometries.

Few differences were observed between imaging the dissolved and the non-dissolved scaffold. In terms of the geometry, there was not a noticeable difference between the scaffolds for both of the neck diameters, suggesting that consistent measurements can be taken before or after scaffold post-processing. It was also noticed that the non-dissolved scaffold had more defined edges at either side of the aneurysm; however, it was not too difficult to distinguish the neck in the dissolved aneurysm as well, so geometries could be characterized at different points of the process. Since either approach to characterization was shown to be acceptable, it may be worth eliminating these steps to save time for future studies.

Once the scaffolds were characterized, the last part of the process was to compare each measured geometry to its original design specifications, which were the measured neck diameters and heights on the Solidworks models. The following section describes the results of the blister aneurysm geometry mold as determined from the Solidworks model.

3.3.5 Solidworks Model Characterization for the Blister Aneurysm Geometry

The blister aneurysm geometry was characterized in Solidworks using the parallel and perpendicular neck diameter and the height. These dimensions were important to compare with results from the scaffold characterization in order to determine how closely the actual scaffold matched the initial scaffold model. In addition, these methods could also be employed in reverse when creating new geometries. Results from the current blister geometry can be found in Table 3.5 below.

Table 3.5: Blister Aneurysm Solidworks Mold Dimensions

Parallel Neck Diam. (mm)	Perpendicular Neck Diam. (mm)	Height (mm)
4.97	5.823	2.25

The Solidworks model dimensions were consistently almost 1 mm larger than all three internal measurements of the scaffolds themselves, as illustrated in Table 3.6 below, which summarizes all dimensions of the blister aneurysm geometry. This suggests that the process does not output the exact dimensions, but the proportions are still very similar. Though these design specifications did not return the exact output, these proportions imply that the shape of the aneurysm was maintained. This demonstrated that if a specific dimension is desired, enough data could be collected in order to determine how much the models would need to be scaled up to obtain the correct output. Since the difference was not large, however, this method of creating aneurysm molds can still be used to create distinct geometries that vary height and neck diameter.

Table 3.6: Summary of Blister Aneurysm Geometry Dimensions

Description or Condition	Ext. Par. Neck Diam. (mm)	Ext. Per. Neck Diam. (mm)	Ext. Height (mm)	Int. Par. Neck Diam. (mm)	Int. Per. Neck Diam. (mm)	Int. Height (mm)
Distal	1.91 ± 0.042	3.05 ± 0.283	5.26 ± 0.113	-	-	1.71
Proximal	1.665 ± 0.134	2.965 ± 0.290	5.81 ± 0.042	-	-	1.67
Dissolved	-	-	-	4.14	5.19	-
Non-Dissolved	-	-	-	4.04	5.20	-
Solidworks	-	-	-	4.97	5.823	2.25

Abbreviations: Ext = External, Par = Parallel, Per = Perpendicular, Int = Internal

3.4 Conclusions

Previously in the lab, aneurysm geometries were characterized only with external dimensions of the width of the neck and the height. While this method was sufficient for preliminary scaffold characterization, it did not provide any information about the actual internal geometry that would interface with devices. Both aneurysm height and neck diameter are relevant for assessing the type of device needed for treatment, and have been commonly used to characterize aneurysms in clinical and in vivo models. It is, therefore, necessary for internal dimensions to be assessed when evaluating customized in vitro aneurysm geometries.

This chapter established consistent characterization methods for both Solidworks models and resulting scaffold geometries. Current geometries were explored to evaluate these new characterization methods as well as to set the foundation for new geometries. To summarize both of the internal neck diameters and aneurysm height were successfully measured for the current blister aneurysm geometry, and measurements were similar enough to the dimensions of the

Solidworks models. This demonstrates that the output of the electrospinning process is an appropriate representation of the model design for new geometries that are similar to the blister aneurysm shape. In addition, the work also showed that these methods are sufficient in determining internal dimensions for future geometries.

In contrast, saccular aneurysm geometries were not successfully characterized. Through height measurements, it was seen that the resulting scaffold did not conform to the intended designed geometry because of the inability of the electrospun fibers to create a narrow neck. The saccular geometry was eliminated from further characterization because of the likely difficulty of distinguishing the edges of the neck. From this, it was learned that future geometries should not be modeled after the current saccular aneurysm without a new method of depositing fibers.

In addition to measurement methods, it was also determined that there was no notable difference between measurements from non-dissolved and dissolved aneurysm scaffolds. At any point during the scaffold creation process after electrospinning, the aneurysm can be measured. Eliminating saran wrapping, melting, and dissolving the wax, can save a lot of time. Future geometries were characterized without melting and dissolving the scaffold; however, it was decided that the saran-wrapping step should be kept because not enough data has shown that this step affects all geometries in the same way that it affected the blister geometry. It was speculated that the heat gun can melt part of the geometry, as seen when measuring the height of the saccular aneurysms, causing variability among different scaffolds. In addition, depending on how well the aneurysm was saran wrapped, the plastic can potentially add height to the aneurysm, and ridges caused by heat shrinking can also slightly alter the geometry. Therefore, this step remained, since it is a crucial part of scaffold creation for aBVM use.

With new characterization methods established, the next chapter will address the second and third aim of this thesis. The techniques of this chapter were employed to accomplish the second aim of this thesis: to create new molds for new geometries, as well as characterize the resulting scaffolds. New geometries were chosen to mimic the ranges found in the rabbit models from Chapter 2. Subsequent experiments then demonstrated completion of the third and final aim of this thesis, which was to test these new geometries for feasibility as aBVMs to evaluate neurovascular devices.

4 Customization of Neck Size and Height in Tissue Engineered Aneurysm Models and Implementation for Early Stage Flow Diverter Testing

4.1 Introduction

The goal of this chapter was to document the work performed towards the second and third aims of this thesis. Specifically, Aim 2 was to fabricate and characterize aneurysm geometry variations based on common rabbit and human anatomies, and Aim 3 was to evaluate new aneurysm geometries for feasible use in blood vessel mimic models. Completion of these aims relied upon the in vivo measurements found through Aim 1, and on the measurement techniques presented in the previous chapter.

After completion of this work for Aim 2 and Aim 3, it was deemed impactful and compelling enough for manuscript preparation and submission. Therefore, the bulk of this chapter was documented in a very specific format for submission to the journal Neuroradiology. This manuscript is currently under review. The manuscript title and co-author information is as follows:

Title: Customization of Neck Size and Height in Tissue Engineered Aneurysm Models and Implementation for Early Stage Flow Diverter Testing

Authors: Camille Villadolid, Brandon Puccini, Benjamin Dennis, Tessa Gunnin, Conor Hedigan, Kristen O'Halloran Cardinal

In addition to what was documented in the manuscript, some additional work was performed towards these aims. That work will be briefly presented here in the following section.

4.2 Other Aneurysm Scaffold Variations

Distinct aneurysm scaffold geometries with varying neck diameter and height were created in order to replicate the ranges of dimensions covered by in vivo rabbit elastase models. During this process, different iterations were designed and tested that allowed for the success of creating these distinct geometries. In the next section, the very first iteration of an aneurysm geometry that was not successfully electrospun is described, followed by two other variations of aneurysms on a 6 mm parent artery.

4.2.1 First Iteration

The first CAD model iteration of an aneurysm mold was created with the goal of being able to control both height and neck diameter. A neck diameter of 2.3 mm was modeled with a specified height of 4 mm. Instead of using the dome feature in Solidworks, a cylinder was extruded from the base of the aneurysm neck to create the dome, which allowed for the height to be controlled as well.

Initial observation of the scaffold neck demonstrated that the fibers did not conform to the geometry, as illustrated by Figure 24 below. Even without SEM imaging, it was clear that the fibers did not conform to the mandrel at the neck, and the true neck size parallel to the parent vessel was larger than 2.3 mm.

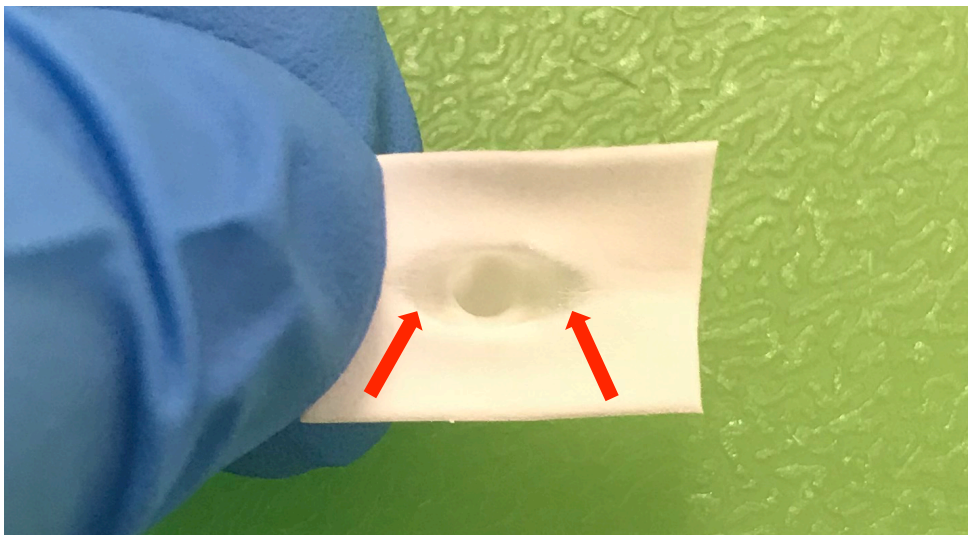

Figure 24: Lumen of the neck of the first iteration of an aneurysm scaffold with a designated neck size of 2.3 mm and a height of 4 mm. Flow direction is oriented horizontally. This aneurysm was designed with a cylindrical dome so that the height could also be controlled. Fibers did not conform to the geometry, and instead, were stretched out over the neck region on either side of the aneurysm, as illustrated by the red arrows. This would increase the parallel neck diameter, indicating that this design did not allow for the internal neck diameter to be controlled.

Similar to the current saccular aneurysm geometry, it seemed that the fibers stretched out at the neck region. For the saccular geometry, this was due to the narrow neck. In this iteration, the cylindrical aneurysm dome created a ninety-degree angle with the parent artery, and it was speculated that this angle was still not large enough to properly expose the neck to the fibers during electrospinning. It was then determined that a cone-shaped aneurysm dome was necessary to expose the neck region to allow for sufficient fiber deposition. The cone shape was achieved by using the dome feature in Solidworks, which limited the height depending on the given neck

size. At this point, it was determined that creating aneurysm scaffolds with accurate neck dimensions was more important than being able to control both neck size and height without any limitations; therefore, all geometries with varying neck sizes were created as cone-shaped using the dome feature. These cone-based iterations are documented in the manuscript.

4.2.2 Aneurysm Scaffold Variations on a 6 mm Parent Vessel

In addition to replicating ranges of heights and neck sizes on a 4 mm parent vessel, aneurysms were also designed on a 6 mm parent vessel, demonstrating further customization of our in vitro models and allowing larger necks to be created. Two different aneurysms were designed on a 6 mm parent vessel: one with a neck size of 5.5 mm, which was also done previously on a 4 mm parent vessel, and another aneurysm with a much larger, elliptical neck containing dimensions of 6 mm for the minor axis and 8 mm for the major axis.

A neck size of 5.5 mm was successfully designed and modeled on a parent vessel with a diameter of 6 mm. SEM images were taken and parallel and perpendicular neck diameters were measured using ImageJ, as seen in Figure 25 below. Three measurements on one scaffold sample of both the parallel and perpendicular neck diameters were taken and averaged.

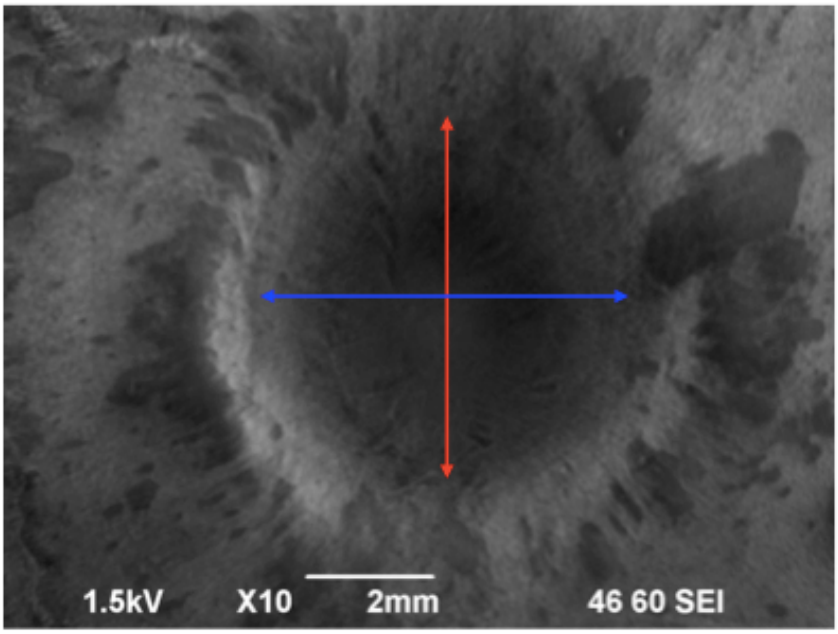

Figure 25: SEM image of the inner lumen of a 5.5 mm neck size aneurysm scaffold on a 6 mm diameter parent vessel at x10 magnification. The red arrow indicates the parallel neck diameter and the blue arrow indicates the perpendicular neck diameter. Flow direction was oriented vertically.

An aneurysm design with a much larger, elliptical neck was modeled and also successfully electrospun. The neck size of the aneurysm was specified to be 6 mm for the perpendicular neck diameter and 8 mm for the parallel neck diameter. The parent vessel diameter was also increased to be 6 mm. SEM images were taken to visualize the luminal neck, as illustrated in Figure 26 below. ImageJ was utilized to measure the neck diameters. Similar to the 5.5 mm neck size scaffold, three measurements were taken and averaged on one scaffold sample for both the parallel and perpendicular neck diameters. Values are presented as mean ± standard deviation. The standard deviation represents the variation in these measurements from the same scaffold sample.

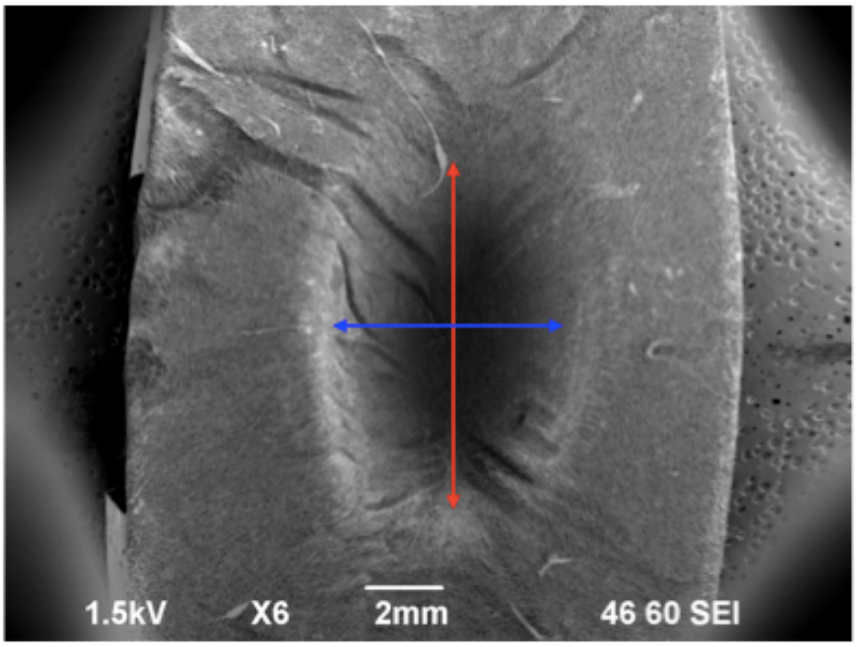

Figure 26: SEM image of the inner lumen of a 6 mm by 8 mm neck size aneurysm scaffold on a 6 mm diameter parent vessel at x6 magnification. The red arrow indicates the parallel neck diameter and the blue arrow indicates the perpendicular neck diameter. Flow direction was oriented vertically.

For both of these aneurysm scaffolds, unexpected measurements were obtained when measuring the neck diameters. For the 5.5 mm neck size scaffold, the parallel neck diameter was measured to be 5.94 mm ± 0.06 mm, and the perpendicular neck diameter was measured to be 5.97 mm ± 0.05 mm, which were both consistently slightly larger than the 5.5 mm neck size scaffold that was electrospun on a 4 mm parent vessel. For reference, those neck sizes measured to be 5.51 mm ± 0.03 mm for the parallel neck diameter, and 5.67 mm ± 0.07 mm for the perpendicular neck diameter, respectively. For the scaffold with the large, elliptical neck aneurysm, the parallel neck diameter was measured to be 9.07 mm ± 0.16 mm and the perpendicular neck diameter was measured to be 6.45 mm ± 0.14 mm, which was also slightly

larger than the specifications on the Solidworks models. This could be due to the saran-wrapping step when creating the wax mandrel. Because the parent vessel was much larger, more saran wrap was utilized to completely cover the mandrel. It was speculated previously that saran wrapping could add height or length due to the thickness of the plastic itself or due to ridges created when the heat gun was applied to shrink the wrap over the mandrel. For the large, elliptical neck aneurysm, skewed measurements could also be due to SEM imaging. Because the aneurysm was much larger, the sample could have been tilted more than expected, which could have affected the measurements.

Even though there was a greater disparity between measurements and specifications with the aneurysms on the 6 mm parent vessel than on the 4 mm parent vessel, the difference was only about 1 mm, and distinct neck sizes were still accurately electrospun. Future work could be done to reduce this difference or to better characterize large scaffolds. Nonetheless, these aneurysms demonstrate that distinct geometries can be electrospun on different parent vessel diameters. In addition, the elliptical neck aneurysm demonstrates that geometries that are larger than the current blister geometry are possible utilizing our current electrospinning process. These examples both enhance the versatility of the aBVM model.

4.2.3 ImageJ Measurement Variation of Scaffolds Due to SEM Imaging

One challenge of taking measurements using ImageJ of SEM images is the resulting variability of measured values. When measuring the neck sizes of the aneurysm scaffolds, any tilting of the sample during imaging can cause the measurements to be slightly skewed. Additionally, clear SEM images were not always obtained due to difficulties in optimizing their

quality. Because of this, it was difficult to determine the edges of the neck of the aneurysm, which lead to a larger variation of measured values due to human judgment.

Table 4.1 and Figure 27 below illustrate the range of the measurements from the varying neck size scaffolds that could reasonably be determined from the SEM images. The smallest and largest values that could potentially be measured for the neck sizes were determined. The ranges of reasonable measurements spanned less than 1.5 mm for all scaffolds, though most ranges spanned around 0.5 mm.

Table 4.1: ImageJ Measurement Variation for Varying Neck Size Scaffolds

Measurement	2.3 mm Neck	3.5 mm Neck	5.5 mm Neck
Smallest Parallel Neck Measurement (mm)	1.74	2.96	5.13
Largest Parallel Neck Measurement (mm)	2.24	3.70	5.69
Smallest Perpendicular Neck Measurement (mm)	1.50	3.04	4.51
Largest Perpendicular Neck Measurement (mm)	2.32	3.69	5.89

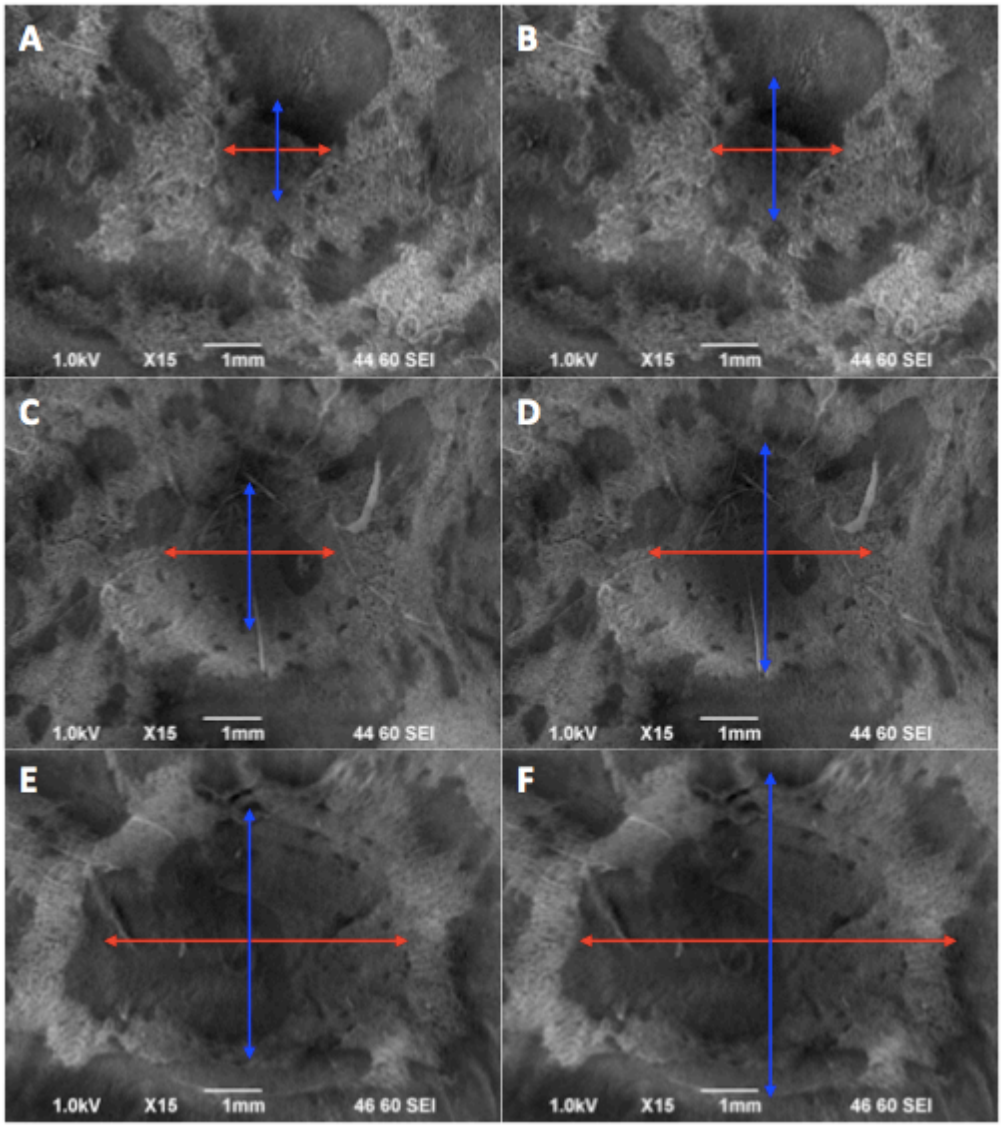

Figure 27: Visualization of reasonable ImageJ measurement variation of varying neck size scaffolds at x15 magnification due to human judgment. The left column represents measurements that could have been made on the lower end of the range, and the right column represents measurements that could have been made on the higher end of the range. The top-most row contains annotated images of the 2.3 mm scaffold. The middle row contains image of the 3.5 mm scaffold. The bottom-most row contains annotated images of the 5.5 mm scaffold. Red arrows indicate the parallel neck diameters and blue arrows indicate the perpendicular neck diameter. Flow direction was oriented horizontally.

A range that encompassed the variation in potential neck size scaffold measurements was also determined for the aneurysm neck size variations that were designed on a 6 mm parent vessel. Table 4.2 and Figure 28 below illustrate this variation that could reasonably be determined. Similar to the varying neck size scaffolds on a 4 mm parent vessel, the smallest and largest values that could potentially be measured for the neck sizes were determined.

Table 4.2: ImageJ Measurement Variation for Varying Neck Size Scaffolds on a 6 mm Parent Vessel

Measurement	5.5 mm Neck	8 x 6 mm Elliptical Neck
Smallest Parallel Neck Measurement (mm)	5.43	8.20*
Largest Parallel Neck Measurement (mm)	7.34	10.88*
Smallest Perpendicular Neck Measurement (mm)	5.17	5.94**
Largest Perpendicular Neck Measurement (mm)	7.05	7.65**

* Parallel neck on elliptical aneurysm base was originally dimensioned to be 8 mm

** Perpendicular neck on elliptical aneurysm base was originally dimensioned to be 6 mm

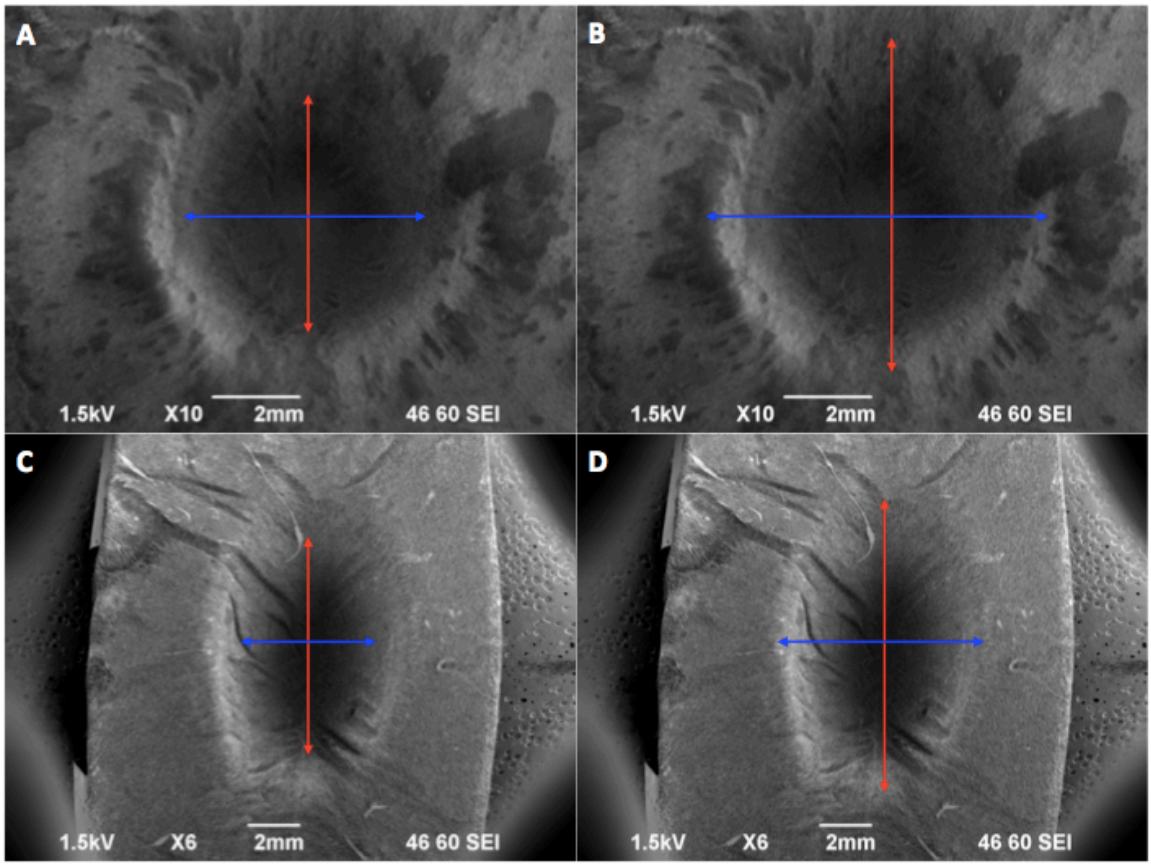

Figure 28: Visualization of reasonable ImageJ measurement variation of varying neck size scaffolds on a 6 mm parent vessel due to human judgment. The left column represents measurements that could have been made on the lower end of the range, and the right column represents measurements that could have been made on the higher end of the range. The top row contains annotated images of the 5.5 mm scaffold at x10 magnification. The bottom row contains annotated images of the elliptical base 6 x 8 mm scaffold at x6 magnification. Red arrows indicate the parallel neck diameters and blue arrows indicate the perpendicular neck diameter. Flow direction was oriented vertically.

The measurement ranges were much larger on the scaffold variations on the 6 mm parent vessels than on the neck variations on the 4 mm parent vessels. This was consistent with the

scaffold measurements that were taken in the previous section because those measurements were not as close to their respective dimensions as the measurements taken of the varying neck scaffolds on 4 mm parent vessels. Since the aneurysms were much larger, it may have been more difficult to adjust the contrast so that the aneurysm dome was completely dark, and a clear edge could be identified, like the current blister aneurysm geometries in the lab. One future project that could build upon this work would be how to best optimize the contrast for different aneurysm sizes in order to get a clear edge to make accurate measurements.

4.3 Conclusion

Aims 2 and 3 were successfully accomplished with new aneurysm geometries varying neck size and height in order to expand the aBVM model for neurovascular device testing. Methods of aneurysm characterization were developed, and scaffolds were tested for feasible use as aBVMs through the implantation of flow diverters.

5 Overall Discussion and Conclusions

5.1 Summary

The work in this thesis demonstrated the development of customized aneurysm scaffolds based off human clinical cases and rabbit elastase models for use as aBVMs for flow diverter implantation.

The first aim of this work was to explore and identify different aneurysm geometries and dimensions found in rabbit models and human clinical settings. Critical dimensions of height and neck size were gathered. It was determined that for human models, the neck diameter can range from 1.35 mm – 9 mm, with the range of 3 mm – 6 mm being the most common, and height can range from 1.27 mm – 14 mm, with the range of 3 mm – 10 mm being the most important to capture in preclinical models. For rabbit elastase models, it was seen that the neck diameter spans a narrower range of 2.3 mm – 5.5 mm. The height can range from 1.7 mm – 16.8 mm, with a more common range between 2 mm – 8 mm. Human models were found to be more variable for height, neck size, and other dimensions compared to rabbit models. In addition, human models were harder to interpret due to their complexity and variability, making the rabbit elastase model a better foundation to replicate aneurysm geometries in vitro. From these values, varying neck diameters and heights were chosen to create new aneurysm scaffold geometries.

The second aim of this thesis was to fabricate and characterize aneurysm geometry variations based on common rabbit and human anatomies. From the literature review, aneurysm neck sizes of 2.3 mm, 3.5 mm, and 5.5 mm and heights of 2 mm, 5 mm, and 8 mm were selected. Before scaffolds could be designed and fabricated, characterization methods for measurement were also put into place. Then, CAD models were machined, custom aneurysm wax mandrels were molded, and scaffolds were successfully electrospun. Scaffolds were cut and successfully

imaged using the scanning electron microscope for visualization of each geometry. These scaffolds were characterized using internal dimensions measured with ImageJ from the SEM images in addition to external dimensions using calipers.

The third and final aim of this thesis was to evaluate new aneurysm geometries for feasibility in aBVM models. Scaffolds of varying neck sizes were set up for use as aBVMs in a perfusion bioreactor system, and constructs were successfully created by depositing human smooth muscle cells and human endothelial cells into the scaffold lumens using a dual-sodding technique. A thick, confluent cell lining was observed throughout all portions of each scaffold. In addition, flow diverters were deployed in these constructs to evaluate this model's capability for testing neurovascular devices. Constructs of all geometries withstood deployment, and cell coverage after 3 days was observed over some stent struts, showing initial healing. In addition, the aneurysms were clearly visualized using SEM imaging, which demonstrated that healing could be tracked across the neck at longer time points.

Overall, these results showed that varying aneurysm dimensions to create different geometries that mimic rabbit and human models can be designed and fabricated. Additionally, these scaffolds are feasible as aBVMs in vitro, and could be used as a preclinical model for testing neurovascular devices.

5.2 Contributions

The aBVM work in the Cal Poly Tissue Engineering research lab mainly started with Shen et al. [82], a previous team of masters students and undergrads. Through published work, Shen et al. demonstrated feasibility of deploying flow diverters in straight BVMs and tracking healing throughout the vessels at different time points. In addition, the team developed a protocol

for creating customized, electrospun aneurysm scaffolds for use as an in vitro model. Using this protocol, blister, saccular, and fusiform aneurysm geometries were successfully electrospun and cell deposition using 3T3s showed feasibility as a proof of concept cell type.

The work presented in this thesis built upon Shen et al. and focused on the creation and characterization of aneurysm scaffolds. In this thesis, distinct aneurysm geometries were created that were defined by dimensions rather than shape; in particular, neck sizes and heights were predetermined and specified during CAD modeling of the aneurysm molds. A consistent method was developed in order to control these dimensions, providing insight on the limitations of possible combinations of neck sizes and heights. Additionally, methods were also developed for evaluating scaffolds through internal dimensions that were specified in the CAD models, which are most critical for neurovascular device testing.

After characterization of these geometries, feasibility studies were performed for scaffolds with varying neck diameters to evaluate their use as in vitro models for testing neurovascular devices. This was the first time demonstrating the possibility of using a dual-sodding technique to deposit both human smooth muscle cells and endothelial cells in aneurysm scaffolds of varying neck size geometries. In addition, these scaffolds with varying neck sizes also withstood flow diverter deployment and exhibited initial healing in the parent vessel. A thick, confluent cell layer was observed in both the aneurysm dome and the parent vessel region in all geometries; however, cell morphology in the aneurysm dome may not be important. Flow diverter treatment relies upon the reconstruction of the parent vessel at the neck of the aneurysm dome. Previous studies have hypothesized that the cells along the parent vessel migrate over neck and utilize the stent as a scaffold to construct the neointima [110, 111], demonstrating that the cells in the dome may not be crucial to the healing process. In contrast, the success of

treatment by embolization coiling can depend on the height and width of the aneurysm dome [85]; however, the initial mechanism of healing relies on clotting the aneurysm sac to prevent blood flow, which leads to the eventual growth of the endothelium from cells originating from the parent vessel [112]. In this case, the cells involved in the healing process are circulating red blood cells in addition to the cells of the parent artery, and not the cells within the aneurysm dome. Because a thin layer of uniaxial fibers in the aneurysm dome was observed in the resulting scaffolds of varying height geometries, it is uncertain if the same success of a thick, confluent cell layer that was seen in varying neck geometries could also be cultivated within these scaffolds. However, because these cells may not play a role in healing aneurysms and, therefore, determine the effectiveness of the device tested, a confluent cell layer in the dome may not be required for the aBVM model to be successful as long as there was a prominent cell layer in the parent vessel region. It can be reasonably concluded that a cell layer could be cultivated in the scaffolds with varying height geometries because their microstructures in the parent artery region were similar in all vessels to those of the varying neck size geometries.

The aBVMs presented in this work have many potential advantages when compared to other preclinical benchtop, in vitro, and in vivo aneurysm models. Though many benchtop models were successful in generating hemodynamic blood flow profiles through an aneurysm [113, 114] and allowed for early stage device testing [71–73], they lacked the biological aspect of cells that comprise the parent vessel. In flow diverters specifically, healing over the aneurysm neck is the primary goal of the device treatment [44, 45]. A few in vitro studies have incorporated human endothelial cells with their aneurysm models [75, 76], but these models were used primarily to study cellular responses due to hemodynamic changes, rather than for device testing. In addition, electrospun scaffolds more closely mimic the extracellular matrix of

native tissue, allowing for increased cell adhesion. When compared to rabbit elastase models, aBVMs have many logistical advantages. The process to create these electrospun scaffolds has the potential to be more reproducible, and can be customized to fit the requirements of specific device studies. aBVMs are less expensive and do not require highly trained technicians. Even though in vitro models will most likely never replace in vivo models, they could be used to screen different device designs before moving to preclinical animal testing.

5.3 Limitations and Next Steps

During development of this thesis work, several limitations were encountered with regard to creation of the geometries. In designing the CAD models, many combinations of neck and height sizes could be achieved; however, due to the limitation of the continuous dome feature on Solidworks, heights were limited by the diameter of the neck, and tall heights could only be accommodated by large neck sizes. It was also determined that saccular geometries could not be accurately electrospun using the current setup because it required the aneurysm neck to be completely exposed in order for the fibers to conform to the designated geometry. Because of this, aneurysm domes were cone-shaped, which was acceptable for this application of flow diverter testing. In other cases, however, aneurysm shape may be important. A future project could work on different ways to deposit fibers onto aneurysm mandrels such as changing the direction of the polymer stream, adding multiple syringes that target the mandrel at a different angle, or adding more movement to the collector to expose different areas of the geometry to the polymer stream.

Regarding the process of creating aneurysm scaffolds, the saran-wrapping step proved to be another limitation. Not only was this step of the process extremely difficult and time

consuming, but it also could have contributed to slight geometric changes. Ridges created by the plastic wrap during shrinking over the mandrel could add variation to the geometry, and exposure to the heat gun could melt the aneurysm dome. This step could be removed from the process by finding a wax that does not affect cell growth on the scaffold, and this would decrease process time and variation of the scaffold outputs.

Many future studies could be done using these aneurysm geometries as aBVMs to test neurovascular devices. Flow diverters were only tested at 3 days for this work, and they could be evaluated at different and longer time points to compare healing over all portions of the vessel. In addition, different devices could also be evaluated in all relevant scaffold variations. For example, embolization coils could be tested using the geometries that vary aneurysm height. In order to incorporate new aneurysm geometries that are similar to human models, larger aneurysms can be created on larger parent arteries and tested for feasible use as aBVMs. Additionally, different vessel configurations with more complex shapes could be designed utilizing these geometries. When researching literature on human models, bifurcation aneurysms were commonly found, and if bifurcated aneurysms could be designed, electrospun, and used as aBVMs, they would be extremely relevant to human models. Additionally, adding bends and curves to replicate the tortuous anatomy found in the Circle of Willis would also create a physiologically relevant model.

Another design consideration that would greatly improve the aBVM model, though beyond the scope of this thesis work, would be to more closely replicate the flow environment seen in the Circle of Willis. Currently, aBVMs utilize a low and steady flow in order to carry nutrients and waste away from the cells; however, the hemodynamics of the current conditions are not close to the shear stresses that endothelial cells experience. Adding pulsatile flow at

physiologically relevant pressures to expose the cells to oscillatory shear is relevant, and the cell phenotype and behavior could possible be closer to what is seen in the disease state.

5.4 Conclusion

In conclusion, the work presented in this thesis accomplished critical steps to creating an appropriate in vitro aneurysm model for early stage preclinical testing of neurovascular devices for treating hemorrhagic stroke. A literature review was performed to establish ranges of aneurysm heights and neck sizes that characterize both human models and rabbit elastase models. New geometries were then designed into molds and machined, and mandrels and scaffolds were generated. Methods were then developed to properly characterize the internal dimensions of these scaffolds. In addition, aBVM constructs were successfully created using a dual-sodding technique to deposit human endothelial and smooth muscle cells onto the scaffolds. Lastly, flow diverters were implanted into a subset of constructs and demonstrated feasibility and initial healing. Custom aneurysm scaffolds can eventually lead to more efficient, accurate preclinical testing of neurovascular devices. Effective preclinical in vitro testing can save time and money throughout the design process of a medical device by reducing the amount of in vivo studies needed for sufficient demonstration of safety. More specifically, the geometric variations of the aneurysms in the model can allow researchers to better understand the cellular responses and aneurysm healing mechanisms in a wide variety of cases, resulting in the creation of better devices that will directly prevent hemorrhagic stroke.

REFERENCES

1. Keedy A (2006) An overview of intracranial aneurysms. McGill J Med
2. Austin GM, Fisher S, Dickson D, Anderson D, Richardson S (1993) The significance of the extracellular matrix in intracranial aneurysms. Ann Clin Lab Sci
3. Schievink WI, Wijdicks EFM, Parisi JE, Piepgras DG, Whisnant JP (1995) Sudden death from aneurysmal subarachnoid hemorrhage. Neurology. doi: 10.1212/WNL.45.5.871
4. Fogelholm R, Hernesniemi J, Vapalahti M (1993) Impact of early surgery on outcome after aneurysmal subarachnoid hemorrhage: A population-based study. Stroke. doi: 10.1161/01.STR.24.11.1649
5. Brisman JL, Song JK, Newell DW (2006) Cerebral Aneurysms. N Engl J Med 355:928–939 . doi: 10.1056/NEJMra052760
6. Jalali Kondori B, Azemati F, Dadseresht S (2017) Magnetic resonance angiographic study of anatomic variations of the circle of willis in a population in Tehran. Arch Iran Med
7. Shahan CP, Gray RI, Croce MA, Fabian TC (2017) Impact of circle of Willis anatomy in traumatic blunt cerebrovascular injury-related stroke. Trauma Surg Acute Care Open. doi: 10.1136/tsaco-2017-000086
8. Castro MA, Putman CM, Sheridan MJ, Cebral JR (2009) Hemodynamic patterns of anterior communicating artery aneurysms: A possible association with rupture. Am J Neuroradiol. doi: 10.3174/ajnr.A1323
9. Stehbens WE (1990) Pathology and pathogenesis of intracranial berry aneurysms. Neurol Res. doi: 10.1080/01616412.1990.11739909
10. Abe M, Tabuchi K, Yokoyama H, Uchino A (2009) Blood blisterlike aneurysms of the internal carotid artery. J Neurosurg. doi: 10.3171/jns.1998.89.3.0419

11. Guo S, Jiang P, Liu J, Yang X, Jiang C, Li Y, Wu Z (2018) A comparative CFD analysis of common carotid fusiform aneurysm in canine models and vertebrobasilar fusiform aneurysm in human patients. Int Angiol. doi: 10.23736/S0392-9590.17.03869-X

12. Friedman AH, Drake CG (2009) Subarachnoid hemorrhage from intracranial dissecting aneurysm. J Neurosurg. doi: 10.3171/jns.1984.60.2.0325

13. Lin CT, Tranmer B, Durham S, Johnson D, Hamlin M, Bolman RM (2017) Ruptured Mycotic Aneurysm and Cerebral Vasospasm in the Setting of Endocarditis and Heart Failure Requiring Cardiothoracic Surgery: Case Report and Literature Review. World Neurosurg. doi: 10.1016/j.wneu.2017.01.076

14. Fennell VS, Kalani MYS, Atwal G, Martirosyan NL, Spetzler RF (2016) Biology of Saccular Cerebral Aneurysms: A Review of Current Understanding and Future Directions. Front Surg. doi: 10.3389/fsurg.2016.00043

15. Starke RM, Chalouhi N, Ali MS, Jabbour PM, Tjoumakaris SI, Gonzalez LF, Rosenwasser RH, Koch WJ, Dumont AS (2013) The role of oxidative stress in cerebral aneurysm formation and rupture. Curr Neurovasc Res

16. Starke RM, Chalouhi N, Ding D, Raper DMS, Mckisic MS, Owens GK, Hasan DM, Medel R, Dumont AS (2014) Vascular Smooth Muscle Cells in Cerebral Aneurysm Pathogenesis. Transl Stroke Res. doi: 10.1007/s12975-013-0290-1

17. Nakagawa T, Hashi K (2009) The incidence and treatment of asymptomatic, unruptured cerebral aneurysms. J Neurosurg. doi: 10.3171/jns.1994.80.2.0217

18. Hirai S, Ono J, Odaki M, Serizawa T, Sato M, Isobe K, Sunami K, Kubota M, Saeki N, Yamaura A (2001) Treatment of asymptomatic unruptured intracranial aneurysms. A clinical decision analysis. Interv Neuroradiol

19. Chicoine MR (2003) Microsurgery and Clipping: The Gold Standard for the Treatment of Intracranial Aneurysms. J Neurosurg Anesthesiol. doi: 10.1097/00008506-200301000-00013

20. Lafuente J, Maurice-Williams RS (2003) Ruptured intracranial aneurysms: The outcome of surgical treatment in experienced hands in the period prior to the advent of endovascular coiling. J Neurol Neurosurg Psychiatry. doi: 10.1136/jnnp.74.12.1680

21. Grasso G, Perra G (2017) Surgical management of ruptured small cerebral aneurysm: Outcome and surgical notes. Surg Neurol Int. doi: 10.4103/2152-7806.171257

22. Gross BA, Du R (2013) Microsurgical treatment of ophthalmic segment aneurysms. J Clin Neurosci. doi: 10.1016/j.jocn.2012.11.005

23. Cerebral Aneurysms. In: AANS Am. Assoc. Neurol. Surg. www.aans.org/Patients/Neurosurgical-Conditions-and-Treatments/Cerebral-Aneurysm.

24. Zhao J, Lin H, Summers R, Yang M, Cousins BG, Tsui J (2017) Current Treatment Strategies for Intracranial Aneurysms: An Overview. Angiology. doi: 10.1177/0003319717700503

25. Zhu Y, Zhang H, Zhang Y, Wu H, Wei L, Zhou G, Zhang Y, Deng L, Cheng Y, Li M, Santos HA, Cui W (2019) Endovascular Metal Devices for the Treatment of Cerebrovascular Diseases. Adv. Mater.

26. Zubillaga AF, Guglielmi G, Vinuela F, Duckwiler GR (1994) Endovascular occlusion of intracranial aneurysms with electrically detachable coils: Correlation of aneurysm neck size and treatment results. Am J Neuroradiol

27. (2017) Endovascular Coiling [Image]. In: Mayo Clin. https://www.mayoclinic.org/diseases-conditions/brain-aneurysm/multimedia/aneurysm-

coil/img-20007617

28. White JB, Ken CGM, Cloft HJ, Kallmes DF (2008) Coils in a nutshell: A review of coil physical properties. Am. J. Neuroradiol.

29. Ota K, Matsubara N, Miyachi S, Izumi T, Ito M, Asai T, Yamanouchi T, Wakabayashi T (2017) Evaluation of the characteristics of various types of finishing coils for the embolization of intracranial aneurysms in an experimental model with radiolucent coils. Interv Neuroradiol. doi: 10.1177/1591019916685713

30. Murphy KJ, Houdart E, Szopinski KT, Levrier O, Guimaraens L, Kühne D, Solymosi L, Bartholdy NJ, Rüfenacht DA (2013) Mechanical Detachable Platinum Coil: Report of the European Phase II Clinical Trial in 60 Patients. Radiology. doi: 10.1148/radiology.219.2.r01ma38541

31. Marks MP, Chee H, Liddell RP, Steinberg GK, Panahian N, Lane B (1994) A mechanically detachable coil for the treatment of aneurysms and occlusion of blood vessels. Am J Neuroradiol

32. Reinges MHT, Krings T, Drexler AY, Ludolph A, Sellhaus B, Bovi M, Geibprasert S, Agid R, Scherer K, Hans FJ (2010) Bare, bio-active and hydrogel-coated coils for endovascular treatment of experimentally induced aneurysms: Long-term histological and scanning electron microscopy results. Interv Neuroradiol. doi: 10.1177/159101991001600205

33. Medical Advisory Secretariat (2006) Coil embolization for intracranial aneurysms: an evidence-based analysis. Ont Health Technol Assess Ser

34. Yoon NK, Awad A-W, Kalani MYS, Taussky P, Park MS (2017) Stent technology in ischemic stroke. Neurosurg Focus. doi: 10.3171/2017.1.focus16507

35. Matsuda Y, Chung J, Keigher K, Lopes D (2018) A comparison between the new Low-profile Visualized Intraluminal Support (LVIS Blue) stent and the Flow Redirection Endoluminal Device (FRED) in bench-top and cadaver studies. J Neurointerv Surg. doi: 10.1136/neurintsurg-2017-013074

36. Piotin M, Blanc R (2014) Balloons and stents in the endovascular treatment of cerebral aneurysms: Vascular anatomy remodeled. Front. Neurol.

37. Leyon JJ, Chavda S, Lamin S (2016) Corking the WEB and coiling through a jailed microcatheter: WEB assisted coiling, a useful technique avoiding the use of stents in treating wide-necked large intracranial aneurysms. J Neurointerv Surg. doi: 10.1136/bcr-2015-011649

38. Takeshita T, Nagamine T, Ishihara K, Kaku Y (2017) Stent-assisted coil embolization of a recurrent posterior cerebral artery aneurysm following surgical clipping. Neuroradiol J 30:99–103 . doi: 10.1177/1971400916678243

39. Kim M, Levy EI, Meng H, Hopkins LN (2007) Quantification of hemodynamic changes induced by virtual placement of multiple stents across a wide-necked basilar trunk aneurysm. Neurosurgery. doi: 10.1227/01.neu.0000306110.55174.30

40. Stoeckel D, Bonsignore C, Duda S (2002) A survey of stent designs. Minim Invasive Ther Allied Technol. doi: 10.1080/136457002760273340

41. Wanke I, Forsting M (2008) Stents for intracranial wide-necked aneurysms: More than mechanical protection. Neuroradiology

42. Benndorf G, Herbon U, Sollmann WP, Campi A (2001) Treatment of a ruptured dissecting vertebral artery aneurysm with double stent placement: Case report. Am J Neuroradiol

43. (2015) Flow Diverter [Image]. http://www.massdevice.com/wp-content/uploads/files/logos/pegasus-device-large-3x2.jpg

44. Linfante I, Mayich M, Sonig A, Fujimoto J, Siddiqui A, Dabus G (2017) Flow diversion with pipeline embolic device as treatment of subarachnoid hemorrhage secondary to blister aneurysms: Dual-center experience and review of the literature. J. Neurointerv. Surg.

45. Durso PI, Lanzino G, Cloft HJ, Kallmes DF (2011) Flow diversion for intracranial aneurysms: A review. Stroke

46. Wakhloo AK, Gounis MJ (2007) Revolution in aneurysm treatment: Flow diversion to cure aneurysms: A paradigm shift. In: Neurosurgery

47. Raymond J, Darsaut TE, Makoyeva A, Bing F, Salazkin I (2013) Endovascular treatment with flow diverters may fail to occlude experimental bifurcation aneurysms. Neuroradiology. doi: 10.1007/s00234-013-1272-4

48. Piotin M, Biondi A, Sourour N, Mounayer C, Jaworski M, Mangiafico S, Andersson T, Soderman M, Goffette P, Anxionnat R, Blanc R (2018) The LUNA aneurysm embolization system for intracranial aneurysm treatment: Short-term, mid-term and long-term clinical and angiographic results. J Neurointerv Surg. doi: 10.1136/neurintsurg-2018-013767

49. Dmytriw AA, Salem MM, Yang VXD, Krings T, Pereira VM, Moore JM, Thomas AJ (2019) Endosaccular Flow Disruption: A New Frontier in Endovascular Aneurysm Management. Neurosurgery. doi: 10.1093/neuros/nyz017

50. Perez MA, Bhogal P, Moreno RM, Bäzner H, Ganslandt O, Henkes H (2017) The medina embolic device: Early clinical experience from a single center. J Neurointerv Surg. doi:

10.1136/neurintsurg-2016-012539

51. Rajah G, Narayanan S, Rangel-Castilla L (2017) Update on flow diverters for the endovascular management of cerebral aneurysms. Neurosurg Focus. doi: 10.3171/2017.3.focus16427

52. (2019) Woven EndoBridge (WEB) Aneurysm Embolization System - P170032 [Image]. In: U.S. Food Drug Adm. https://www.fda.gov/medical-devices/recently-approved-devices/woven-endobridge-web-aneurysm-embolization-system-p170032

53. Murthy SB, Shah S, Shastri A, Venkatasubba Rao CP, Bershad EM, Suarez JI (2014) The SILK flow diverter in the treatment of intracranial aneurysms. J. Clin. Neurosci.

54. Bender MT, Colby GP, Jiang B, Lin LM, Campos JK, Xu R, Westbroek EM, Vo CD, Zarrin DA, Caplan JM, Huang J, Tamargo RJ, Coon AL (2019) Flow diversion of posterior circulation cerebral aneurysms: A single-institution series of 59 cases. In: Clinical Neurosurgery

55. Ryan RW, Khan AS, Barco R, Choulakian A (2017) Pipeline flow diversion of ruptured blister aneurysms of the supraclinoid carotid artery using a single-device strategy. Neurosurg Focus. doi: 10.3171/2017.3.focus1757

56. Hamamdzic D, Wilensky RL (2013) Porcine Models of Accelerated Coronary Atherosclerosis: Role of Diabetes Mellitus and Hypercholesterolemia. J Diabetes Res. doi: 10.1155/2013/761415

57. Bouzeghrane F, Naggara O, Kallmes DF, Berenstein A, Raymond J (2010) In vivo experimental intracranial aneurysm models: A systematic review. Am. J. Neuroradiol.

58. Ysuda R, Strother CM, Aagaard-Kienitz B, Pulfer K, Consigny D (2012) A large and giant bifurcation aneurysm model in canines: Proof of feasibility. Am J Neuroradiol. doi:

10.3174/ajnr.A2789

59. da Silva Morais A, Oliveira JM, Reis RL (2018) Small animal models. In: Advances in Experimental Medicine and Biology

60. Brinjikji W, Ding YH, Kallmes DF, Kadirvel R (2016) From bench to bedside: Utility of the rabbit elastase aneurysm model in preclinical studies of intracranial aneurysm treatment. J. Neurointerv. Surg.

61. Mapara M, Thomas BS, Bhat KM (2012) Rabbit as an animal model for experimental research. Dent Res J (Isfahan). doi: 10.4103/17353327.92960

62. Wancket LM (2015) Animal Models for Evaluation of Bone Implants and Devices: Comparative Bone Structure and Common Model Uses. Vet Pathol. doi: 10.1177/0300985815593124

63. Altes TA, Cloft HJ, Short JG, Degast A, Do HM, Helm GA, Kallmes DF (2000) Creation of saccular aneurysms in the rabbit: A model suitable for testing endovascular devices. Am J Roentgenol. doi: 10.2214/ajr.174.2.1740349

64. Rietschel B, Arrey TN, Meyer B, Bornemann S, Schuerken M, Karas M, Poetsch A (2009) Elastase digests: new ammunition for shotgun membrane proteomics. Mol Cell Proteomics

65. Zeng Z, Kallmes DF, Durka MJ, Ding Y, Lewis D, Kadirvel R, Robertson AM (2011) Hemodynamics and anatomy of elastase-induced rabbit aneurysm models: Similarity to human cerebral aneurysms? Am J Neuroradiol. doi: 10.3174/ajnr.A2324

66. Wang S, Dai D, Kolumam Parameswaran P, Kadirvel R, Ding YH, Robertson AM, Kallmes DF (2018) Rabbit aneurysm models mimic histologic wall types identified in human intracranial aneurysms. J Neurointerv Surg. doi: 10.1136/neurintsurg-2017-013264

67. Ding Y, Dai D, Kadirvel R, Lewis DA, Kallmes DF (2010) Creation of large elastase-induced aneurysms: Presurgical arterial remodeling using arteriovenous fistulas. Am J Neuroradiol. doi: 10.3174/ajnr.A2205

68. Ding YH, Dai D, Lewis DA, Danielson MA, Kadirvel R, Mandrekar JN, Cloft HJ, Kallmes DF (2006) Can neck size in elastase-induced aneurysms be controlled? A retrospective study. Am J Neuroradiol

69. Kainth D, Salazar P, Safinia C, Chow R, Bachour O, Andalib S, McKinney AM, Divani AA (2017) A Modified Method for Creating Elastase-Induced Aneurysms by Ligation of Common Carotid Arteries in Rabbits and Its Effect on Surrounding Arteries. J Vasc Interv Neurol

70. Chivukula VK, Levitt MR, Clark A, Barbour MC, Sansom K, Johnson L, Kelly CM, Geindreau C, Rolland du Roscoat S, Kim LJ, Aliseda A (2019) Reconstructing patient-specific cerebral aneurysm vasculature for in vitro investigations and treatment efficacy assessments. J Clin Neurosci. doi: 10.1016/j.jocn.2018.10.103

71. Gester K, Luchtefeld I, Busen M, Sonntag SJ, Linde T, Steinseifer U, Cattaneo G (2016) In vitro evaluation of intra-aneurysmal, flow-diverter-induced thrombus formation: A feasibility study. Am J Neuroradiol. doi: 10.3174/ajnr.A4555

72. Boyle AJ, Landsman TL, Wierzbicki MA, Nash LD, Hwang W, Miller MW, Tuzun E, Hasan SM, Maitland DJ (2016) In vitro and in vivo evaluation of a shape memory polymer foam-over-wire embolization device delivered in saccular aneurysm models. J Biomed Mater Res - Part B Appl Biomater. doi: 10.1002/jbm.b.33489

73. Dholakia RJ, Kappel AD, Pagano A, Woo HH, Lieber BB, Fiorella DJ, Sadasivan C (2018) In vitro angiographic comparison of the flow-diversion performance of five

neurovascular stents. Interv Neuroradiol. doi: 10.1177/1591019917748317

74. Sugiu K, Tokunaga K, Sasahara W, Watanabe K, Nishida A, Katsumata A, Kusaka N, Date I, Ohmoto T, Rufenacht DA (2017) Training in Neurovascular Intervention Usefulness of in-Vitro Model and Clinical Practice. Interv Neuroradiol. doi: 10.1177/15910199040100s118

75. Kaneko N, Mashiko T, Namba K, Tateshima S, Watanabe E, Kawai K (2018) A patient-specific intracranial aneurysm model with endothelial lining: A novel in vitro approach to bridge the gap between biology and flow dynamics. J Neurointerv Surg. doi: 10.1136/neurintsurg-2017-013087

76. Levitt MR, Mandrycky C, Abel A, Kelly CM, Levy S, Chivukula VK, Zheng Y, Aliseda A, Kim LJ (2019) Genetic correlates of wall shear stress in a patient-specific 3D-printed cerebral aneurysm model. J Neurointerv Surg. doi: 10.1136/neurintsurg-2018-014669

77. Touroo JS, Williams SK (2012) A tissue-engineered aneurysm model for evaluation of endovascular devices. J Biomed Mater Res - Part A. doi: 10.1002/jbm.a.34256

78. Cardinal KO, Bonnema GT, Hofer H, Barton JK, Williams SK (2006) Tissue-Engineered Vascular Grafts as In Vitro Blood Vessel Mimics for the Evaluation of Endothelialization of Intravascular Devices . Tissue Eng. doi: 10.1089/ten.2006.12.ft-268

79. Gibbons MC, Foley MA, Cardinal KO (2012) Thinking Inside the Box: Keeping Tissue-Engineered Constructs In Vitro for Use as Preclinical Models . Tissue Eng Part B Rev. doi: 10.1089/ten.teb.2012.0305

80. Touroo JS, Dale JR, Williams SK (2012) Bioengineering Human Blood Vessel Mimics for Medical Device Testing Using Serum-Free Conditions and Scaffold Variations. Tissue Eng Part C Methods. doi: 10.1089/ten.tec.2012.0311

81. Herting S, DiBartolomeo A, Pipes T, Kunz S, Temnyk K, Truty J, Ur S, Cardinal KO (2016) Human Umbilical Versus Coronary Cell Sources for Tissue-Engineered Blood Vessel Mimics. Appl Vitr Toxicol. doi: 10.1089/aivt.2016.0012

82. Shen TW, Puccini B, Temnyk K, Herting S, Cardinal KO (2019) Tissue-engineered aneurysm models for in vitro assessment of neurovascular devices. Neuroradiology. doi: 10.1007/s00234-019-02197-x

83. Elahi MF, Lu W (2013) Core-shell Fibers for Biomedical Applications-A Review. J Bioeng Biomed Sci. doi: 10.4172/2155-9538.1000121

84. Simpson DG, Bowlin GL (2006) Tissue-engineering scaffolds: Can we re-engineer mother nature? Expert Rev. Med. Devices

85. Fang C, Li MH, Zhu YQ, Tan HQ, Zhang PL, Xu HW, Wang W, Zhou B (2010) The Effectiveness and Feasibility of Endovascular Coil Embolization for Very Small Cerebral Aneurysms: Mid- and Long-Term Follow-Up. Ann Vasc Surg. doi: 10.1016/j.avsg.2009.10.005

86. Pierot L, Spelle L, Vitry F (2008) Immediate clinical outcome of patients harboring unruptured intracranial aneurysms treated by endovascular approach: Results of the ATENA study. Stroke. doi: 10.1161/STROKEAHA.107.512756

87. Brinjikji W, Cloft HJ, Kallmes DF (2009) Difficult aneurysms for endovascular treatment: Overwide or undertall? Am J Neuroradiol. doi: 10.3174/ajnr.A1633

88. Fujiwara NH, Kallmes DF (2002) Healing response in elastase-induced rabbit aneurysms after embolization with a new platinum coil system. Am J Neuroradiol

89. Ben-Joseph O, Bensussen S (2018) Neurovascular Device Market: Poised for Growth. MedTech Strateg 5:19–26

90. FDA (2016) Recommended Content and Format of Non-Clinical Bench Performance Testing Information in Premarket Submissions

91. FDA (2015) General Considerations for Animal Studies for Medical Devices

92. Pugliese L, Marconi S, Negrello E, Mauri V, Peri A, Gallo V, Auricchio F, Pietrabissa A (2018) The clinical use of 3D printing in surgery. Updates Surg.

93. Jia ZY, Shi H Bin, Miyachi S, Hwang SM, Sheen JJ, Song YS, Kim JG, Lee DH, Suh DC (2018) Development of New Endovascular Devices for Aneurysm Treatment. J Stroke. doi: 10.5853/jos.2017.02229

94. Wang JL, Yuan ZG, Qian GL, Bao WQ, Jin GL (2018) 3D printing of intracranial aneurysm based on intracranial digital subtraction angiography and its clinical application. Medicine (Baltimore). doi: 10.1097/MD.0000000000011103

95. Seo J-H, Eslami P, Caplan J, Tamargo RJ, Mittal R (2018) A Highly Automated Computational Method for Modeling of Intracranial Aneurysm Hemodynamics. Front Physiol. doi: 10.3389/fphys.2018.00681

96. Zhang XJ, Gao BL, Li TX, Hao WL, Wu SS, Zhang DH (2018) Association of basilar bifurcation aneurysms with age, sex, and bifurcation geometry. Stroke. doi: 10.1161/STROKEAHA.118.020829

97. Rajabzadeh-Oghaz H, Varble N, Shallwani H, Tutino VM, Mowla A, Shakir HJ, Vakharia K, Atwal GS, Siddiqui AH, Davies JM, Meng H (2018) Computer-Assisted Three-Dimensional Morphology Evaluation of Intracranial Aneurysms. World Neurosurg. doi: 10.1016/j.wneu.2018.07.208

98. King RM, Brooks OW, Langan ET, Caroff J, Clarençon F, Tamura T, Wainwright JM, Gounis MJ, Marosfői M, Puri AS (2018) Communicating malapposition of flow diverters

assessed with optical coherence tomography correlates with delayed aneurysm occlusion. J Neurointerv Surg. doi: 10.1136/neurintsurg-2017-013502

99. Marosfoi M, Langan ET, Strittmatter L, Van Der Marel K, Vedantham S, Arends J, Lylyk IR, Loganathan S, Hendricks GM, Szikora I, Puri AS, Wakhloo AK, Gounis MJ (2017) In situ tissue engineering: Endothelial growth patterns as a function of flow diverter design. J Neurointerv Surg. doi: 10.1136/neurintsurg-2016-012669

100. Park H, Nakagawa I, Yokoyama S, Wada T, Motoyama Y, Kichikawa K, Nakase H (2019) Central Retinal Artery Thromboembolism without Ophthalmic Artery Occlusion During Stent-Assisted Coil Embolization of Ophthalmic Artery Aneurysm. World Neurosurg. doi: 10.1016/j.wneu.2018.09.184

101. Shi L, Yu J, Zhao Y, Xu K, Yu J (2018) Clipping treatment of posterior communicating artery aneurysms associated with arteriosclerosis and calcification: A single center study of 136 cases. Exp Ther Med. doi: 10.3892/etm.2017.5525

102. OISHI H, TERANISHI K, YATOMI K, FUJII T, YAMAMOTO M, ARAI H (2018) Flow Diverter Therapy Using a Pipeline Embolization Device for 100 Unruptured Large and Giant Internal Carotid Artery Aneurysms in a Single Center in a Japanese Population. Neurol Med Chir (Tokyo). doi: 10.2176/nmc.oa.2018-0148

103. Jiang P, Liu Q, Wu J, Chen X, Li M, Yang F, Li Z, Yang S, Guo R, Gao B, Cao Y, Wang R, Di F, Wang S (2018) Hemodynamic findings associated with intraoperative appearances of intracranial aneurysms. Neurosurg Rev. doi: 10.1007/s10143-018-1027-0

104. Rahman M, Smietana J, Hauck E, Hoh B, Hopkins N, Siddiqui A, Levy EI, Meng H, Mocco J (2010) Size ratio correlates with intracranial aneurysm rupture status: A prospective study. Stroke. doi: 10.1161/STROKEAHA.109.574244

105. Li Z, Zhao R, Fang X, Zhou J, Jiang G, Huang Q, Liu J (2017) AMD3100 Accelerates Reendothelialization of Neointima in Rabbit Saccular Aneurysm After Flow Diverter Treatment. World Neurosurg. doi: 10.1016/j.wneu.2017.07.128

106. Hoh BL, Rabinov JD, Pryor JC, Ogilvy CS (2004) A modified technique for using elastase to create saccular aneurysms in animals that histologically and hemodynamically resemble aneurysms in human. Acta Neurochir (Wien). doi: 10.1007/s00701-004-0276-6

107. Li ZF, Fang XG, Zhao R, Yang PF, Huang QH, Liu JM (2018) Stromal cell-derived factor 1α facilitates aneurysm remodeling in elastase-induced rabbit saccular aneurysm. Cytokine. doi: 10.1016/j.cyto.2017.07.020

108. Tronc F, Mallat Z, Lehoux S, Wassef M, Esposito B, Tedgui A (2000) Role of matrix metalloproteinases in blood flow-induced arterial enlargement: interaction with NO. Arterioscler Thromb Vasc Biol

109. Short JG, Fujiwara NH, Marx WF, Helm GA, Cloft HJ, Kallmes DF (2001) Elastase-induced saccular aneurysms in rabbits: Comparison of geometric features with those of human aneurysms. Am J Neuroradiol

110. Kallmes DF, Ding YH, Dai D, Kadirvel R, Lewis DA, Cloft HJ (2007) A new endoluminal, flow-disrupting device for treatment of saccular aneurysms. Stroke. doi: 10.1161/STROKEAHA.106.479576

111. Alderazi YJ, Shastri D, Kass-Hout T, Prestigiacomo CJ, Gandhi CD (2014) Flow diverters for intracranial aneurysms. Stroke Res. Treat.

112. Brinjikji W, Kallmes DF, Kadirvel R (2015) Mechanisms of healing in coiled intracranial aneurysms: A review of the literature. Am. J. Neuroradiol.

113. Sedlacik J, Frölich A, Spallek J, Forkert ND, Faizy TD, Werner F, Knopp T, Krause D,

Fiehler J, Buhk JH (2016) Magnetic particle imaging for high temporal resolution assessment of aneurysm hemodynamics. PLoS One. doi: 10.1371/journal.pone.0160097

114. Amili O, Schiavazzi D, Moen S, Jagadeesan B, Van De Moortele PF, Coletti F (2018) Hemodynamics in a giant intracranial aneurysm characterized by in vitro 4D flow MRI. PLoS One. doi: 10.1371/journal.pone.0188323

APPENDICES

APPENDIX A: DIAGRAMS AND ARTISTIC RENDITIONS OF CLINICAL ANEURYSM STUDIES

Purpose:

This appendix shows artistic renditions and diagrams of human aneurysm models (A.1-A.7) from the literature review in Chapter 2.

Figures

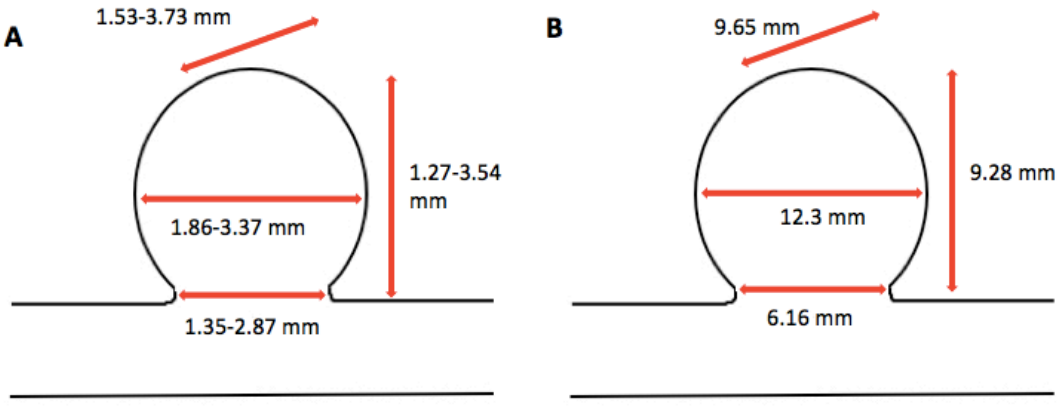

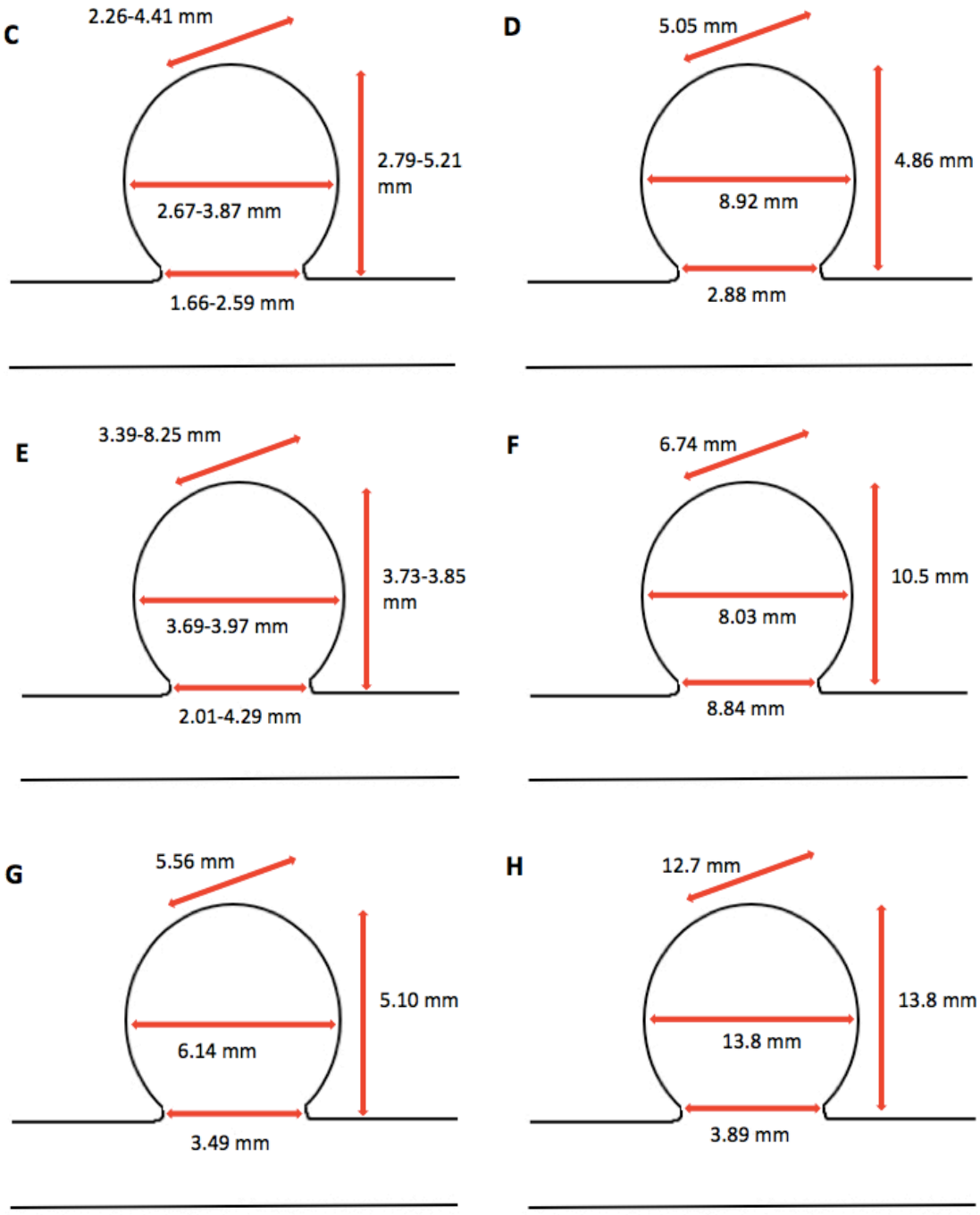
C
2.26-4.41 mm
2.79-5.21 mm
2.67-3.87 mm
1.66-2.59 mm
D
5.05 mm
4.86 mm
8.92 mm
2.88 mm
E
3.39-8.25 mm
3.73-3.85 mm
3.69-3.97 mm
2.01-4.29 mm
F
6.74 mm
10.5 mm
8.03 mm
8.84 mm
G
5.56 mm
5.10 mm
6.14 mm
3.49 mm
H
12.7 mm
13.8 mm
13.8 mm
3.89 mm

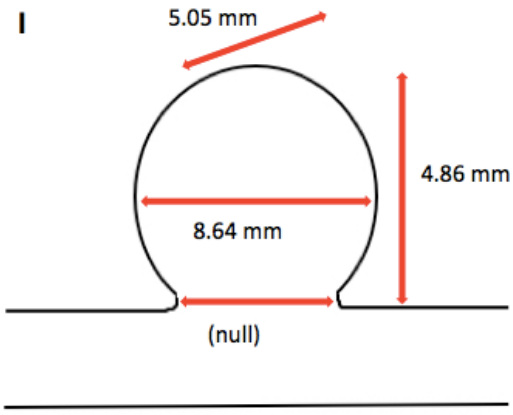

Figure A.1: Aneurysms studied from Wang et al. [94] Similar ranges were noted in a single diagram, and aneurysms that were much larger were depicted separately. Most neck sizes were similar to the dome diameter and height of the aneurysm. Large aneurysms increase in dome size, but not necessarily in neck size. A) Left and right middle cerebral artery aneurysms (N=3). B) Large middle cerebral artery aneurysm. C) Anterior communicating artery aneurysms (N=3). D) Large anterior communicating artery aneurysm. E) Left and right posterior communicating artery aneurysms (N=2). F) Large posterior communicating artery aneurysm. G) Left internal carotid artery aneurysm. H) Large right internal carotid artery aneurysm. I) Left vertebral artery dissecting aneurysm. No dimension was given to define the neck of the aneurysm because of the general shape of a dissecting aneurysm.

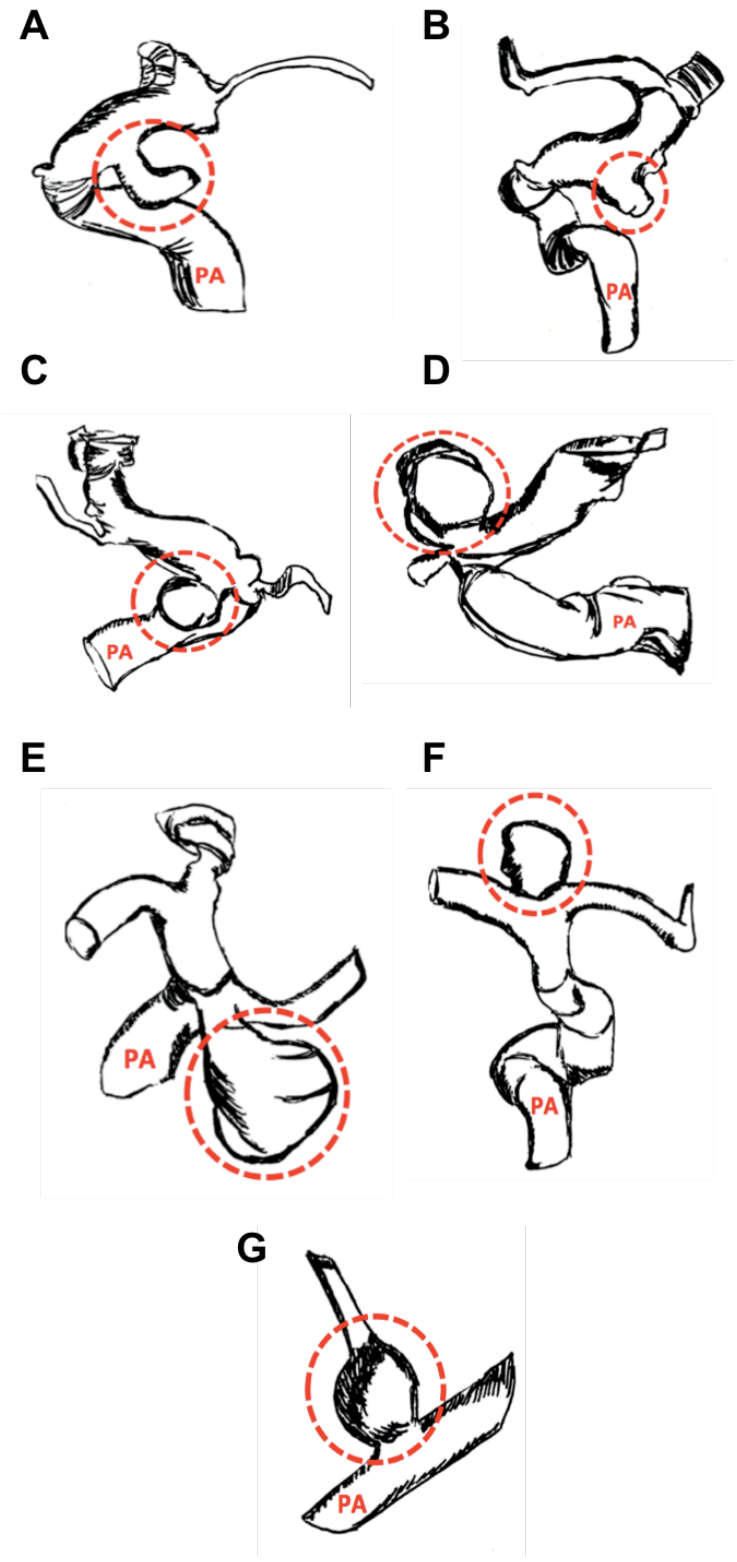

Figure A.2: Aneurysms from Seo et al. [95] Aneurysms were analyzed based on the type of aneurysm on a bifurcation, branch point, or sidewall of a vessel. Most aneurysms were saccular.

The size ratio (SR), which is the maximum aneurysm size divided by the parent vessel diameter, was measured for each type. The average SR was calculated to be 1.39, indicating that most aneurysms were not that much larger than the parent artery. A-D) Saccular sidewall aneurysms with SR = 1.5, 0.77, 1.29 and 1.7, respectively. E, F) Saccular bifurcation aneurysms with SR = 1.87 and 1.33, respectively. G) Fusiform branching aneurysm with SR = 1.28.

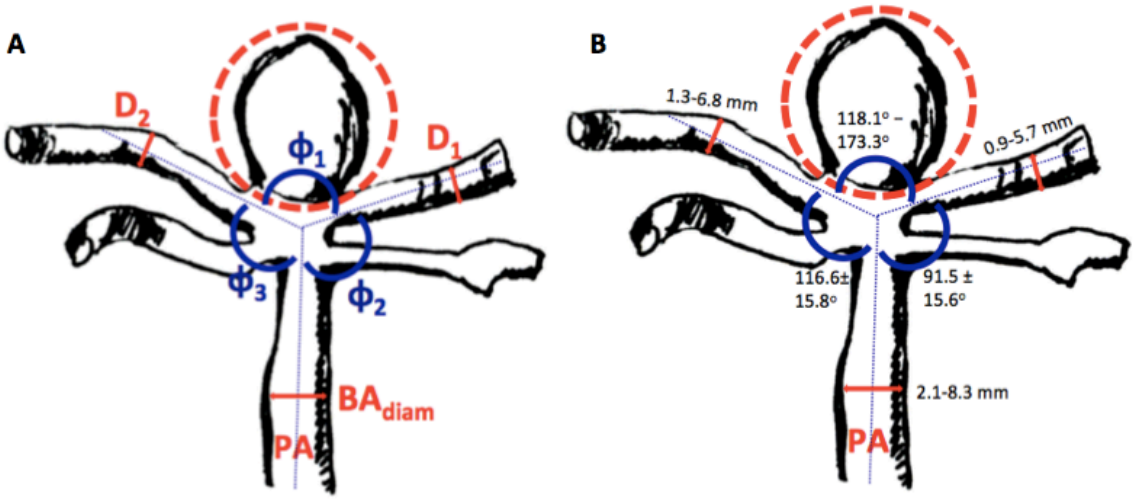

Figure A.3: Artistic rendition of a basilar artery bifurcation aneurysm annotated with the dimensions explored by Zhang et al. [96] A large Φ_1 was associated with basilar aneurysm formation. A large variety of aneurysm sizes were also discovered. This geometry is an example of an aneurysm that can be further characterized by certain dimensions unique to only that kind, and further variations of this geometry can be determined. A) Annotated dimensions. The diameters of the adjacent arteries, D_1 and D_2, and the angles that create the bifurcation, Φ_1, Φ_2, and Φ_3, as well as the diameter of the basilar artery, BA diameter, have been previously found to affect the shape of the aneurysm at the bifurcation. B) Established ranges of dimensions.

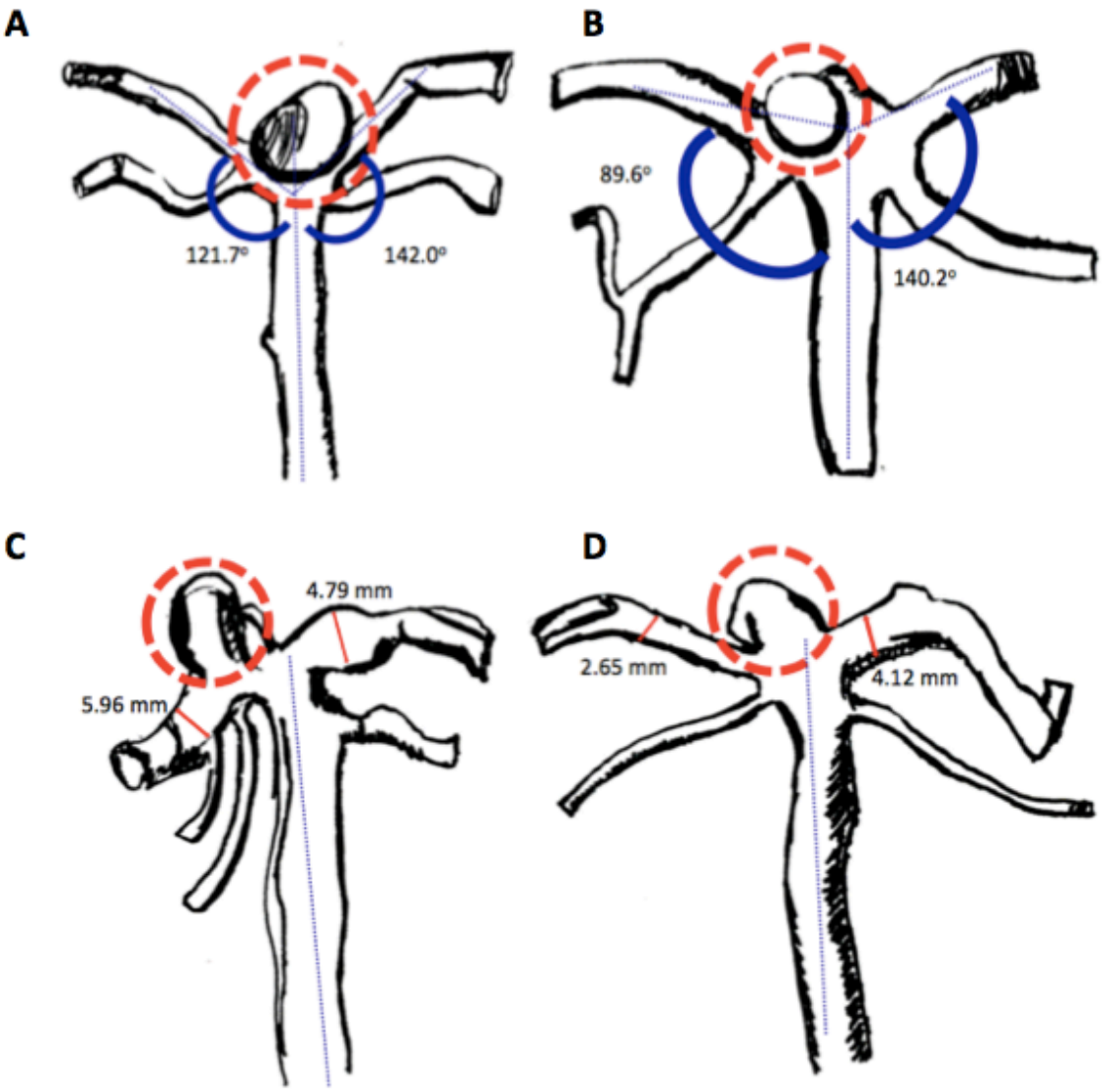

Figure A.4: Basilar artery bifurcation aneurysm deviations based on geometry of surrounding vasculature from Zhang et al. [96] A, B) Deviations due to different lateral angles. The deviation towards the smaller angle (B) is more commonly seen. C, D) Deviations due to different diameters of adjacent arteries. The deviation towards the smaller lateral adjacent artery diameter (D) is more commonly seen.

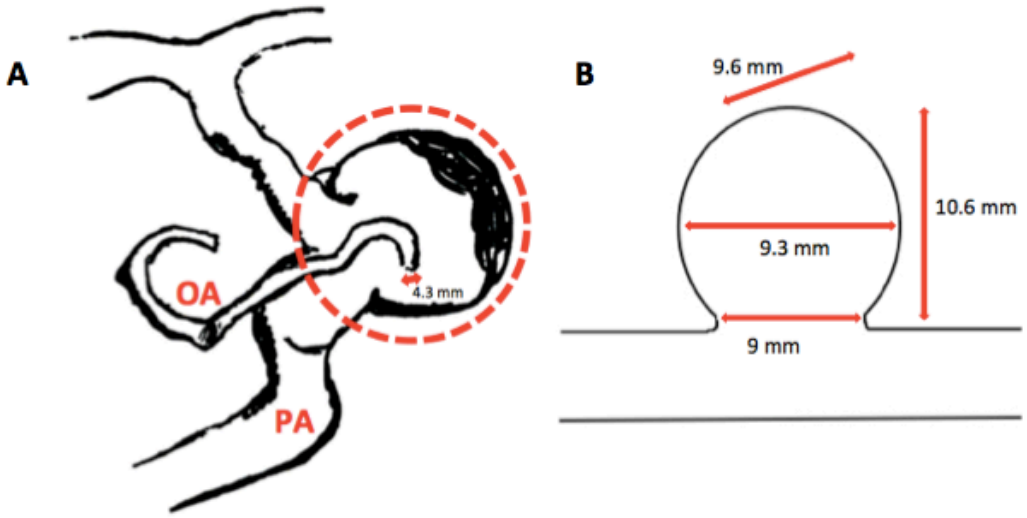

Figure A.5: A unique clinical case from Park et al. [100] of a giant right internal carotid artery aneurysm with a 4.3 mm neck arising from the branch of the ophthalmic artery. This case was an example among many demonstrating that not all aneurysms can be categorized. A) Artistic rendition. B) Aneurysm dimensions without the neck from the branch of the ophthalmic artery.

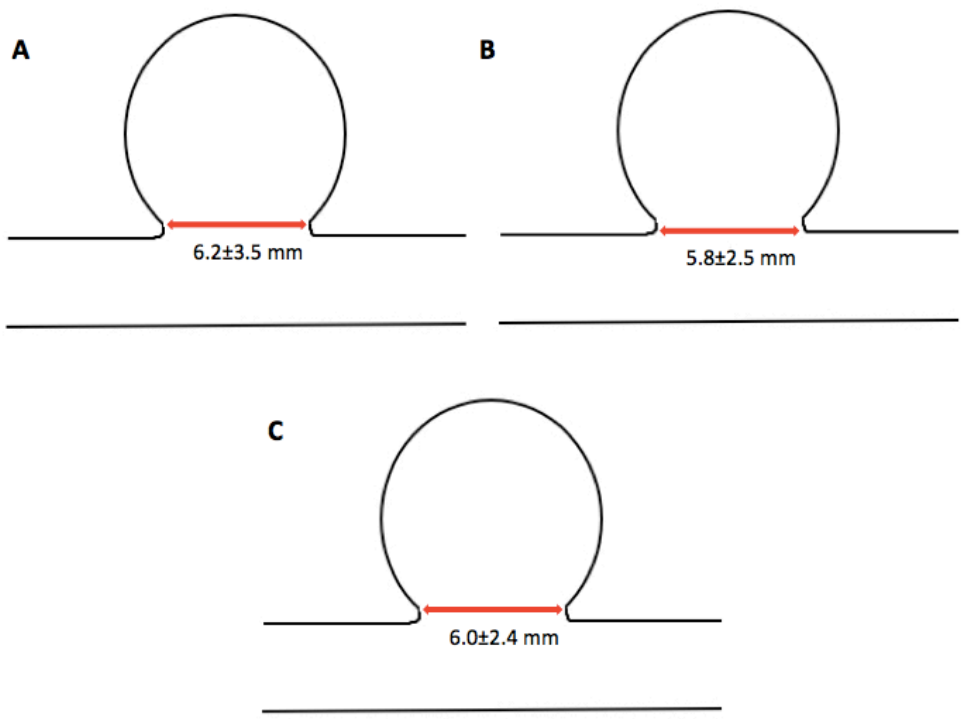

Figure A.6: Wide neck posterior communicating artery aneurysms associated with arteriosclerosis and calcification of parent vessel from Shi et al. [101]. This was the only study that included solely the diameter of the neck to characterize their aneurysms. A) Diagram of Type I aneurysms, or aneurysms with arteriosclerosis and calcification of the aneurysm neck (N=4). B) Diagram of Type II aneurysms, or aneurysms with arteriosclerosis and calcification of the parent artery (N=86). C) Diagram of Type III aneurysms, or aneurysms with arteriosclerosis and calcification of the aneurysm and parent artery (N=46).

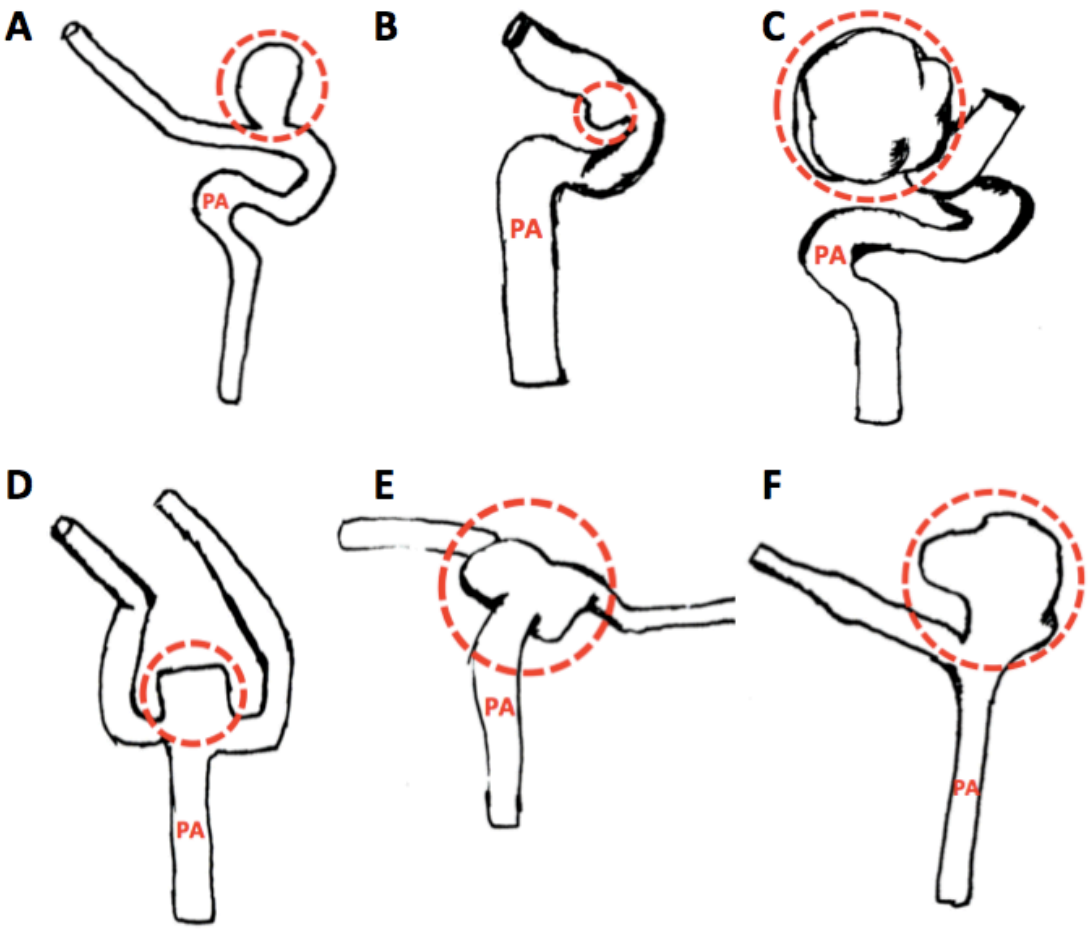

Figure A.7: Artistic rendition of aneurysms from Rajabzadeh-Oghaz et al. [97] This study characterized aneurysms based on their type and location in addition to two dimensions, which helped provide a better picture of each geometry. A) Internal carotid artery aneurysm. B) Blister internal carotid artery aneurysm. C) Giant internal carotid artery aneurysm. D) Middle cerebral artery aneurysm. E) Basilar artery aneurysm. F) Anterior communicating artery aneurysm.

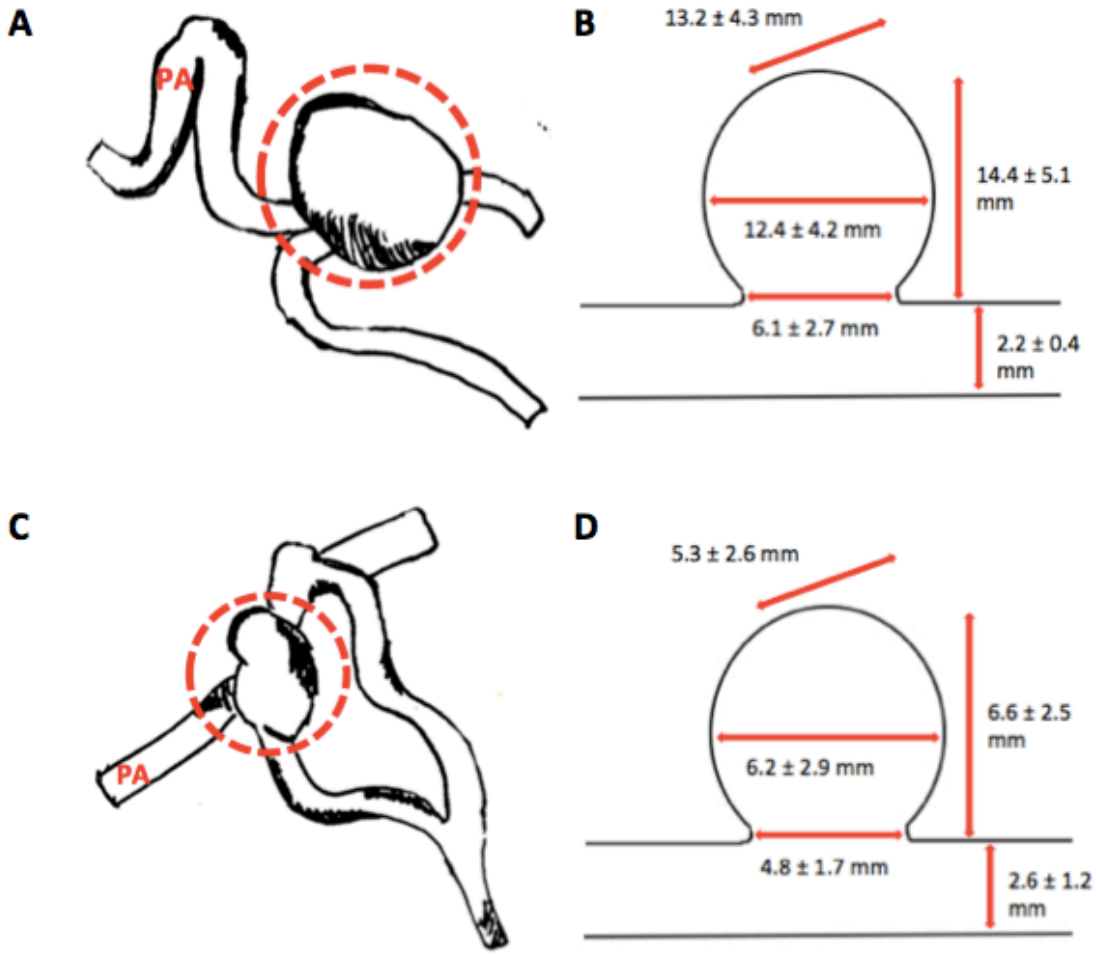

Figure A.8: Middle cerebral artery bifurcation aneurysms from Jiang et al. [103] This study most comprehensively characterized aneurysms using dimensions of all clinical cases, making it very easy to distinguish between geometries. A, B) Artistic rendition and diagram of average dimensions of thick-walled aneurysms (N=18). C, D) Artistic rendition and diagram of average dimensions of thin-walled aneurysms (N=23).

APPENDIX B: TABLE OF EXTRA VALUES DETERMINED FROM PRELIMINARY CHARACTERIZATION OF CURRENT BLISTER AND SACCULAR ANEURYSM GEOMETRIES

Purpose:

This appendix shows tables of extra values determined during preliminary characterization of current blister and saccular geometries.

The following table, Table B.1, describes the internal parallel neck diameter of blister and saccular aneurysms used in preliminary characterization. These values were determined not to be as accurate because the neck diameter could have been stretched out slightly due to cutting during sample preparation. In addition, these values are unnecessary because a better way of measuring the parallel neck diameter using the image of the bottom view of the aneurysm was developed.

Table B.1: Internal Parallel Neck Diameter of Blister and Saccular Aneurysms

Aneurysm Type	Aneurysm Position	Parallel Neck Diameter (mm)
Blister	Distal	5.83
	Proximal	5.52
Saccular	Distal	7.11
	Proximal	6.56